MEASUREMENT OF TEMPERATURE PROFILE IN THE REACTOR CAVITY COOLING SYSTEM

A Thesis

by

TARIQ YAQOOB SAYED AHMAD ABDULRAHIM ALHASHIMI

Submitted to the Office of Graduate and Professional Studies of
Texas A&M University
in partial fulfillment of the requirements for the degree of

MASTER OF SCIENCE

Chair of Committee,	Yassin A. Hassan
Committee Members,	William Marlow
	Maria King
Head of Department,	Yassin A. Hassan

December 2014

Major Subject: Nuclear Engineering

ABSTRACT

The Reactor Cavity Cooling System (RCCS) is an important passive cooling safety system used to cool the cavity of generation IV Very High Temperature Reactors (VHTR). Texas A&M University built a 1/8 scale experimental facility for the air-cooled Reactor Cavity Cooling System (RCCS) based on General Electric Modular High Temperature Gas Cooled Reactor (MHTGR) design to study the thermal hydraulic phenomena occurring in the upper plenum. The facility consists of four vertical parallel riser ducts welded to the upper plenum which has two exhaust chimneys. Blowers are used to drive air through in-line heaters which are connected to the bottom end of the riser ducts. Experiments were conducted to measure the temperature spatial profile in the plenum. Type T thermocouples were mounted on six moveable racks inside the upper plenum, which were moved during the experiments to measure the temperature profile across 6 different planes. Measurements were taken for four different cases with different boundary conditions. Two cases operated with heated air flow in all four risers, whereas the other two were performed with flow in a single riser only. The obtained temperature profiles were asymmetric and suggested the presence of reverse flow from one of the chimneys in both single riser cases and in one of the four riser cases. The other four riser case exhibited a symmetric temperature spatial profile indicating even distribution of the flow across the exhaust chimneys.

DEDICATION

I dedicate this thesis to my loving parents. Their endless love gave me the inspiration, encouragement, support and perseverance I needed to complete this work. Their prayers and backing relieved my stress during the toughest times of my study.

I also dedicate this work to my sisters Hind, Maryam, Asma, Huda and Sara and to my brothers Abdullah and Mohamed. Their continuous support raised my spirit and helped me overcome the most stressful times.

ACKNOWLEDGEMENTS

I direct my sincere gratitude to my mentor Dr. Elvis Dominguez the proctor of the University Services Building at Texas A&M University and the leader of the air-cooled RCCS project. By far Dr. Dominguez is the finest experimentalist I have ever met. Dr. Dominguez is the mastermind behind all of the RCCS experiments at TAMU. He was extremely generous with his time and knowledge and never complained about how much I bothered him over the past 18 months. This work would have never been complete without his guidance and support. I learnt many things from him regarding experiments and work ethic. I again thank him for all the help I received from him.

Special thanks go to my senior colleague Shamsul Sulaiman the PhD student working on the air-cooled RCCS project. Along with Dr. Dominguez, Sham was the primary designer of the air-cooled RCCS facility at TAMU. Sham worked really hard with me to build the facility and to obtain the necessary data for this thesis. Many of the figures used in this work were also produced by Sham. I sincerely admire his hard work and diligence and wish him success in continuing what we've started together.

I would like to acknowledge my colleague John Budd who joined the project 9 months ago. John was a key player in the installation of the instrumentation in the facility and he helped me in conducting many experiments. John and I suffered for a long time during the installation and calibration of the thermocouples; along with Dr. Dominguez guidance, John's patience and perseverance enabled us to overcome one of the toughest phases of the project

Thanks also go to Mario Matos the undergraduate student from the Engineering Technology department. Mario proved himself as one of the key players in the RCCS project. In fact, the toughest jobs are mostly assigned to Mario due to his competency and skill.

Special thanks are directed to my chair Dr. Hassan for his guidance and support. His weekly visits to the lab encouraged us to achieve more. He is truly an influential person with passion in nuclear engineering.

I would also like to acknowledge my committee members Dr. William Marlow and Dr. Maria King for their time and dedication.

Thanks also go to my friends at Texas A&M University who made my 5 and a half years journey in college station pass by with peace. I would like to thank my friend Talal who helped in running one of the experiments. Thanks to Razag for helping me in one time during the assembly of the different part of the facility.

Finally, I direct my thanks to anyone who made this work successful and I apologize if I forgot to acknowledge him by name.

TABLE OF CONTENTS

Page

LIST OF FIGURES

Page

Page

Page

Page

Page

Page

LIST OF TABLES

1. INTRODUCTION

The Very High Temperature Reactor (VHTR) is a promising generation IV type reactor. The VHTR is envisaged to operate with a core outlet temperature of 1000^{o}C. The high core outlet temperature will allow the VHTR to supply the necessary energy for a broad spectrum of heat applications. Examples of industrial applications which may utilize the VHTR capability to supply heat include hydrogen and ammonia production (Vaghetto, 2011). Moreover, the process heat supplied by the VHTR can also be used in cement and iron manufacturing. If the VHTR concept is applied to support these processes, the emission of greenhouse gases will significantly reduce as fossil fuel burning is the primary energy source for heat-intensive applications.

However, in case of loss of coolant accident, or pump failure the reactor temperature may rise to dangerous levels (Corradini et al., 2012). If the rise of temperature is not halted, core meltdown is inevitable. Passive safety systems can prevent the core meltdown by providing an ultimate heat sink without the need for any power source or human intervention. Passive heat removal systems are capable of removing decay heat from the pressure vessel to an ultimate heat sink (Sulaiman, et al., 2014). The Reactor Cavity Cooling System (RCCS) grabbed the attention as a leading passive heat removal design for generation IV type reactors.

The RCCS is a passive safety system designed to remove the decay heat produced in the core of the reactor to an ultimate heat sink under all accident scenarios (Sulaiman, et al., 2014). The RCCS prevents the core cavity structure from overheating

and provide continuous cooling for the reactor pressure vessel (RPV). The RCCS design consists of a series of pipes or ducts facing the RPV. Heat is mainly transferred from the RPV walls to the pipe/ducts via radiation. The heat is then removed by the coolant flowing through the pipe/ducts. Current RCCS designs use water and air as cooling fluids. Most water and air cooled RCCS designs operate using natural circulation. As the coolant is heated, the density decreases. The change in density creates a buoyancy pressure head which enables natural circulation. Table 1 below shows a list of water and air cooled RCCS designs.

Table 1. List of Current RCCS Designs (Sulaiman, et al., 2014).

Country	**Reactor**	**Power (MWt)**	**RCCS Coolant**	**Circulation Method**
Japan	HTTR	30	Water	Forced
China	HTR-10	10	Water	Natural
South Africa	PBMR	265	Water	Natural
Russia	GT-MHR	600	Air	Natural
USA	MHTGR	450	Air	Natural

1.1 The Japanese HTTR

The Japanese High Temperature Engineering Test Reactor (HTTR) is a $30MW_{th}$ reactor which is cooled by helium and moderated by graphite (Corradini et al., 2012). The HTTR is the first High Temperature Gas Cooled Reactor (HTGR) to be built in Japan with a nominal outlet temperature of 950°C (Idaho National Laboratory, date accessed: Oct-5-2014). The HTTR uses prismatic block core with an active core height of 290cm and an effective diameter of 230cm (Idaho National Laboratory, date accessed: Oct-5-2014). The Japanese HTTR has three cooling systems: the main cooling system (MCS), the auxiliary cooling system (ACS), and the vessel cooling system (VCS) (Idaho National Laboratory, date accessed: Oct-5-2014). Figure 1 below shows a schematic of the cooling systems in the HTTR.

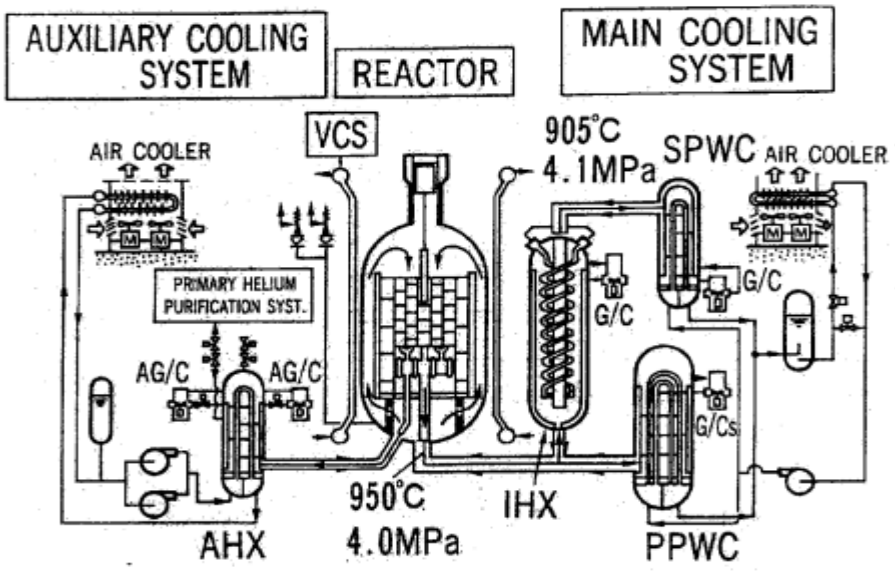

Figure 1. The HTTR Cooling Systems (Idaho National Laboratory, date accessed: Oct-5-2014).

The MCS is designed to cool the reactor during normal operation. The ACS operates when there is a scram, while the VCS comes into play when there is a rupture in the piping of the primary cooling system which prevents forced circulation (Idaho National Laboratory, date accessed: Oct-5-2014). The VCS is a unique type of RCCS which acts as a residual heat removal system in case of piping rupture in the primary system. The VCS also operates under normal conditions to cool the reactor's concrete walls. It is not a passive type of RCCS which uses water as coolant. It consists of two independent sets of cooling panels equipped with emergency power supplies (Idaho National Laboratory, date accessed: Oct-5-2014). As shown in fig.1 above, the VCS is lined along the internal surface of the reactors concrete walls.

1.2 The Chinese HTR-10

The Chinese High Temperature Gas Cooled Reactor (HTR-10) is a small research reactor with a thermal output of 10MW. The HTR-10 is a pebble-bed type reactor which operates at a pressure of 3MPa (Oh, et al., 2007). It is helium cooled and has nominal inlet and outlet temperatures of 250 and 700^{o}C, respectively (Oh, et al., 2007). The Chinese HTR-10 has two independent water-cooled RCCSs which completely rely on natural circulation (Oh, et al., 2007). Figure 2 below shows a schematics of the HTR-10 which includes the RCCS. The RCCS water coolers are placed along the inner concreate walls of the containment. Heat is transferred to the water coolers via radiation and conduction. Air coolers are placed on the top of the

reactor positioned in the chimneys (Oh, et al., 2007). On the top of the reactor building, the water coolers are connected to air coolers (Oh, et al., 2007). Heat is transferred from water to air and the heat is then disposed to the atmosphere by the chimney.

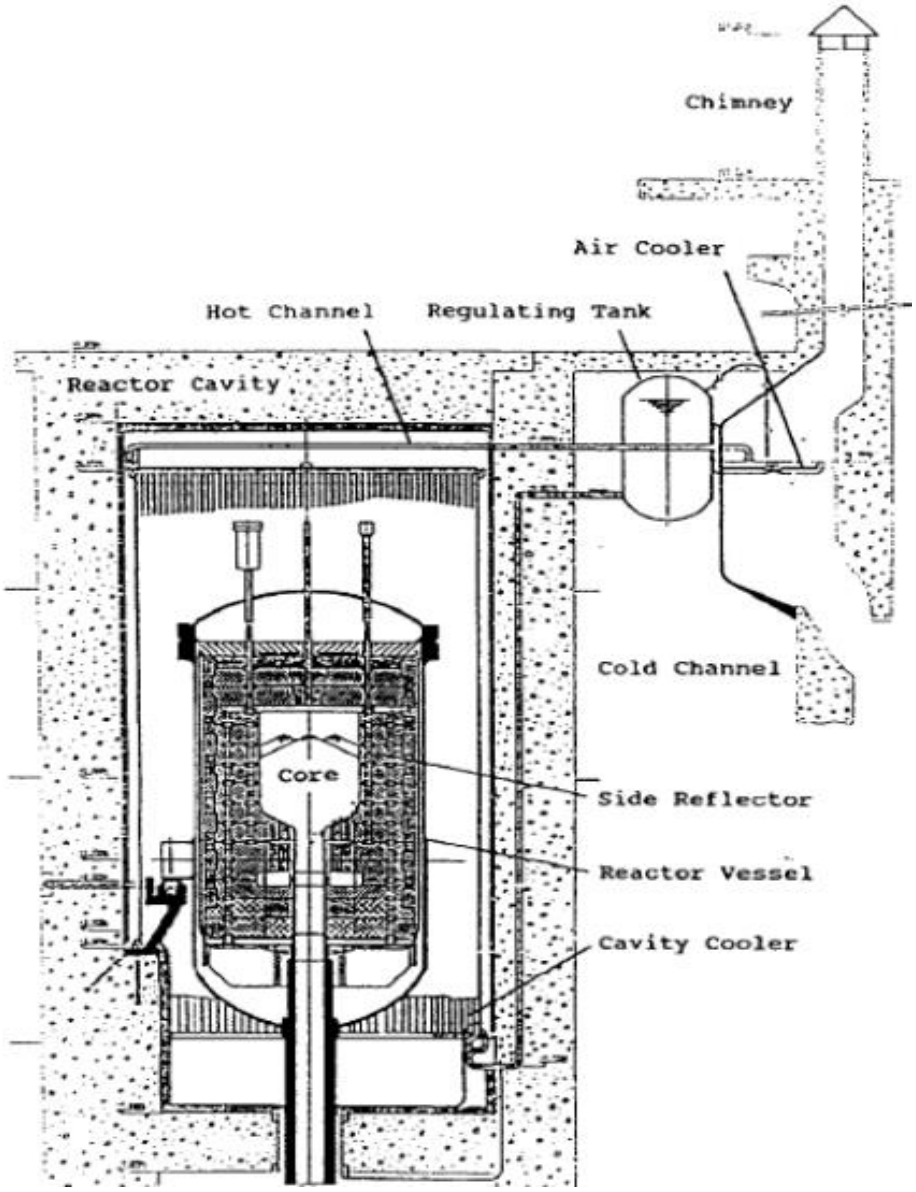

Figure 2. The Chinese HTR-10 including the reactor core, pressure vessel and RCCS (Wei, 2009).

1.3 The South African PBMR

The South African Pebble Bed Modular Reactor (PBMR) is a helium-cooled, graphite moderated HTGR with a thermal power of 265MW (Corradini, et al., 2012). The reactor has nominal inlet and outlet temperatures of 500 and 900^{o}C, respectively (International Atomic Energy Agency, 2011). Similar to the HTR-10 RCCS, the PBMR uses water-cooled RCCS with passive water to air heat exchange for ultimate heat rejection to the atmosphere (Corradini, et al., 2012). The PBMR has three independent RCCSs which utilize natural convection to passively cool the cavity of the reactor (Corradini, et al., 2012). The heat radiated from the reactor pressure vessel is transferred to the water in the RCCS. The change in temperature causes a change in density, which drives the flow of water in the system. Hot water flows upwards and is cooled using an intermediate heat exchanger which rejects the heat to the outside atmosphere. The cooled water then flows down and gets heated again on its way up.

1.4 The Russian GT-MHR

The Russian Gas Turbine Modular Helium Reactor (GT-MHR) is a prismatic type reactor with a thermal power output of 600MW (Corradini, et al., 2012). The reactor will adopt a Brayton cycle for power conversion and is estimated to have a relatively high thermal efficiency. The design was developed by General Atomics in cooperation with Russia's OKMB.A prototype is planned to be constructed in Russia in

the near future. The GT-MHR employs a natural convection, air-cooled RCCSs for passive safety. The GT-MHR's RCCS is composed of cooling panels installed around the RPV (Oh, et al., 2007). Air circulating through the cooling panels from outside removes the heat transferred by radiation and conduction from the RPV (Oh, et al., 2007). Unlike the previous water-cooled designs, this design does not need an intermediate heat exchanger to reject the heat to the environment as the air entering the cooling panels directly exits to the atmosphere.

1.5 The GA-MHTGR

The General Atomics Module High Temperature Gas Cooled Reactor (MHTGR) is a 450MW_{th} reactor currently being developed by GA in the US. The reactor is cooled by helium and uses a prismatic core. The MHTGR RCCS consists of a set of ducts installed along the cavity walls. There are two loops with a total of 227 ducts (Corradini, et al., 2012). Each duct is 19.2m tall and has a cross section of 10x2cm (Corradini, et al., 2012). The flow of air is driven by buoyant forces, in other words, natural circulation. Air will enter the RCCS through an inlet plenum with a temperature of 43^{o}C. The air will flow downwards through a set of downcomers before moving upwards through the risers (Corradini, et al., 2012). The air will exit the system through chimneys located above the reactor building.

Figure 3 below shows how heat is transferred from the RPV to the RCCS and ground. As shown in the figure, heat is transferred from the RPV to the RCCS cooling

panels by radiation and natural convection. Heat is also conducted to the ground beneath the RPV. The heat collected by the air circulating in the cooling panels is disposed to the atmosphere through the chimneys as shown in the figure below.

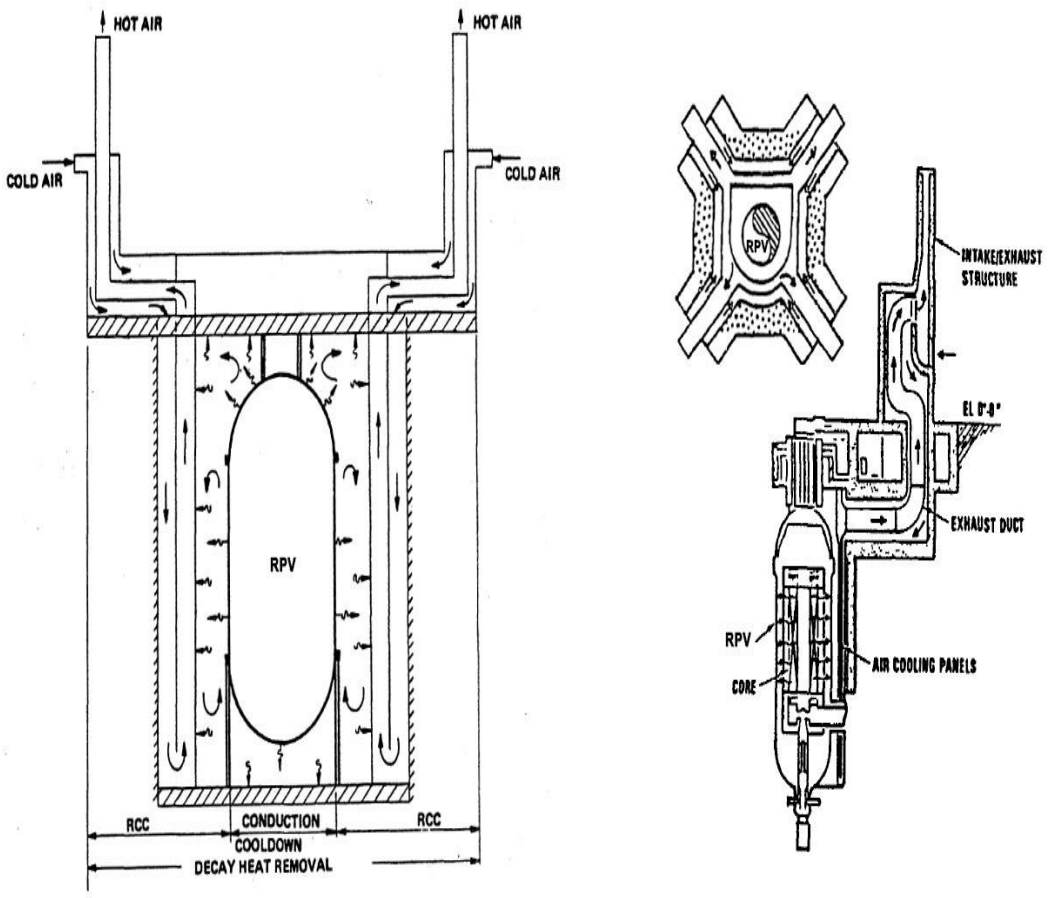

Figure 3. The figure shows how heat is transferred from the RPV to the RCCS (Sulaiman, et al., 2014).

1.6 Inverse Distance and Kriging Interpolations

Interpolations are used to predict an unknown value at a given location by weighing the surrounding known values. Interpolation was very important for this thesis as all of the measured temperatures were interpolated to obtain a full temperature field. Two types of interpolations were used: the inverse distance and kriging interpolation.

Inverse distance interpolation works under the assumption that the predicted value is proportional to the inverse of the distance from the surrounding measured values (Flitter, et al., 2013). In other words, measured values closer to the point of prediction will have more similarity compared to the values measured at a further distance. The method applies a weight to the surrounding measured values based on the separation distance. Measured values close to the point of prediction will have a larger weight and thus larger influence on the predicted value. Measured values at a further location will have lower weights and hence a smaller influence on the predicted value. The general form of the inverse distance is shown in the equation below (Flitter, et al., 2013).

$$\hat{v} = \frac{\sum_{i=1}^{n} \frac{1}{d_i} v_i}{\sum_{i=1}^{n} \frac{1}{d_i}} \quad (1)$$

Where $\hat{v}$ is the predicted value, v_i is the measured value at location I, and d_i is the distance between point i and the predicted value. Some variations of the method add an exponent to the distance term for better control on the influence of the distance.

The Kriging method is very similar to the inverse distance weighting with the exception that in addition to the separation distance, the former takes into account the three-dimensional arrangement of the data (Bohling, 2005). Inverse distance interpolation is categorized as a deterministic type of interpolation with the predicted value being directly proportional to the surrounding measured points. Kriging is a geostatistical type of interpolation which correlates the measured points using statistical models before applying a weighting factor to each measured point. The general form of the Kriging method is as follows (Makhnin, 2014):

$$\hat{v} = \sum_{i=1}^{n} \lambda_i v_i \tag{2}$$

Where in the above equation λ_i is a weighting factor dependent on both the separation distance and correlation between the measured values. Depending on the spatial configuration, the two methods yield similar results in many cases.

1.7 Thermocouple Uncertainty

Thermocouples were used in this experiment to obtain the needed temperature measurements. There are many factors that affect the accuracy of the thermocouples which can be divided into two groups: random and systematic error. The source of random errors in an experiment is usually unknown and irregular. Random errors can be caused by variations in the outside environment or the instrumentation used in an experiment. Due to their unpredictability, random errors are quantified using statistical

models. It's usually assumed that random errors have a normal distribution. Based on the normal distribution assumption, the standard error associated with the mean can be calculated by dividing the standard deviation by the square root of the number of samples.

$$\mu_{error} = \frac{\sigma}{\sqrt{N}} \tag{3}$$

Systematic error is usually easier to identify and correct. This type of error is usually caused by the instruments. Unlike random errors, systematic errors persist throughout the duration of the experiment. They do not occur suddenly as in the random error case. Sandia National Lab developed a model for quantifying the error accompanying the thermocouple readings as shown in Fig.3. The model takes into account many factors affecting the thermocouple readings.

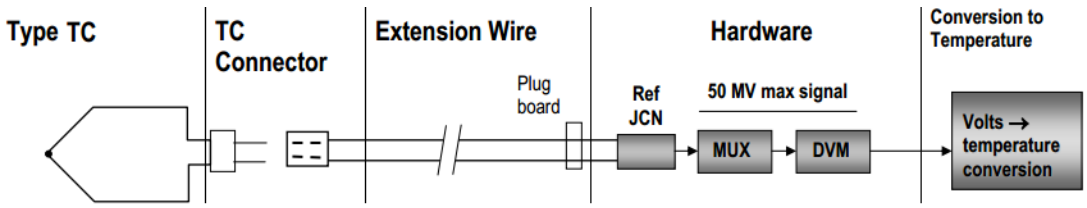

Figure 4. Sandia National Lab model for quantifying the error associated with the thermocouple reading. The figure displays the sources of systematic error for a thermocouple reading (Nakos, 2004).

The first source of systematic error was the type of thermocouple. Each type of thermocouple has an accuracy established by the manufacturer. The errors reported by the manufacturer are assumed to be maximum values. Thermocouple connectors also contribute to the systematic error when there is a temperature difference across the

connector. Depending on the length of the thermocouple wire or the extension wire used, an error is introduced to the system due to the noise picked up by the signal and the voltage divider effect. The error introduced by the length of the wire can be quantified with the following equation (DATAQ, 2012):

$$(1 - \frac{R_a}{R_a + R_t}) * 100 \tag{4}$$

Where R_a is the input resistance of the Data Acquisition System (DAQ) hardware, and R_t is thermocouple wire resistance which is dependent on the length of the wire. The DAQ hardware also contributes to the systematic error, and can be quantified using equations provided by the manufacturer. The main sources of error in the DAQ include the cold junction compensation (CJC), offset and gains and noise (National Instruments, 2012). The CJC is usually the main contributor to the DAQ error. The CJC is used to compensate for the voltages created by cold junctions. A thermocouple consists of two dissimilar materials connected at both ends. One end is referred to as the hot end and the other is referred to as the cold end. The output of the thermocouple is basically the difference between the hot and cold ends (Pyromotion, 2014). However, people are interested in the hot end temperature not the difference between the hot and cold ends. This is where the CJC comes into play. The CJC measures the temperature of the cold end and adds it to the output of the thermocouple so that the hot end temperature is obtained. The CJC error is mainly related to the error of the thermistor used to measure the temperature of the cold end. Noise is also a key contributor to the DAQ error due to the fact that the thermocouple signals are very small

(millivolt range) rendering them vulnerable to noise introduced by the external environment or the device itself. In addition, a thermocouple produces voltage that is converted into a temperature reading. The conversion formula depends on the type of thermocouple and has a given nominal error. The total systematic error can be calculated using equation 5 below (Nakos, 2004). The combined systematic and random errors can be combined using equation 6 (Nakos, 2004):

$$S_{total} = (S_1^2 + S_2^2 + S_3^2 + S_4^2 + ..)^{\frac{1}{2}} \quad (5)$$

$$Error_{total} = +/- (S_{total} + R_{total}) \quad (6)$$

1.8 Project Technical Objective

Texas A&M University constructed a small test facility for the RCCS based on the GA-MHTGR design. The goal behind the construction of the facility was to study the complex thermal hydraulics phenomena occurring in the upper plenum of the RCCS. A good understanding of the flow behavior and underlying phenomena is needed for the development of passive safety systems for generation IV reactors. Temperature and velocity measurements along with computational fluid dynamics (models) were needed to understand the behavior of the flow. The technical objective of this project was to measure the temperature profile in the RCCS's upper plenum with different configurations. The temperature measurements will be used to predict the flow behavior in the upper plenum. This project along with future velocity measurements will provide the necessary experimental results to validate future CFD models. The necessary

experiments for the temperature measurements were conducted at Texas A&M University's thermal hydraulics laboratory located in the University Services Building (USB). Texas A&M's RCCS test facility was used to gather all the data. The experimental setup and procedure will be mentioned in details in the following sections.

2. EXPERIMENTAL FACILITY

Texas A&M University built a small scale test facility for the air-cooled RCCS based on General Atomic's concept of the MHTGR. The facility was built to investigate the multifaceted thermal hydraulics phenomena and the thermal stratification occurring in the upper plenum of the air-cooled RCCS. The experimental facility is 1/8 scale of the full GA design which represents a 10^{o} slice sector. The schematic shown below illustrates the layout of the components in the RCCS test facility. The main components of the experimental apparatus include:

1. Risers
2. Upper plenum
3. Two symmetrically positioned chimneys
4. Blowers
5. Heater

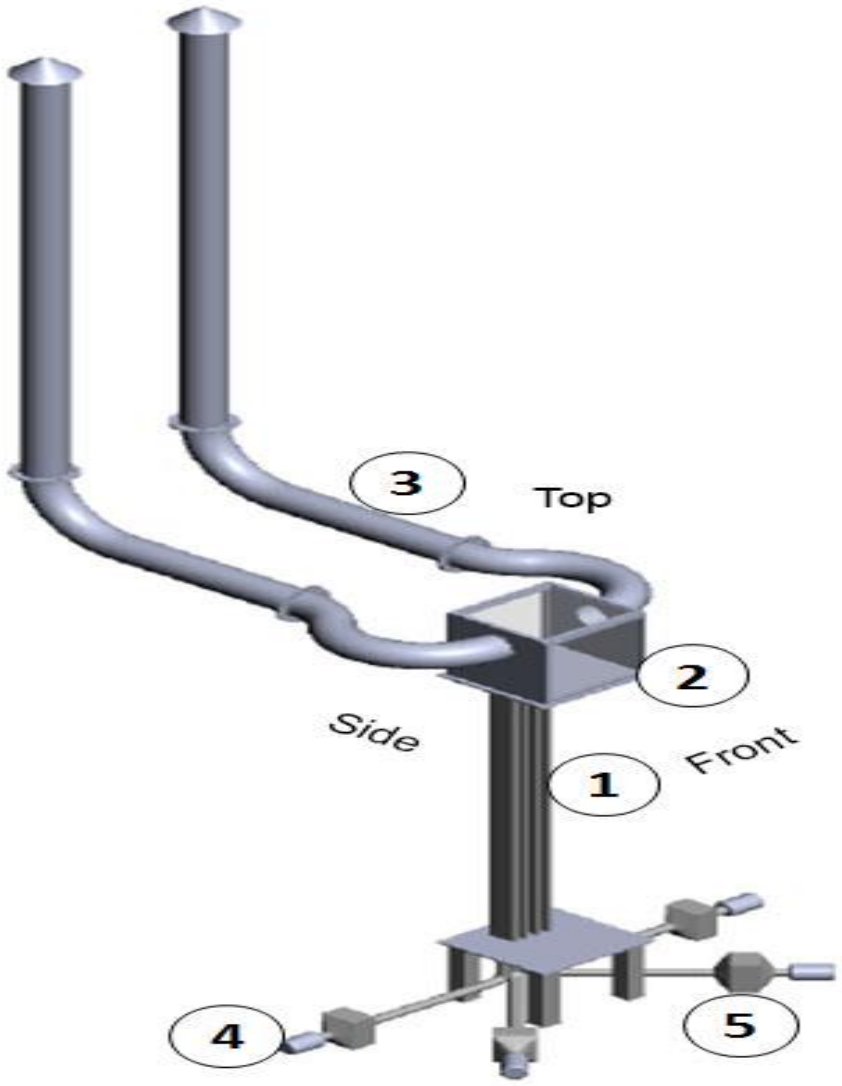

Figure 5. The layout of TAMU's RCCS test facility.

Air enters the system through the four blowers marked with number 4 in the above schematic. The blowers increase the velocity of the circulating air using rotating impellers. The flowing air is then channeled to four in line heaters which are connected to the outlet of each blower. The heater converts electric power into thermal energy using heating coils which ramp the temperature up. Heated air then flows through the

four risers before it penetrates into the upper plenum. Air from the four risers mix inside the upper plenum and departs through two symmetrically positioned chimneys. While the flow in the GA-MHTGR design of the RCCS uses natural convection, the TAMU facility uses forced convection to reach the same boundary conditions at the inlet of the upper plenum. The main purpose of the experimental facility was to study the phenomena occurring in the upper plenum. By having the same boundary conditions, it was expected that the most notable phenomena will be maintained. The use of a blowers and heaters provides flexibility for the experimentalists at TAMU as they can simulate a number of different conditions very easily by changing the boundary conditions. While a natural convection scaled facility with radiant heaters was important in order to study the flow behavior in the risers, a forced convection facility with blowers and heaters enabled the users to manipulate the boundary conditions at the inlet of the plenum very easily. Since UW and ANL already constructed natural convection facilities, TAMU decided to focus its efforts on the upper plenum, so that the experiments are not repeated. Accordingly, a forced convection facility was constructed at TAMU.

2.1 Scaling

As mentioned earlier in the section, the TAMU's air-cooled RCCS test facility was scaled to be 1/8 of the GA's original design. University of Wisconsin (UW), one of the collaborators in the RCCS investigation, built a test facility that was ¼ scale of the GA design. Another air-cooled RCCS facility was built in Argonne National Lab (ANL) which was a half scale of the GA-MHTGR. The scaling laws developed and analyzed by the UW and ANL were adopted for TAMU's design. The purpose of using scaling laws was to preserve vital thermal hydraulics phenomena occurring in the system. Scaling also allowed for the construction of smaller test facilities, which reduced the overall cost.

The main difference between the scaled and full-scale facilities was the reduced axial length l_R, which affected all of the similarity groups. The facility at TAMU had a reduced axial and radial dimensions of 1/8 and ½ of the GA-MHTGR RCCS. Due to the complexity of the flow in the RCCS, two scaling methodologies were adopted for different sections of the system. The first methodology was the top down scaling which basically worked by non-dimensionalizing the 1-D conservation equations in order to derive similarity groups (Lomperski, et al., 2011). The similarity groups were found by finding the ratio of the model parameter to the prototype parameter (Lomperski, et al., 2011).

$$\Psi_R = \frac{\Psi_{Model}}{\Psi_{Prototype}} \tag{7}$$

The similarity groups taken into consideration were: the time ratio T_R^*, power Q, heat flux q'', reference velocity U, and temperature rise ΔT. The scaling analysis performed by UW and ANL established the following similarity relationships (Lomperski, et al., 2011):

$$T_R^* = \sqrt{l_R} \tag{8}$$

$$q'' = l_R^{-0,5} \tag{9}$$

$$Q = \sqrt{l_R} \tag{10}$$

$$\mathrm{Re} = \sqrt{l_R} \tag{11}$$

$$U = \sqrt{l_R} \tag{12}$$

$$\Delta T = 1 \tag{13}$$

The rise in temperature across the risers was meant to be preserved in order to simulate the thermal hydraulics phenomena present in the system. This explained why the ratio between the model and prototype was equal to unity. Given the scaled parameters of TAMU‘s experimental facility, table 2 shown below summarized the similarity groups and their corresponding values.

Table 2. Summary of the similarity groups for different scales (Sulaiman, at el, 2014)

		ANL	UW	TAMU
Parameter	**Scaling Ratios**	**Values for $l_R = 0.50$**	**Values for $l_R = 0.25$**	**Values for $l_R = 0.125$**
Lateral (radial)	-	1.00	1.00	0.50
Velocity, U	$U_{oR} = (l_R)^{1/2}$	0.707	0.50	0.35
Time ratio, T_R^*	$T_R^* = \frac{l_R}{U_{oR}} = (l_R)^{1/2}$	0.707	0.50	0.35
Temperature rise, ΔT	$\Delta T_{oR} = \frac{\dot{Q}_R}{U_{oR} A_{oR}}$	1.00	1.00	1.00
Power, $\dot{Q}$	$\dot{Q}_R = U_{oR} = (l_R)^{1/2}$	0.707	0.50	0.354
Heat flux, q''	$q_R'' = (l_R)^{-1/2}$	1.414	2.00	2.828

As mentioned earlier, the top down scaling methodology was generally used to non-dimensionalize the 1-D conservation equations. The top-down technique was applicable to regions where the flow could be sufficiently characterized by the 1-D conservation equations. However, this method of scaling cannot capture the multifaceted phenomena occurring in the upper plenum. Anticipated phenomena in the upper plenum include thermal stratification, jet entrainment and flow recirculation (Lomperski, et al., 2011). Therefore, another methodology called the bottom-up scaling was employed to account for the complex flow behavior in the upper plenum. The bottom-up methodology was the basis of the upper plenum design for TAMU's RCCS test facility. The parameter of interest was the maximum ceiling height X_M for the upper plenum. The bottom-up scaling technique evaluated X_M while taking the anticipated phenomena into consideration. Experimental data collected by Turner suggested that X_M was proportional to the momentum flux F (Lomperski, at el., 2011). The maximum ceiling

height was derived in terms of the scaled dimensions as shown in Eq.14. Given the scaled parameters of the experimental facility, the maximum ceiling of the upper plenum was found to be ¼ of the full-scale facility.

$$X_m = D_{jR}^{1/2} l_R^{1/2} = 0.25 \tag{14}$$

2.2 Facility Parts Description

As shown in Fig.5 above, the main parts of the RCCS facility were risers, upper plenum and the chimneys. This section will discuss the dimensions and the design considerations of the different parts of the RCCS. All of the parts were made using stainless steel. An illustration of the front, side and top views of the experimental facility are shown in Fig.6. The figures shown in this section were produced using Solidworks. Only the designed parts will be discussed in this section. The blowers and heaters will be discussed in the instrumentation section

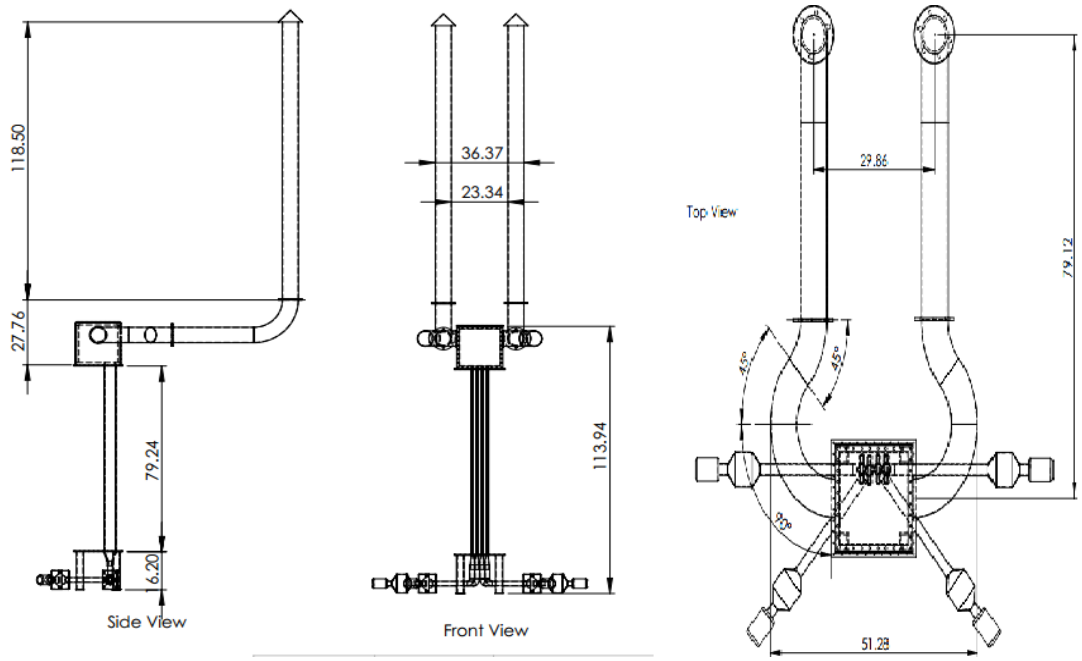

Figure 6. Schematic of the RCCS facility including side, front and top views.

2.2.1 Risers

The TAMU RCCS facility had four parallel risers which were 79.24” tall. The height was only 1/8 of the GA-MHTGR design. The number of risers was selected to be 4 to preserve the flow symmetry present in the original design. The risers had a rectangular cross-section with outer dimensions of 1.05x5.03” and a thickness of 0.18” as illustrated in Fig.7. Each riser had fillets on its four corners with a radius of 0.28”. The separation between each riser was 1”. Each riser was manufactured separately before being arranged in a parallel fashion. The risers were welded from the bottom to a lower plate and from the top to an upper plate. The lower plate served as a support for the risers while the upper plate was basically the bottom part of the upper plenum.

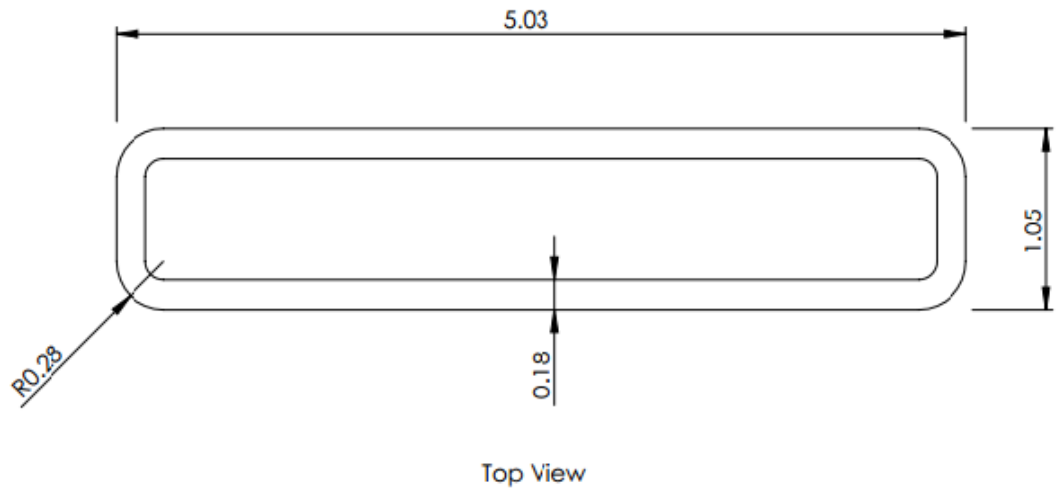

Figure 7. The cross-section of the riser.

2.2.2 Riser Connectors

While the risers were rectangular in shape, the air being pumped and heated traveled through a circular pipe before entering the ducts. Therefore, four riser connectors were manufactured to connect the circular pipes to the rectangular risers. The riser connectors' dimensions are shown in Fig.8 below. It's important to note that the hydraulic diameter of the circular pipe is equal to the hydraulic diameter of the ducts as to reduce the disturbance to the flow. Figure 9 showed the front, side and top views of the four risers combined.

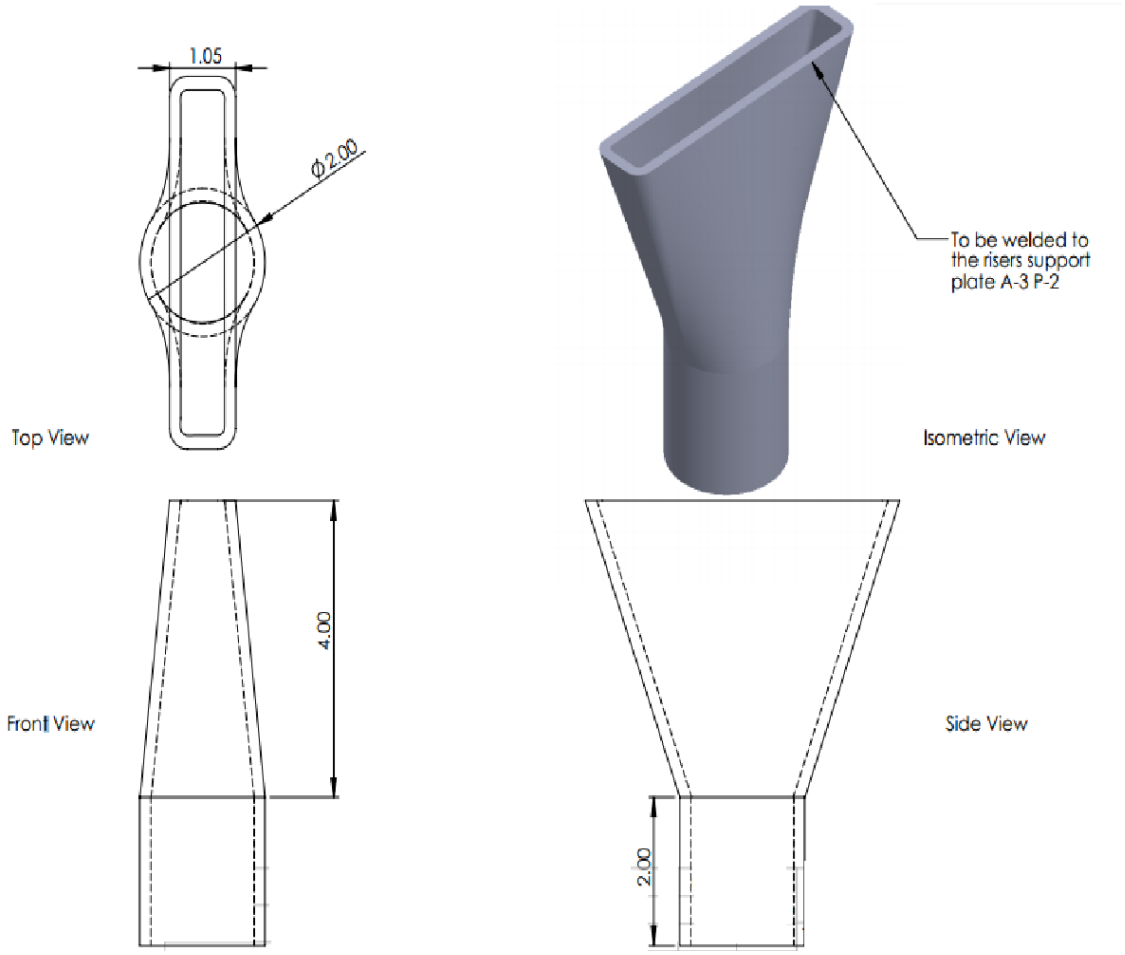

Figure 8. The riser connector front, side, top and isometric views.

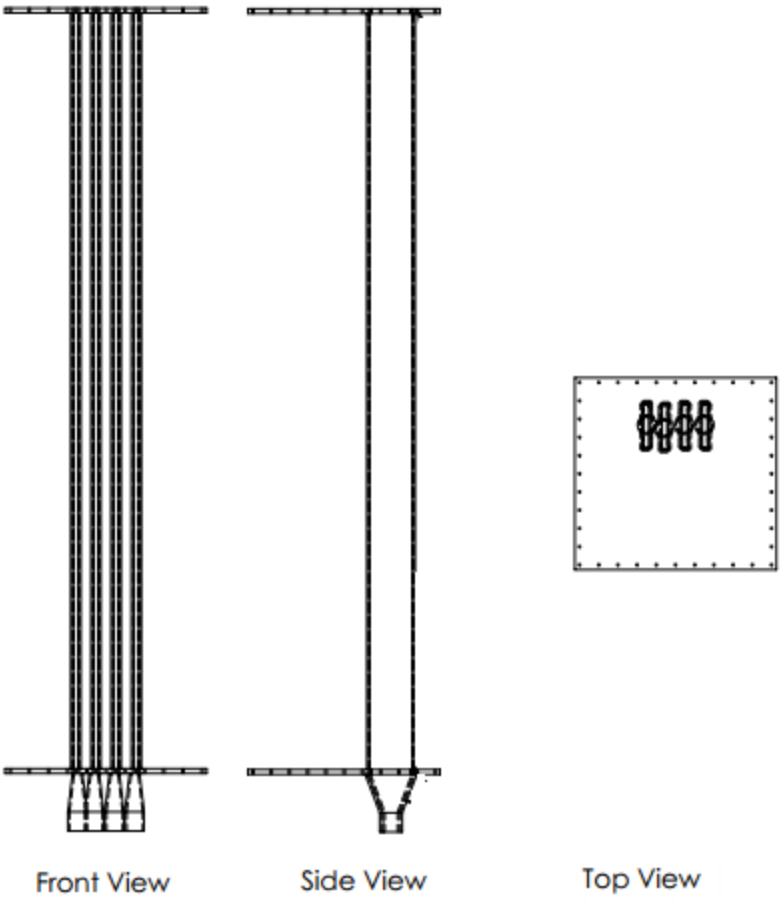

Figure 9. A schematic of the risers including the front, side and top views.

Each riser had 6 holes for 1/8” and three holes for 3/8” Female National Pipe Thread connections (FNPT) as shown in Fig.10. The 1/8” connections were used for temperature and pressure probes while the 3/8” connections were used to insert borescopes for visualization purposes. The locations of the probes are shown in the schematic displayed below.

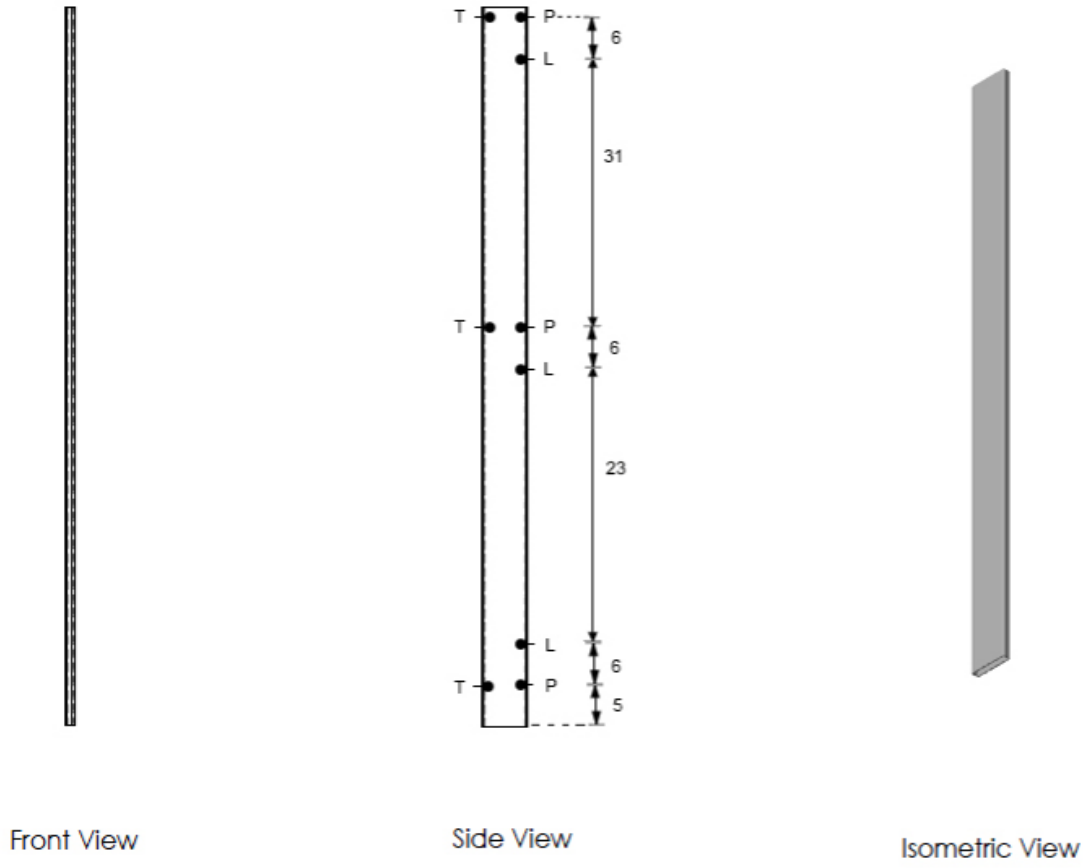

Figure 10. Riser port locations. The letters P and T represent the pressure and temperature ports, while the letter L represents the borescope ports.

2.2.3 Upper Plenum

The upper plenum was the main focus of the research efforts at TAMU. As mentioned earlier, a forced convection facility was constructed specifically for the purpose studying the flow behavior in the upper plenum with different conditions. The parallelepiped upper plenum had a cross section of 19x18", height of 17" and wall thickness of 1". Two circular holes with a diameter of 6" were drilled on the side faces

which allowed the flow to exit the box. The two holes served as the inlet of the chimneys which will be discussed later. The front, back and top faces were manufactured with glass in order to facilitate flow visualization using particle imagery velocimetry (PIV).

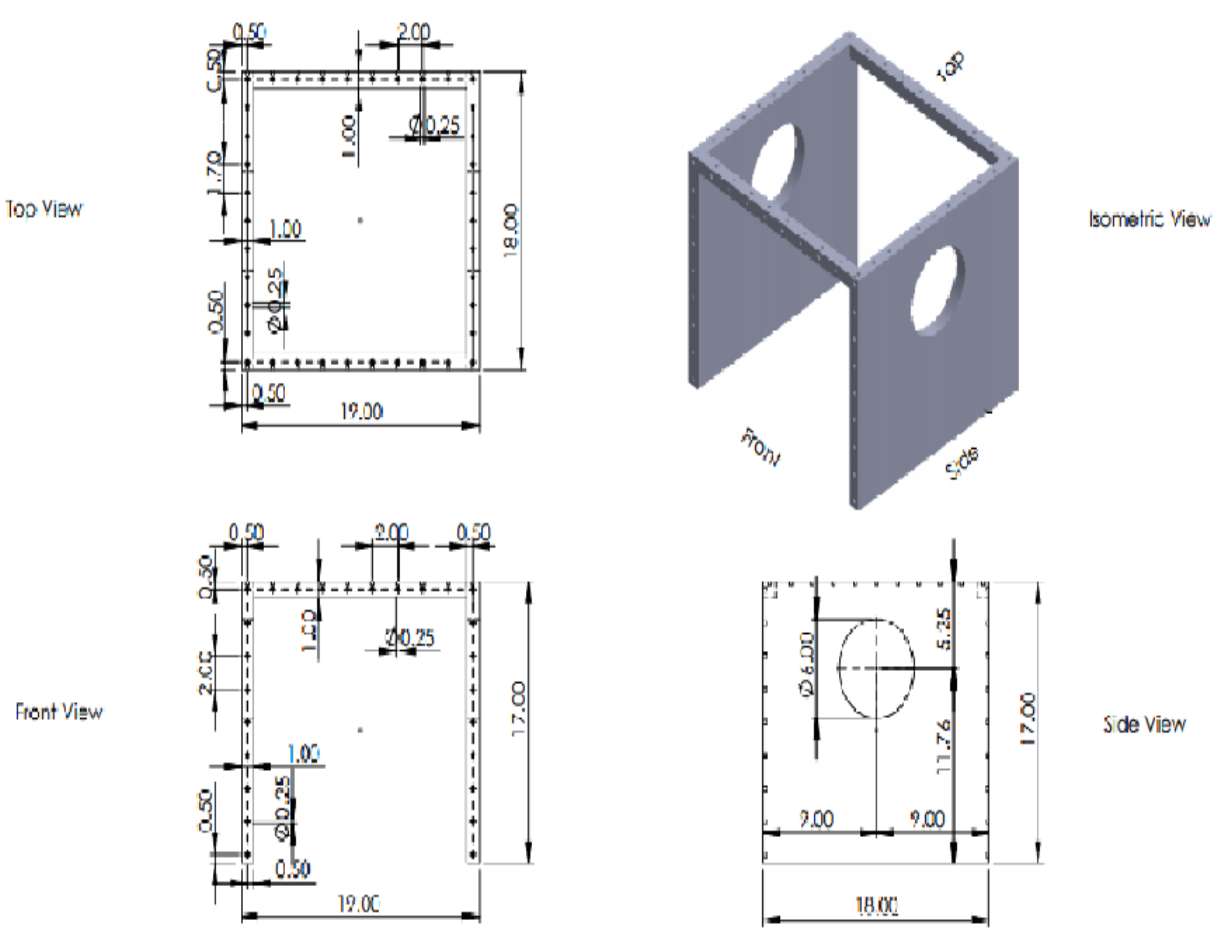

Figure 11. The upper plenum including front, side, top and isometric view.

Seven holes were drilled into the bottom, right side, left side plates of the upper plenums to permit ¼" FNPT connections. Six holes were positioned symmetrically on the plates, whereas the seventh hole was placed at the center. Figures 11,12 and 13 show

the exact locations of the ports. The center hole was used to insert the probe measuring the pressure inside the upper plenum, whereas the six symmetrically positioned holes are used to insert six metallic rods from the bottom and the right side plates. Each pair of parallel rods with the same elevation was connected with a cross bar. In other words, three cross bars were used for the bottom and right side plates. Each cross bar had 14 thermocouples mounted on it. The reason behind the orientation of the cross bars and the mechanism used to move the bars will be discussed later.

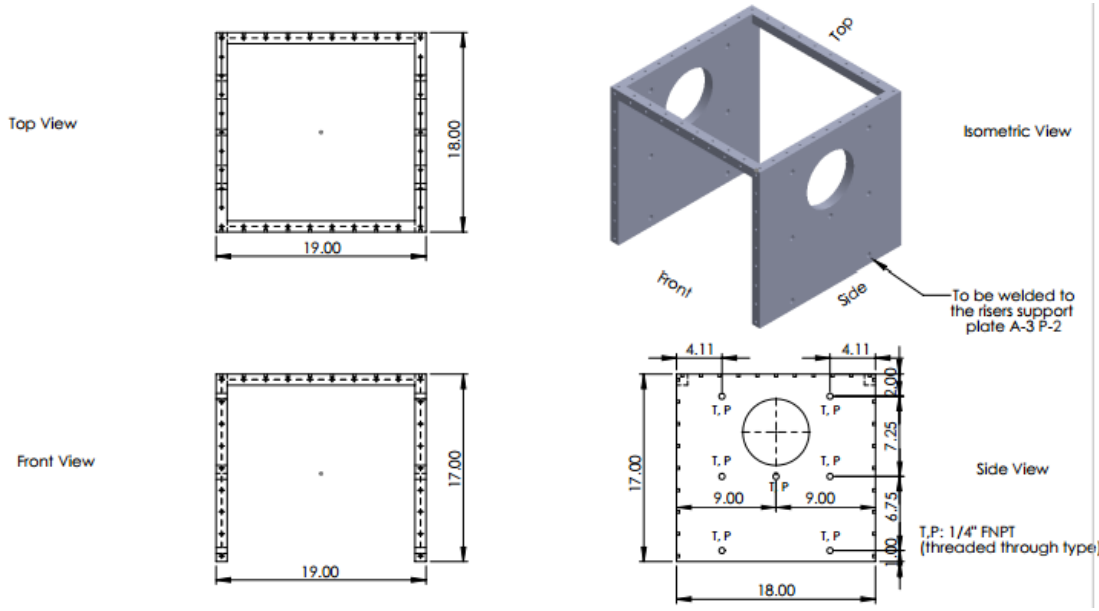

Figure 12. The positions of the ports on the side plates of the upper plenum.

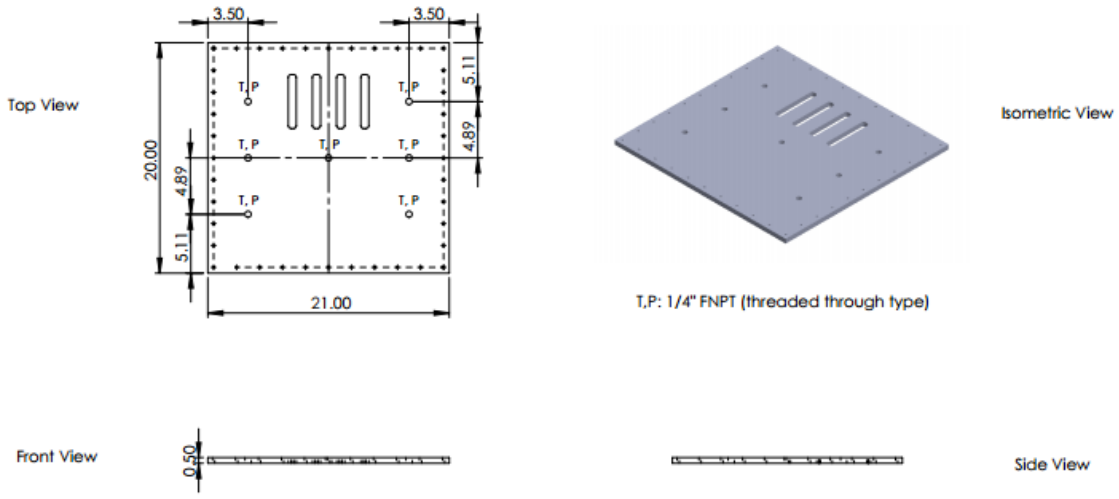

Figure 13. Positions of the ports on the bottom plate of the upper plenum.

2.2.4 Chimney

Two symmetric chimneys link the upper plenum to the outside environment. The heated air exits the upper plenum through these two chimneys. The chimney exhausts were 118.5” tall and had an inner and outer diameters of 6.41 and 6.63”. Due to their large size, each chimney was manufactured as six separate pieces. Some pieces were welded together while others were coupled. Figures 14 and 15 show different views of the chimneys with their dimensions. Similar to the risers, holes were drilled into different parts of the chimneys to enable temperature and pressure measurements in addition to borescopes insertion. The sizes of the holes were exactly the same as the risers’ holes. Figure 16 depicts the exact locations of the ports.

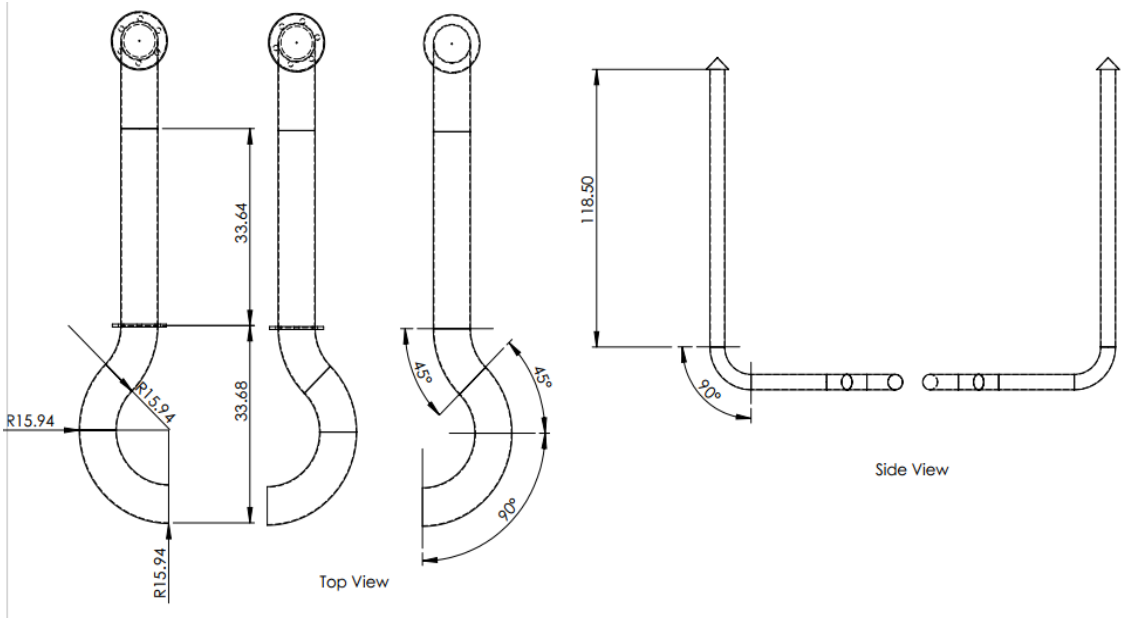

Figure 14. The chimney schematic including the top and side view.

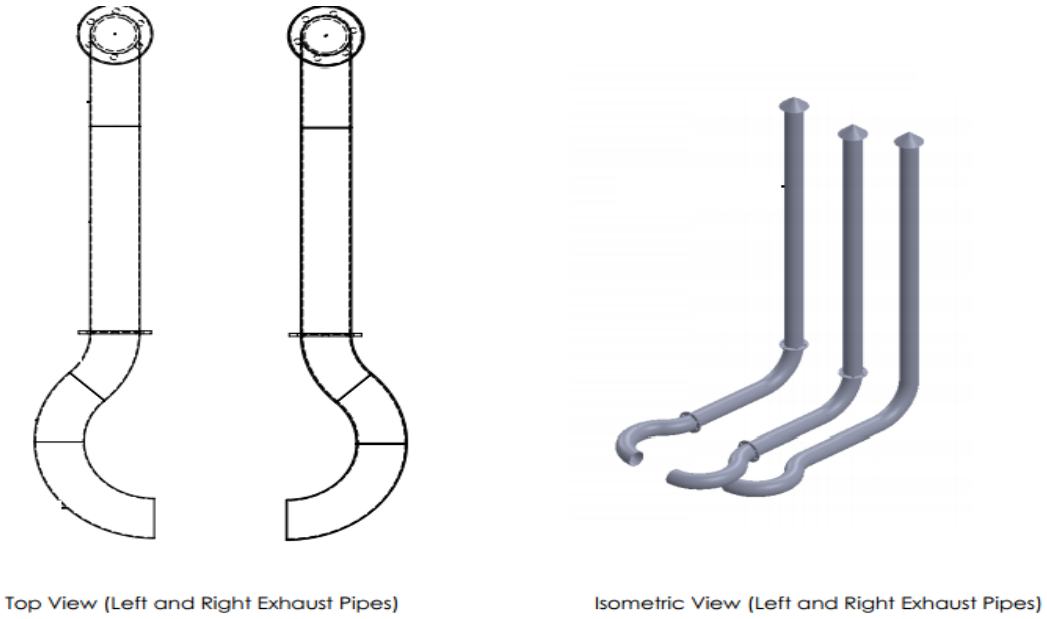

Figure 15. The top and isometric views of the chimneys.

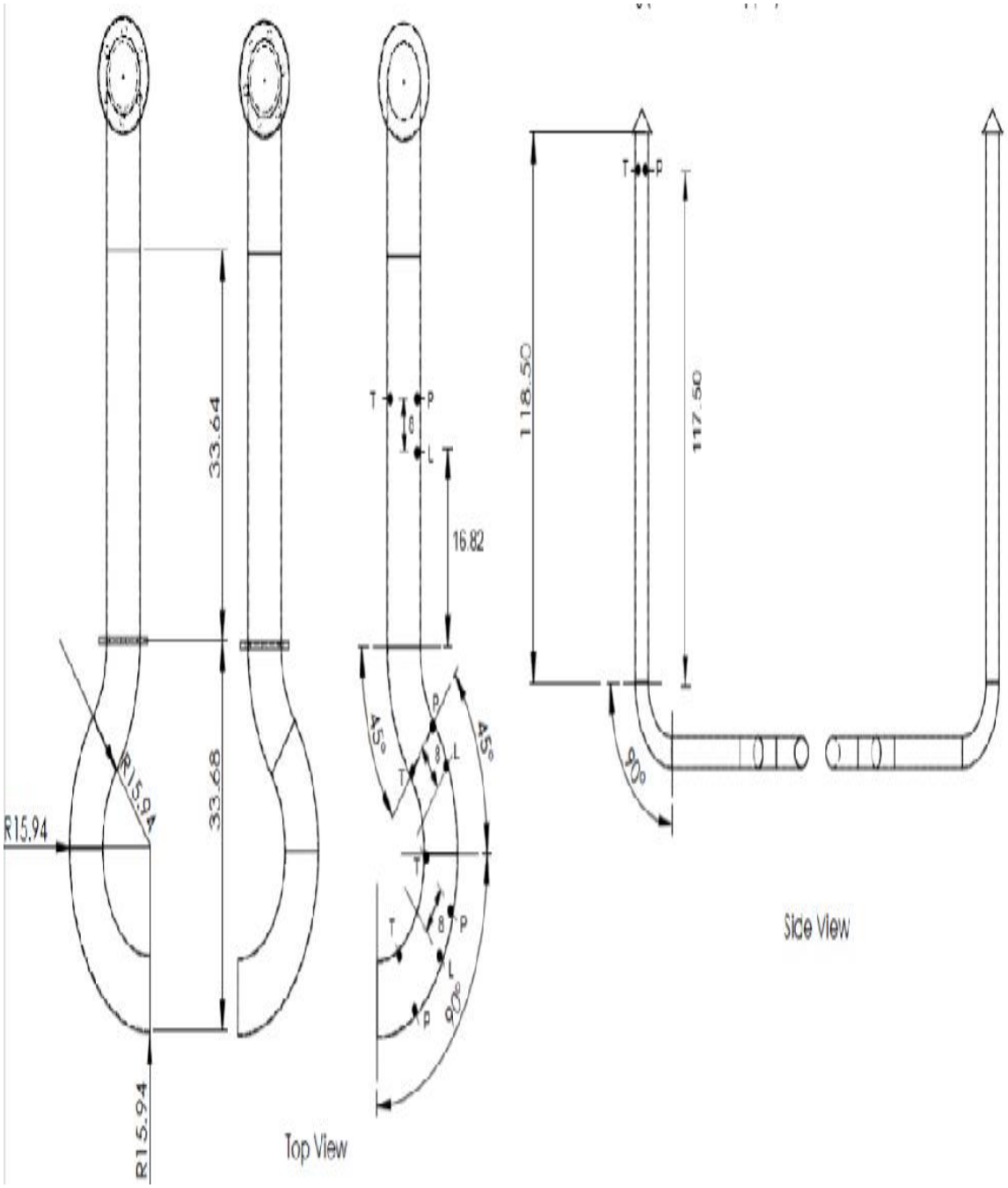

Figure 16. The locations of the ports on the chimneys.

2.3 Supporting Structure

The supporting structure was built using storage pallet racks. The structure was composed of six pallet rack frames; each frame had a height of 240” and a width of 42” as shown in Fig.17 below.

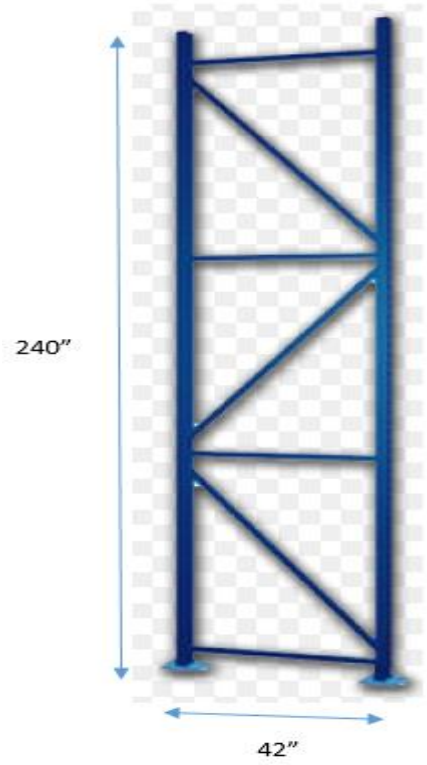

Figure 17. The pallet rack frame used for supporting the RCCS.

Each three frames were placed beside each other and were connected using couplings. The arrangement of each trio was illustrated in Fig.18 and the row separators were displayed in Fig.19.

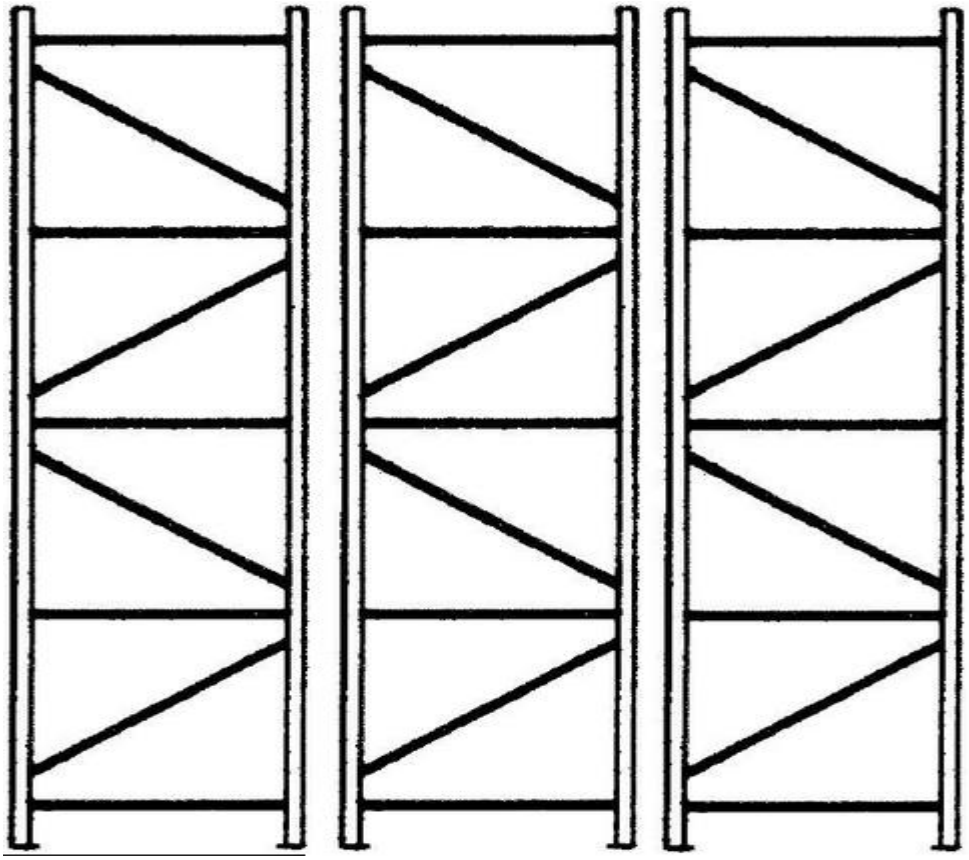

Figure 18. Pallet rack frames arrangement

Figure 19. The row separators between the the pallet rack frames.

The pallet racks were then placed against each other and connected with 144” beams to enhance the stability of the structure. Figure 20 showed the structure after the attachment of the beams.

Figure 20. The pallet rack after being connected by the beams.

Beams were specifically placed at an elevation of 5 and 11ft to support the first and second floors. Mesh decking panels were installed on these beams; half inch thick ply wood was then placed on the mesh and drilled into the supporting beams. Non-slip decks were glued to the wooden floors to prevent tripping hazard. Mesh decking panels and ply wood were installed at the ends of the central pallet rack; the middle of the central pallet rack was left open in order to accommodate the risers and the upper plenum. Lumber beams were installed at the edges of the first and second floors to prevent stuff from falling. Beams were also installed 3ft above each floor to prevent people from falling. A ladder was also mounted to ease the transition to first and second floors. Two floors were needed for many reasons. The first reason was to simplify the installation and reparation of the measuring instruments. For instance, thermocouples can easily break and they need to be fixed very often. Moreover, thermocouples were placed at different locations in the facility, including the risers, upper plenum and chimneys; the elevation between the risers and the upper plenum is close to 80”; the elevation between the ground and the outlet of the chimney is close to 260”; the availability of the first and second floors provided an easy access to the different instrumentation of the facility. In addition, the data acquisition system needed to be really close to the different parts of the facility as to reduce the length of the thermocouples wires connected between the system and the different parts of the facility. Accordingly, the decision was made to have 2 floors in the facility. Figures 21 and 22 show the first and second floors of the RCCS facility structure.

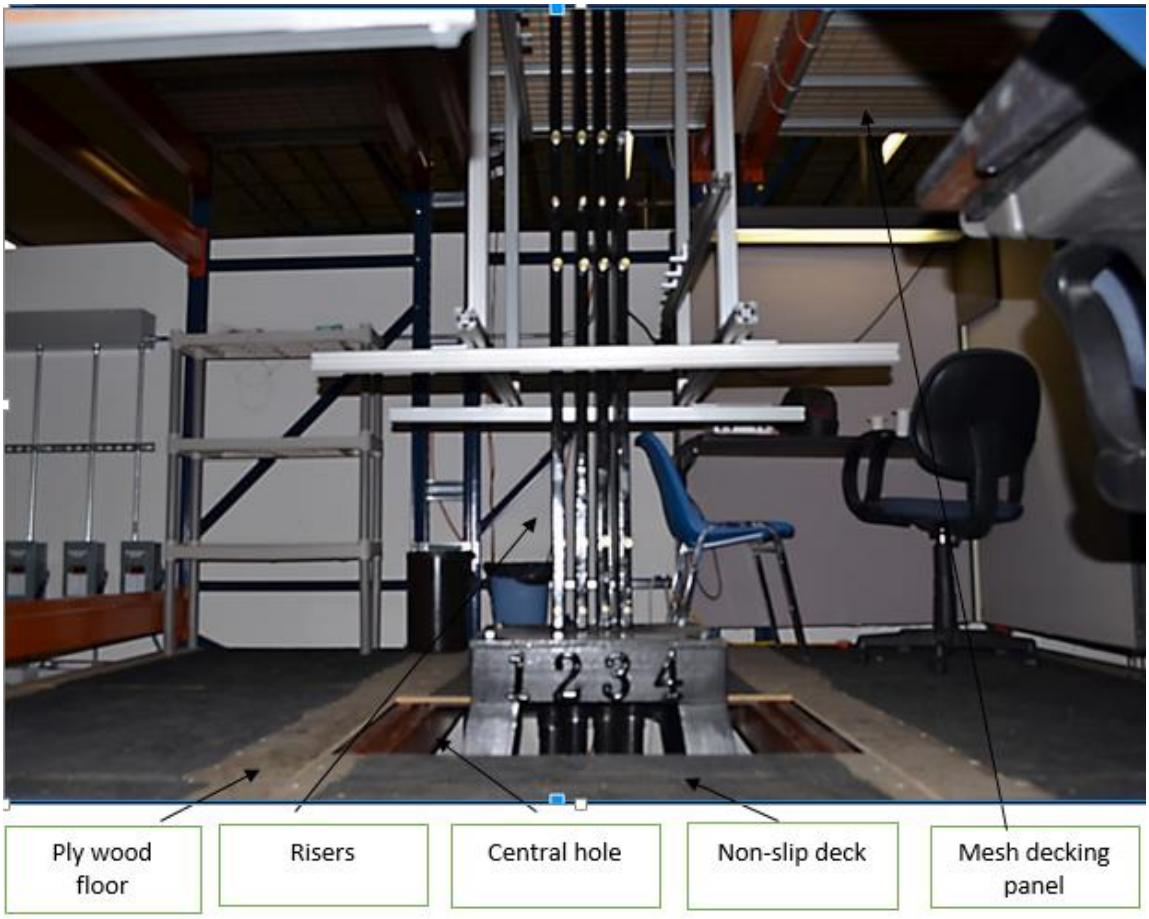

Figure 21. Picture of the first floor showing the ply wood, non-slip decks and the middle section left open to accommodate the risers.

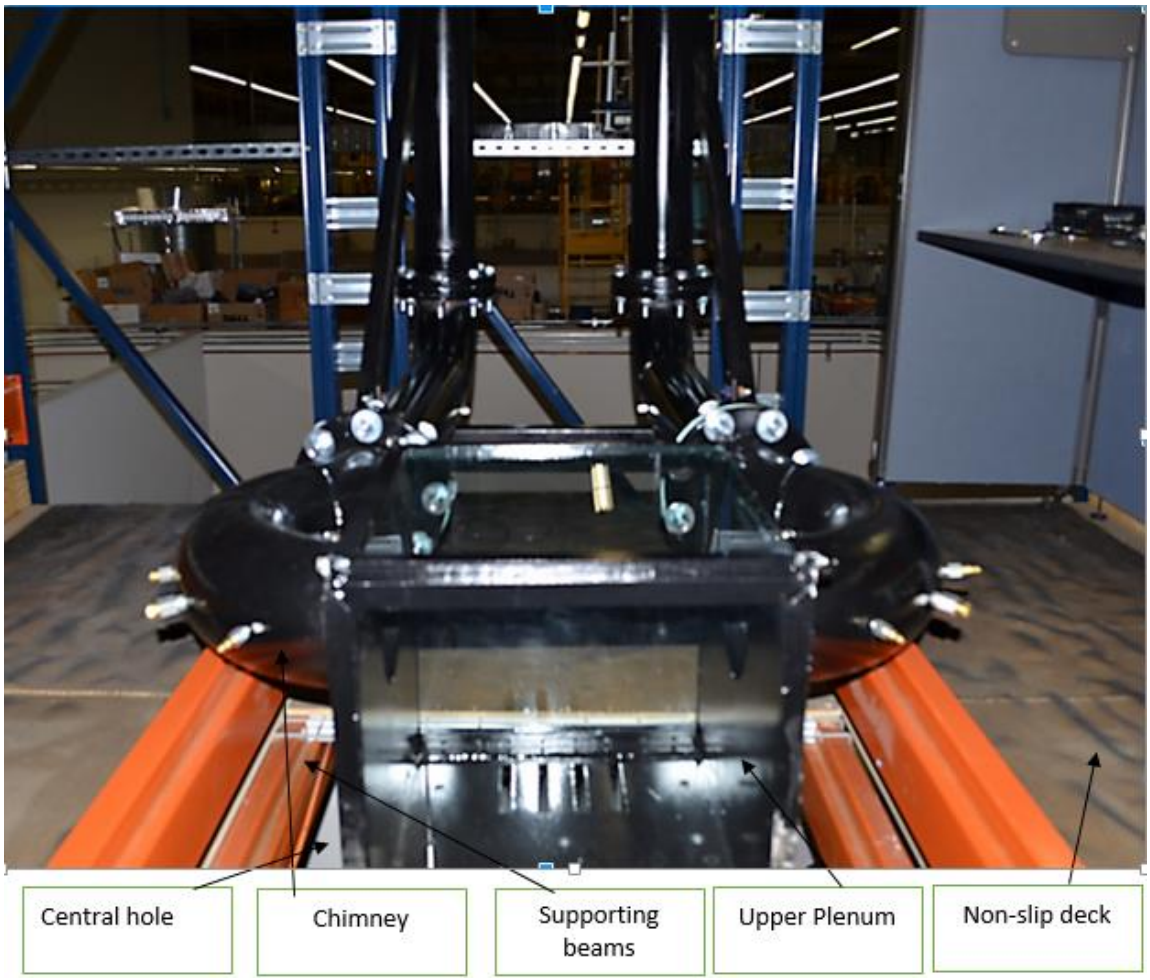

Figure 22. Picture of the second floor which include the central hole, chimney, upper plenum, non-slip deck.

3. INSTRUMENTATION

The RCCS test facility at TAMU was equipped with different kinds of instruments for two chief goals: obtaining boundary conditions similar to those found in natural convection facilities, and measuring, recording and monitoring specific parameters of interest such as air temperature and velocity. This section described the instrumentation used for the purposes of this project only. Other instrumentation including flow visualization devices were not discussed.

3.1 Blowers

The experimental facility for the RCCS had four blowers to control the air flow in each riser independently. The use of blowers enabled the personnel at TAMU to manipulate the flow boundary conditions at the inlet of the upper plenum as needed. Various velocities corresponding to different conditions of the VHTR can be easily obtained. There were two types of blowers that are being used: the GBM 2360 and the TE5005 models. The only reason for using two different types of blowers was that they were attained from another lab.

The GMB 2360 was manufactured by Thermo Andersen Instruments. The blower is basically a centrifugal fan used to control the flow of air. The blower forces air to flow into a pipe connected the outlet of the blower at one end and to a heater at the other end with a slight pressure increase. The blower has a number of rotating blades driven by an

electric motor. The rotating blades cause the air pressure to increase which drives the flow. The GBM 2360 blower operates with a voltage range of 0-110V; it requires a current of 8 Amps; and it is 50/60 Hz compatible.

The TE-5005 blower was manufactured by TISCH Environmental. Similarly, this blower is also a centrifugal fan with a number of rotating blades. This blower also operates with a current of 8 Amps and a voltage range of 0-110V. The blower is 50/60 Hz compatible with a maximum flow rate of 60 CFM. All blowers are enclosed by a customized stainless steel connection boxes to minimize leakage.

3.2 Variable Autotransformer

Variable autotransformers were used in the experiment to control the voltage of the blowers. The air velocity is directly proportional to the voltage of the blower. Thus, to reach the desired air velocity, the voltage was varied accordingly. The autotransformer used in the experiment was manufactured by Stacy Energy Products Company. The variable autotransformer used in this experiment has an input voltage of up to 120V and a maximum output voltage of 140V. It's 50 Hz compatible and has an amperage rate of 6 to 12 Amps. Figure 23 shows the variable autotransformer along with connection box and the blower inlet.

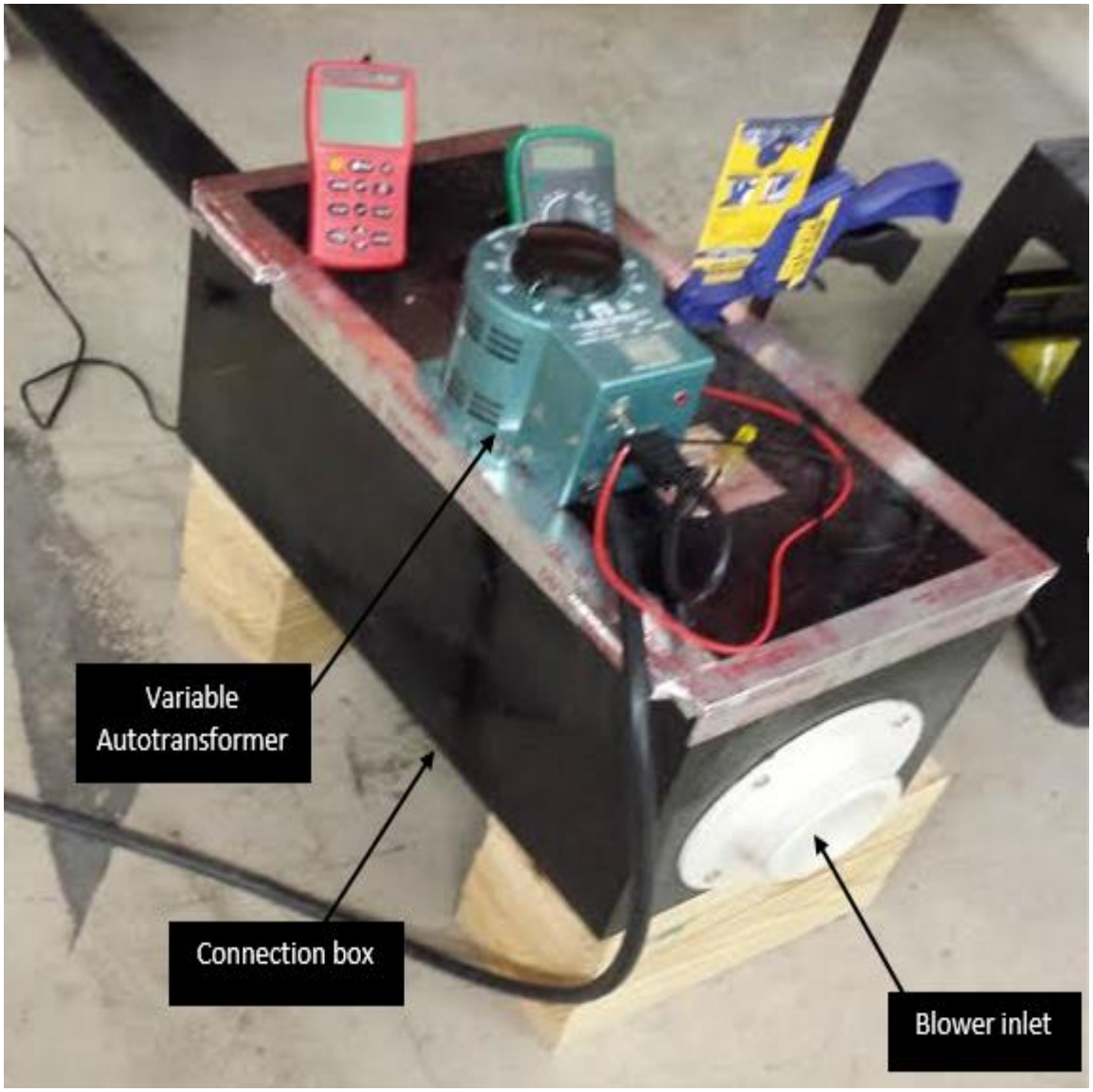

Figure 23. The connection box used for the blower with the blower inlet and variable autotransformer shown.

3.3 Flowmeter

The air flowmeter used in this experiment is the VelociCalc 9545-A. This probe type air velocity meter was manufactured by TSI and has a range of 0 to 30 m/s (TSI, Incorporated, 2014). The accuracy of this type of flowmeter is +/-3% or of the reading or +/- 0.015m/s, whichever is greater; the probe has a temperature range of -10 to 60^{o}C (TSI, Incorporated, 2014**)**. The measured air flow can be displayed as a velocity or volumetric flow rate. The probe has a length of 40" and has an articulated section with a length of 7.8" (TSI, Incorporated, 2014). The flowmeter was used to measure the velocity of the air at the inlet of the plenum to ensure the correctness of the boundary conditions. The flowmeter was shown in Fig. 24.

Figure 24. The flowmeter used to measure the air velocity (TSI, Incorporated, 2014).

3.4 Heaters

While the blowers are used to reach the required inlet velocity, the heaters are used to satisfy the inlet temperature requirement. The heater used in this experiment is a custom made flow torch heater manufactured by Farnam Custom Products. It's an in-line and open coil heater designed to accommodate high flow rates with minimal pressure drop. The heater is used to heat the air coming from the blower before it travels upwards through the risers. The heater has a maximum flow rate and pressure of 500SCFM and 3 PSIG, respectively. It operates at 10kW with a cycle rate setting, whereas the maximum outlet temperature is 482^{o}C. Four heaters were used to control the temperature in each riser independently. This gives TAMU's RCCS facility the freedom to choose the inlet temperature of the RCCS facility. Each thermocouple has its own separate controller. The controllers are equipped with two K-type thermocouples for temperature control. The controllers also have high limit circuit which shuts off the internal safety relay in case the high temperature limit is exceeded. Various alarms and status functions are integrated to monitor different aspects of the heaters. Figures 25 and 26 showed the one of the heaters and the controllers, respectively.

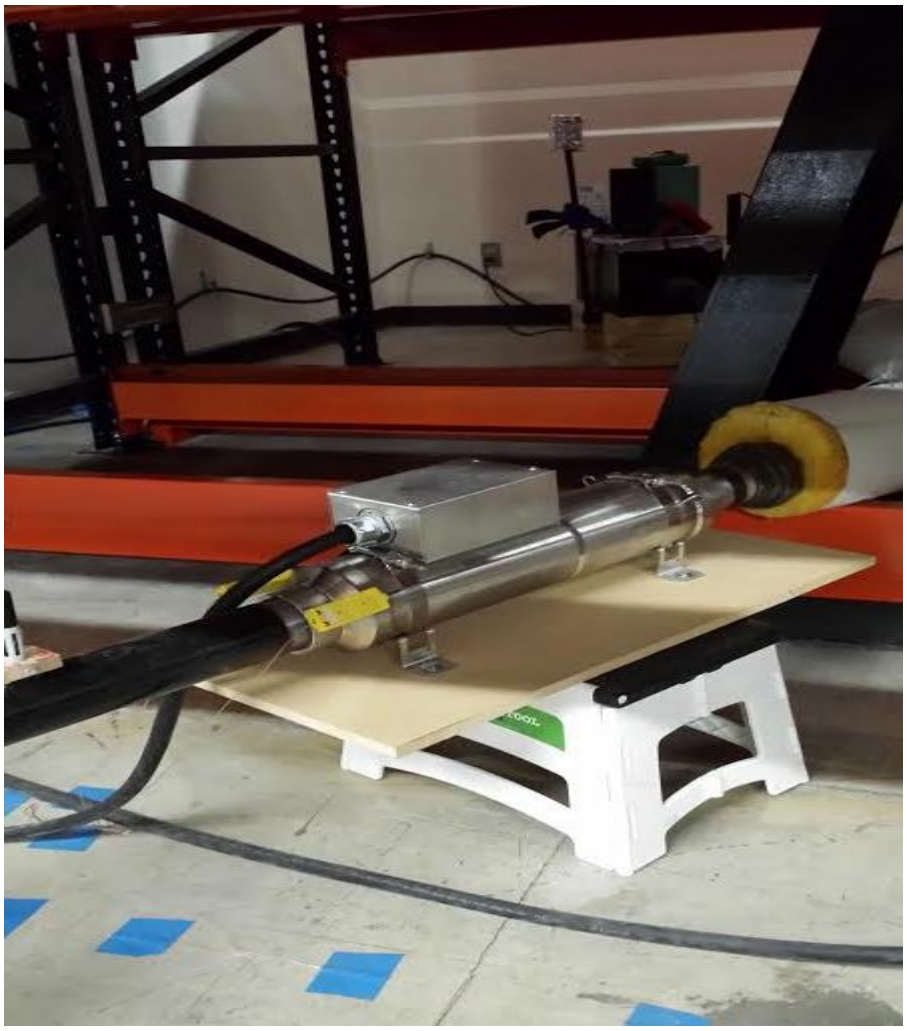

Figure 25. The in-line heater used to heat the air before it travels up through the risers.

Figure 26. The heater controllers used to control the heater settings.

3.5 Thermocouples

Thermocouple wire are made of two dissimilar materials which produce a measurable voltage as a result of heating or cooling. The voltage can then be converted to a temperature reading using a mathematical formula. Fine wire duplex insulated thermocouple wire purchased from OMEGA was used for the air-cooled RCCS test facility. The thermocouple wire used was made of copper and constantan with copper being the positive wire and constantan being the negative wire. The two materials were joined at the end using a fine wire welder to form the sensing end. The thermocouple wire used was type T with special limits of error (SLE). T-type SLE wires have a slightly better accuracy than the normal T-type thermocouple wires. This type of wire can measure any temperature between -267 and 260^{o}C. The associated error is the greater of 0.5^{o}C or 0.4%.

Type-T sheathed probe thermocouples, shown in Fig. 27, were also utilized for this project. The probe thermocouple has three types of junctions: grounded, ungrounded or exposed junction. The probe used in this experiment is an exposed T-type thermocouple, and is made from SLE material. In the exposed junction thermocouples, the sensing junction sticks out of the tip of the sheath exposing it to the surrounding environment. The sheath diameter is 0.062 and is made of 304 Stainless Steel. The probe has a length of 6”. The probe thermocouple has the same temperature range and error as the fine thermocouple wire.

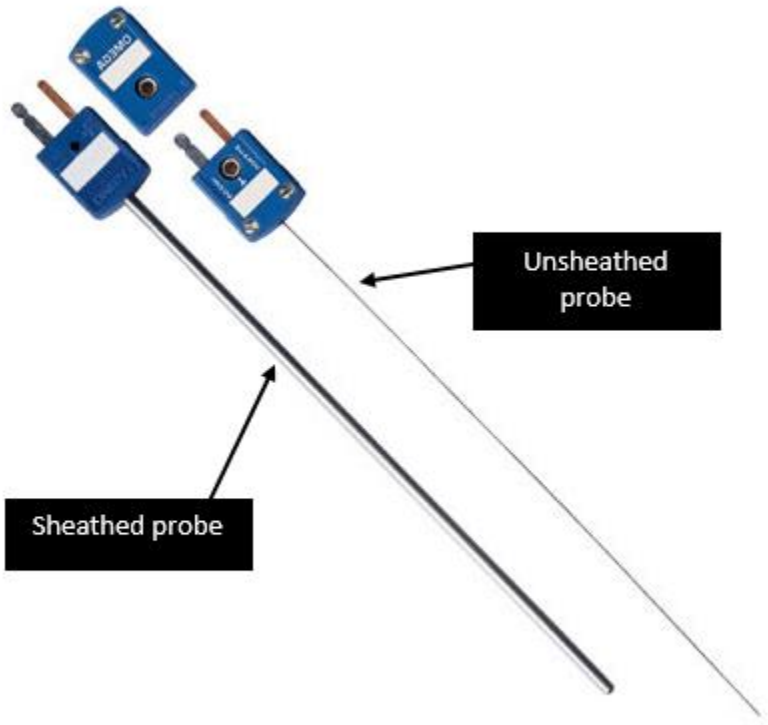

Figure 27. The t-type probe thermocouple used in the air RCCS facility (Omega, 2014).

The RCCS facility was fitted with a total of 96 thermocouples including probes and fine wire combined at various locations. Twelve probe thermocouples were installed on the four risers with three probes per each. The probes were installed at an elevation of 5, 40 and 77" measured from the bottom of the risers as shown in Fig.10 in the previous section. It was ensured that the tip of the probe, the sensing part, was positioned at the center of the riser to avoid contact with the walls which may affect the reading. The probes were inserted horizontally from the shorter side of the rectangular ducts. On the other hand, the upper plenum had the lion's share with 84 fine wire thermocouples

placed at various locations. As shown in Fig.11 from the previous section, holes were drilled at different locations in the upper plenum. Twelve metallic hollow rods were inserted into the upper plenum through these holes. Six rods were inserted from the bottom plate of the upper plenum, whereas the other six were inserted from the right side. Figure 28 below showed where the insertion rods were installed.

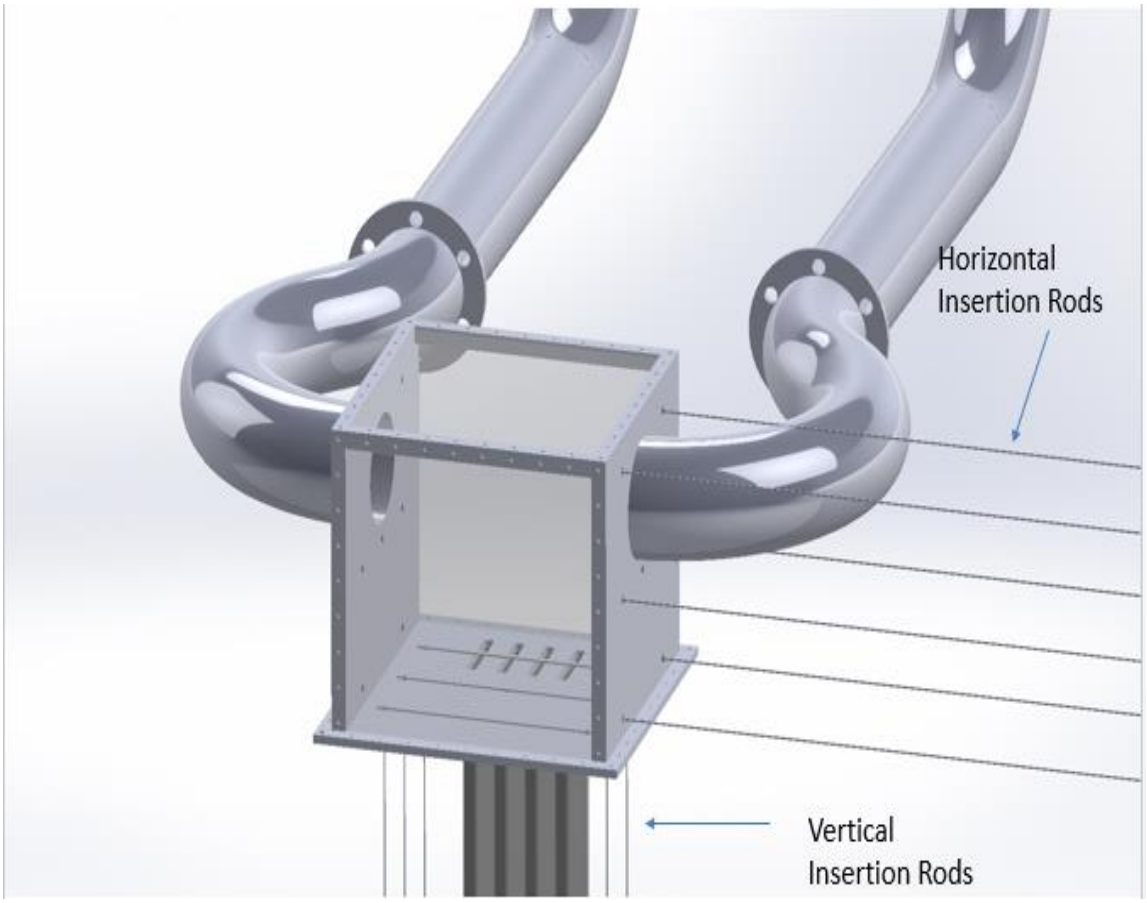

Figure 28. The upper plenum with the horizontal and vertical insertion rods.

Each pair of axially symmetric insertion rods was linked with a 15” cross-bar. The thermocouple wires were inserted into the upper plenum through the hollow

insertion rods. Seven thermocouples were inserted through each insertion rod. The wires were then evenly arranged across the cross bars with 1" spacing. JB weld was used to fix the thermocouples on the cross-bars. The cross-bars attached to the rods inserted from the bottom are referred to as the vertical rack, while the cross-bars inserted from the right side were called the horizontal rack. The thermocouples were named according to their respective position. The vertical rack had three cross-bars referred to as A, B, and C with A being the closest to the risers' outlets and C being the furthest. Similarly, the horizontal racks also had three cross bars referred to as A, B, and C with A being the cross-bar at the highest elevation and C being the lowest. The thermocouples were then given these codes VTX# and HTX#, where VT and HT stand for vertical and horizontal thermocouple, X for the letter corresponding to the cross-bar position, A, B or C, and # for the thermocouple number which can be from 1 to 14 as shown in Fig.29. Figure 30 showed the actual view of the upper plenum from the top.

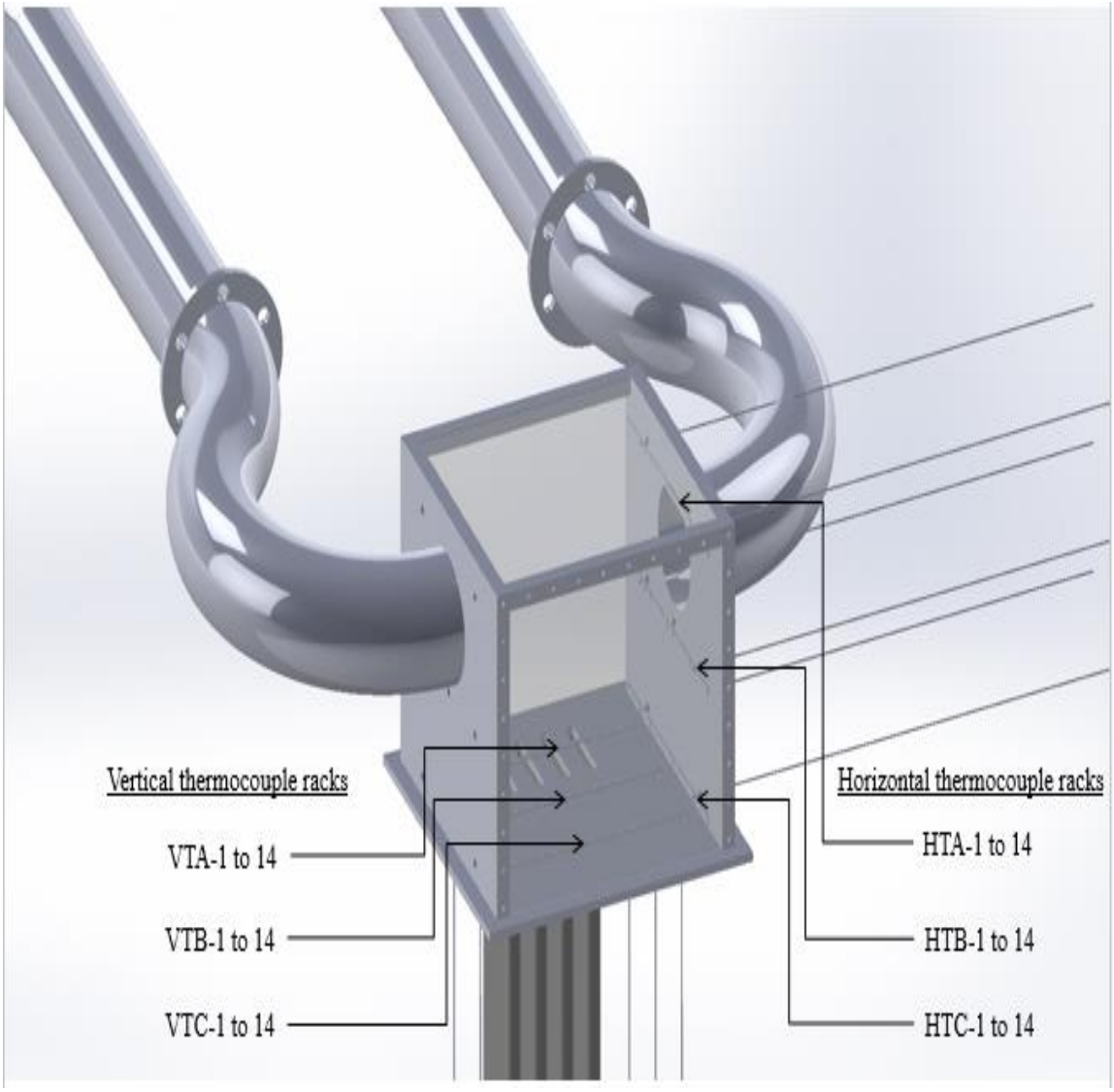

Figure 29. The upper plenum with the vertical and horizontal cross bars. The picture depicts how the thermocouples were placed on the racks.

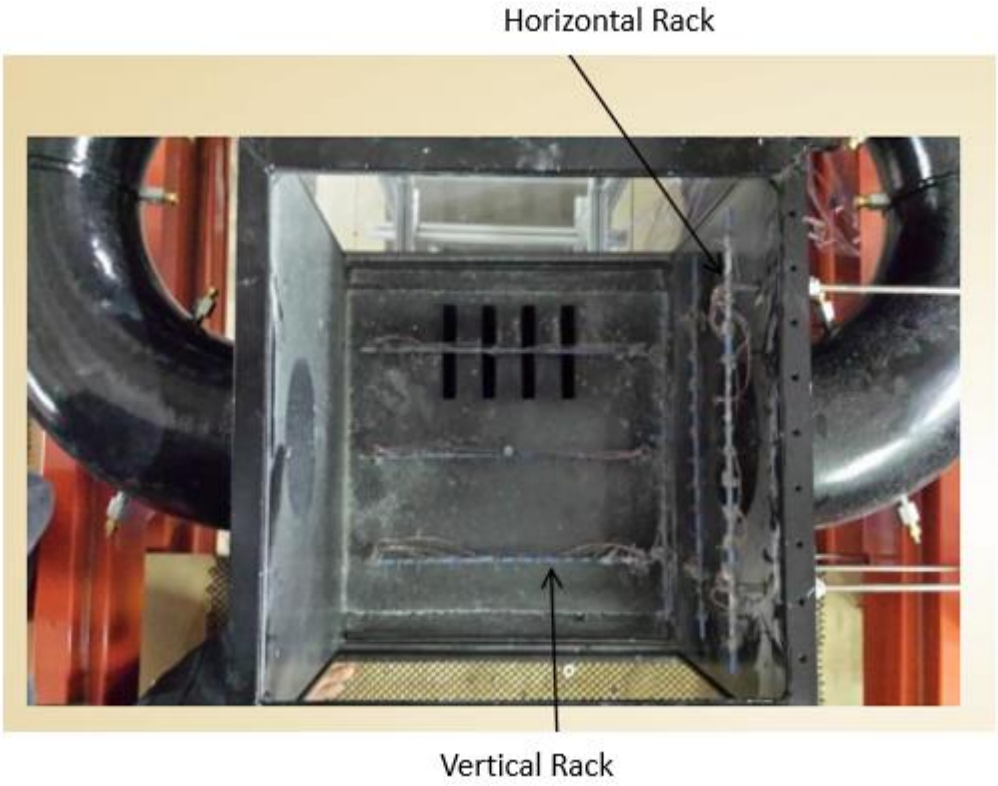

Figure 30. The top view of the upper plenum with horizontal and vertical racks.

The horizontal racks were designed to move in the x direction to form three horizontal planes as depicted in Fig.31, whereas the vertical racks moved in the z direction to form three vertical planes as illustrated in Fig.32. The movement of the racks was controlled manually using vertical and horizontal insertion systems constructed out of 80/20 frames. The insertion systems were fitted with plastic scales calibrated to indicate the thermocouples position inside the upper plenum.

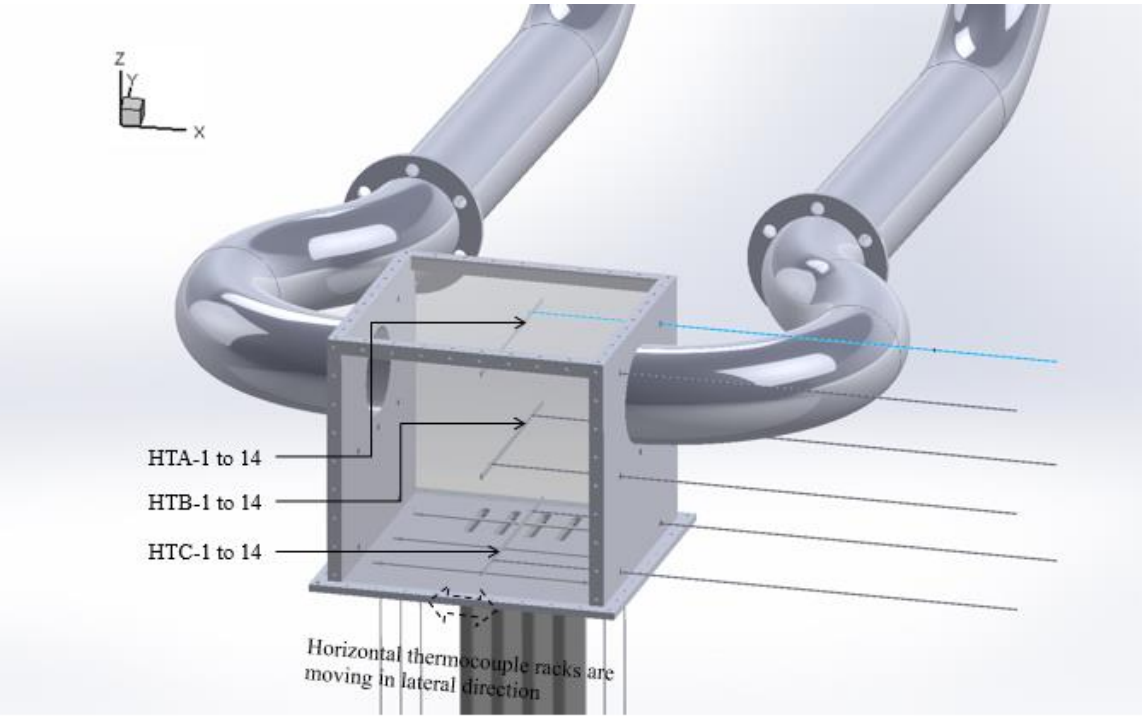

Figure 31. The horizontal cross-bars being inserted into the middle of the upper plenum. The picture illustrates the movement direction of the horizontal racks.

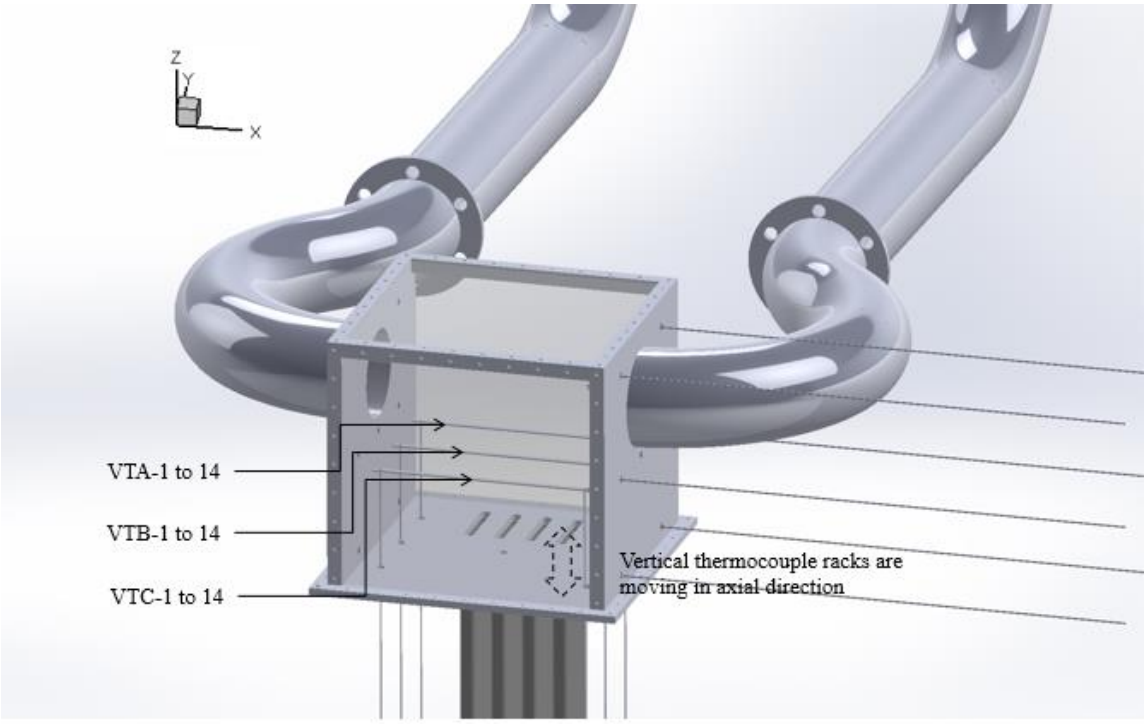

Figure 32.The vertical cross-bars being inserted into the middle of the upper plenum. The picture illustrates the movement direction of the verical racks.

All of the thermocouples were calibrated using Fluke II. Fluke 52 II is a fast response dual input thermometer with an accuracy of +/- 0.3^{o}C. It was manufactured by Fluke and can be used for different thermocouple types including K, J, T and E. The fluke was also used to monitor the ambient temperature during experiments. The fluke was shown in Fig.33.

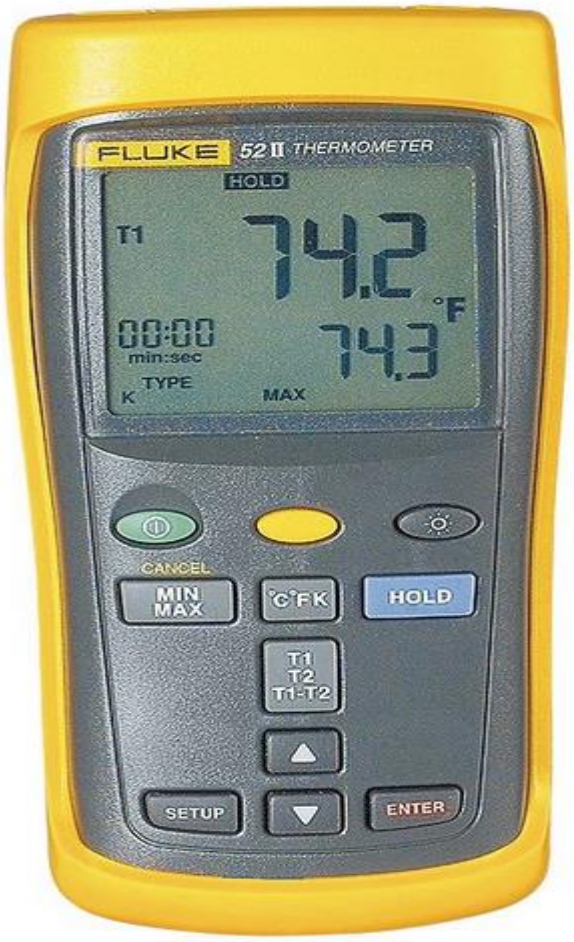

Figure 33. The fluke used to monitor the ambient temperature and thermocouple calibration (Fluke, 1999).

The thermocouple junctions were made using a wire welder by Omega depicted in Fig.34. The junction relates the electric potential to the temperature which enables the measurement of temperature. The wire welder used can weld wires up to 1.1 mm diameter. The energy output range was between 0 and 60 Joules.

Figure 34. The fine wire welder used to form the thermocouple junctions.

3.6 Data Acquisition System

The NI PIXe 1078 was a 9 slot modular instrumentation platform used for taking measurements, building automated systems, and electronic control. It was the data acquisition system (DAQ) used to record the measurements for the RCCs facility. It consists of three major components: chassis, controller and peripheral modules. The chassis is the heart of the system which supplies power, heat removal, and the data transfer buses. The NI PIXe 1078 has a portable, high performance, and low noise

chassis. The chassis contains a controller slot on the left side. The NI PIXe 1078 controller slot enables control via a laptop, desktop, or a workstation. A workstation was used for control in the RCCS experimental facility. The modules are instruments installed in the chassis for data acquisition, digital input/output, or synchronization. The modules used in the experimental facility were data acquisition type that receive and process signals before being sent the controller. In the RCCS case, thermocouples were attached to the modules; the modules received signals from the thermocouples in the form of electric current and convert them into temperatures; the data was then sent to the chassis and can be acquired by the controller. Figure 35 showed the DAQ used in the RCCS facility.

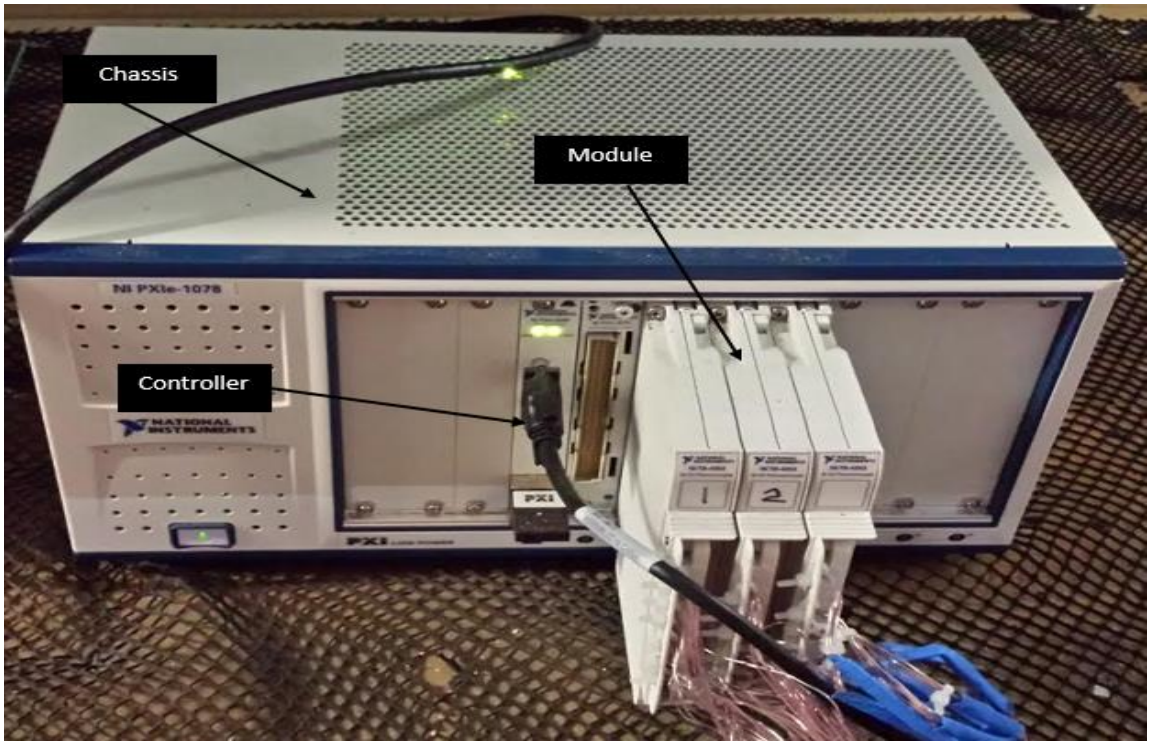

Figure 35. The data acquisition system with the three main components shown.

3.7 Thermocouple Connector and Mounting Bezel Strip

Miniature thermocouple connectors were used in this experiment. The connectors are designed to connect the thermocouples to the temperature controller, which in this case was the NI PIXe 1078. The thermocouple connectors consisted of a male plug with two flat poles and a matching female connector with two prong thermocouple jack. The thermocouple wires were connected to the male connector, while the DAQ was linked to the female connector. Each connector had a write-on window so that each couple can be distinguished. The thermocouple connectors were manufactured by OMEGA.

The bezel strip was essentially a flat panel with rectangular cutouts to enable insertion of the thermocouple connectors. The bezel strip used for the RCCS facility was purchased from OMEGA and has 96 positions. The thermocouples were mounted on the bezel strip to ease identification when one needed to be repaired. It also allowed the wires to be arranged in an orderly manner. The bezel strip was shown in Fig.36.

Figure 36. The bezel strip with the thermocouple connectors installed.

4. EXPERIMENTAL SETUP AND PROCEDURE

This section described the required preparation for the RCCS test facility in order to measure the temperature profile in the upper plenum. The spatial temperature profile was measured for four different cases listed in table 3 below. A number of experiments were conducted to obtain the required boundary conditions. The outlet velocities of the risers were obtained by running an experiment and plotting the velocity versus voltage curve. The heater settings were adjusted to obtain the required temperature by empirical means. A number of experiments were also carried out to determine the optimal increment for taking temperature measurement. This section also illustrates how the experiment can be repeated step by step.

Table 3. A list of the cases with their corresponding conditions

	Case 1	Case 2	Case 3	Case 4
Velocity (m/s)	5	5	2.25	2.25
Upper Plenum Inlet Temperature (C^o)	120	120	120	120
Risers in Operation	R1, R2, R3 and R4	R4 only	R1, R2, R3 and R4	R4 only
Rack Movement Interval	0.5”	0.5”	0.5”	0.5”

4.1 Velocity Calibration

As mentioned in the previous section, a variable autotransformer was used to control the voltage of the blower. The air flow was directly proportional to the voltage of the blower. Since TAMU's air-cooled RCCS experimental facility was projected to operate with different velocities, an experiment was ran to find the velocity as a function of voltage for each riser. The voltage was varied from 10 to 40V at a 2.5V interval. The velocity was measured at the outlet of the risers using VelociCal 9545-A discussed earlier. The probe was placed at the center of the riser. Figure 37, 38, 39 and 40 below showed the velocity as a function of the voltage for risers 1 through 4.

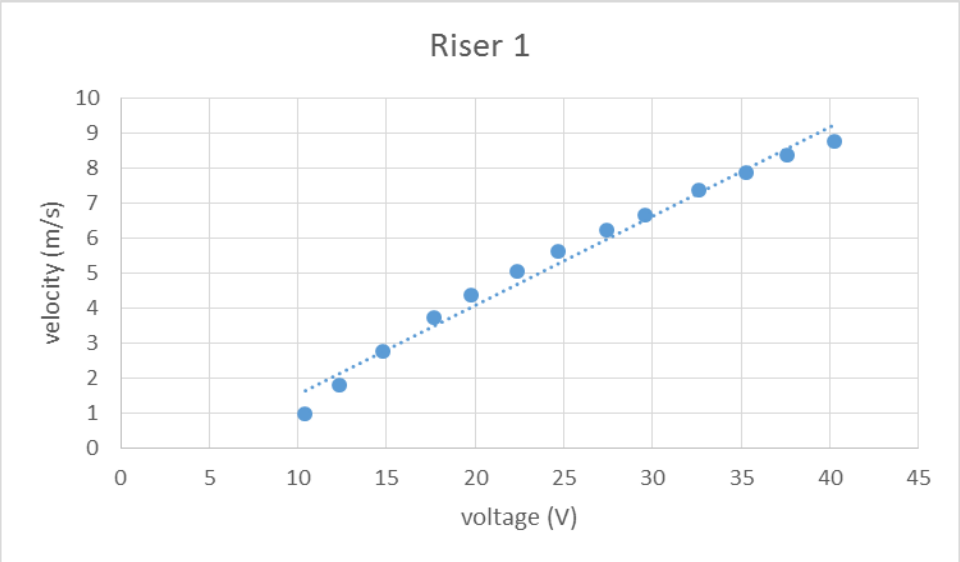

Figure 37. Riser 1 velocity-voltage curve.

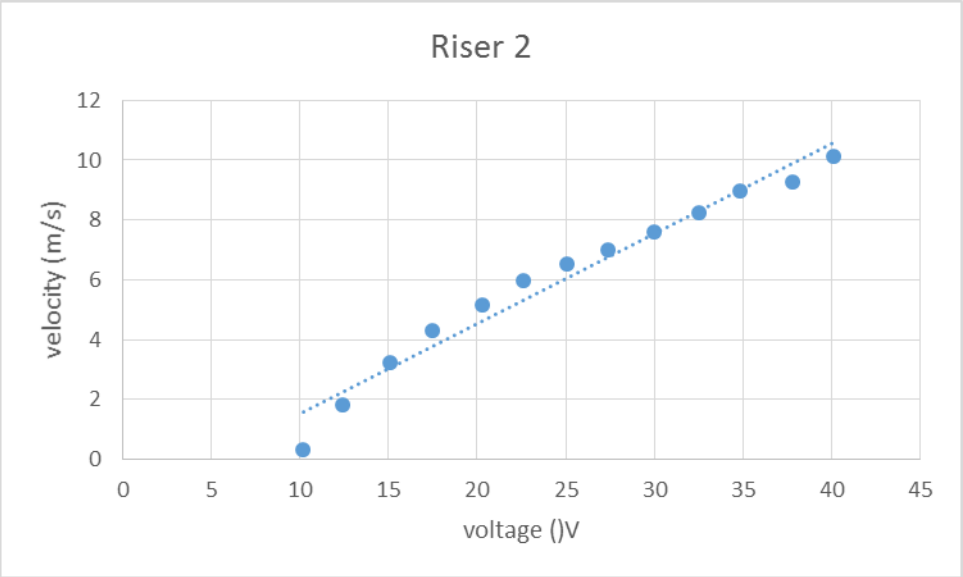

Figure 38. Riser 2 velocity-voltage curve.

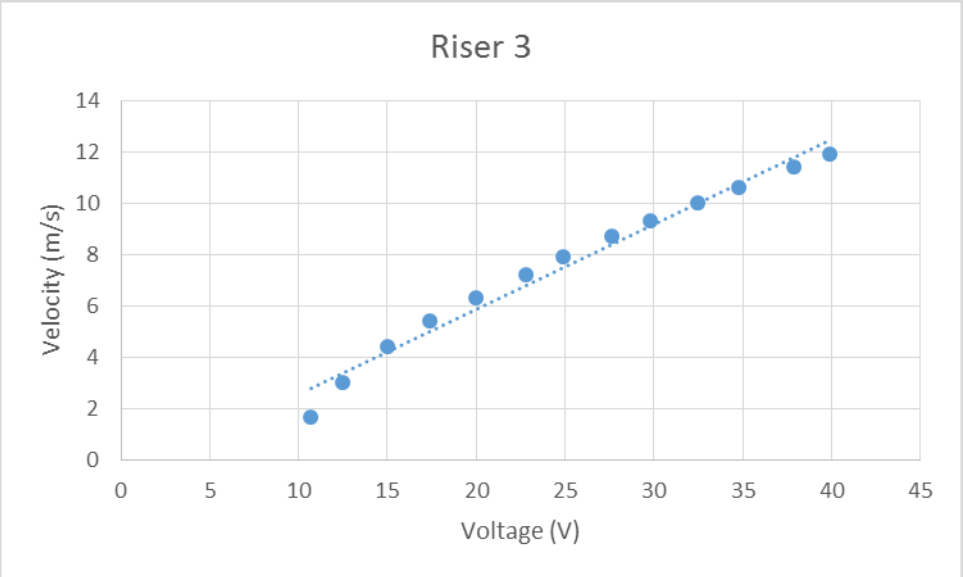

Figure 39. Riser 3 velocity-voltage curve.

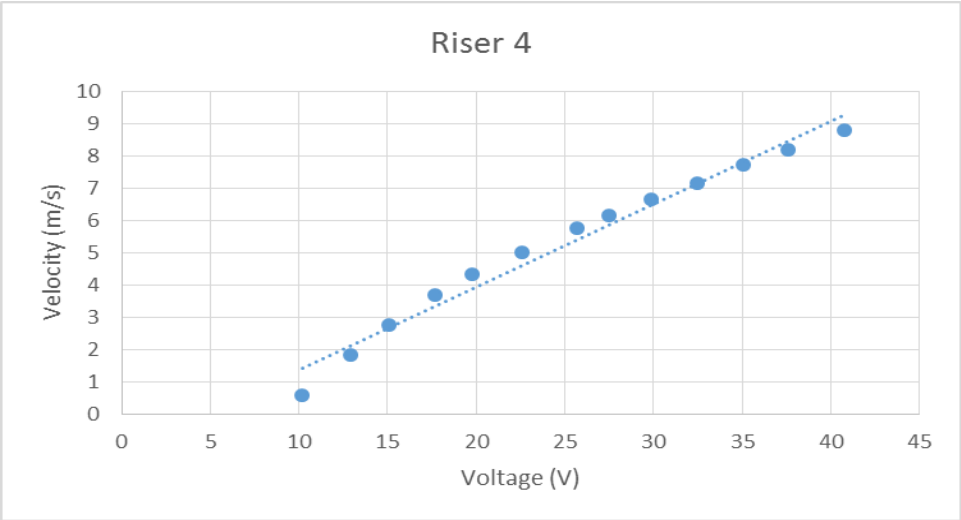

Figure 40. Riser 4 velocity-voltage curve.

It was important to note the curves were actually close to being linear if the first two points were omitted. The blowers blades did not start to rotate until the voltage was close to 10V. Between 10 and 15V the blowers started to overcome the rotational inertia, whereas after 15V the blades seemed to rotate without any resistance. The above curves were used as a basis to determine voltage required to obtain a certain velocity for all of the experiments.

4.2 Heater Settings

The heater settings were adjusted to obtain an outlet riser temperature of 120^{o}C by empirical means. The risers were set at a certain velocity and the heater settings were modified so that the required outlet temperature was obtained. The settings for each riser were not identical. This was possibly due to uneven heat loss in the risers, uneven

ambient temperature distribution, and the way the heaters operated. Table 4 below listed the required heater settings to get an outlet temperature of 120^{o}C.

Table 4. The heater settings required to obtain a riser outlet temperature of 120^{o}C.

	Velocity=2.5 (m/s)				Velocity=2.5 (m/s)			
Setting	Riser1	Riser2	Riser3	Riser4	Riser1	Riser2	Riser3	Riser4
PS	168	184	160	200	220	190	215	226
Hi	400	400	400	400	400	400	400	400
Lo	38	38	38	38	38	38	38	38
dL	28	28	28	28	28	28	28	28
AC	00	00	00	00	00	00	00	00
Cr	01	01	01	01	01	01	01	01
Pb	70	70	70	70	70	70	110	70
Re	115	115	115	115	115	115	199	115
rA	05	05	05	05	05	05	02	05
CA	00	00	00	00	00	00	00	00
At	Off	Off	Off	Off	Off	Off	Off	Off
Fb	02	02	02	02	02	02	02	02
Fp	10.0	10.0	10.0	10.0	10.0	10.0	10.0	10.0
tu	C	C	C	C	C	C	C	C
Hd	00	00	00	00	00	00	00	00

4.3 Riser Velocity Profile

Even though the velocity-voltage curve was used to determine the variable autotransformer settings, the velocity profile across each riser was measured before the start of any experiment. The velocity-voltage curves provided the velocity at the middle of the risers only. Each riser was expected to have a profile, therefore, the velocity distribution was measured and the average value was used for each experiment. In other words, the average value of each riser had to be approximately 5 m/s for cases 1 and 2, and 2.25 m/s for cases 3 and 4. The velocity profile was measured using the VelociCal by placing the probe at the points shown in Fig.41. A sample velocity profile also shown in Fig.42.

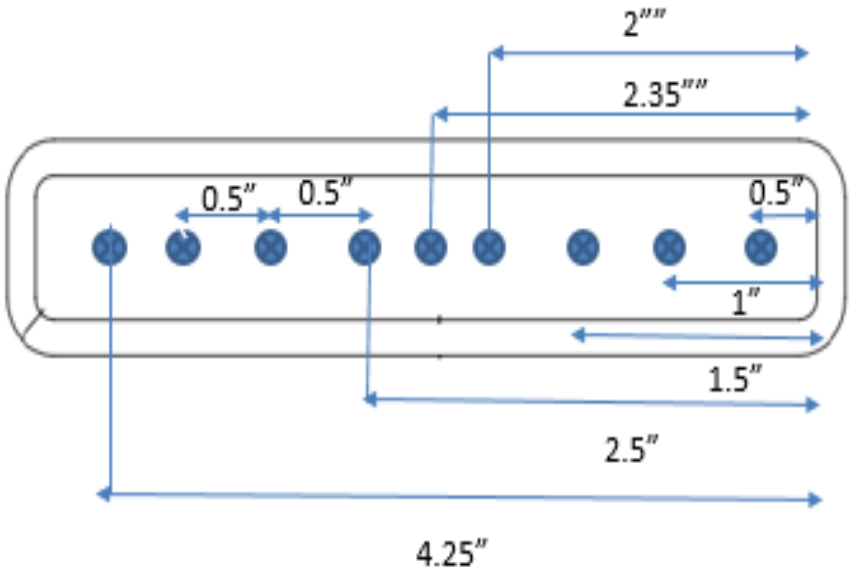

Figure 41. The riser cross section showing the points where velocity measurements were taken.

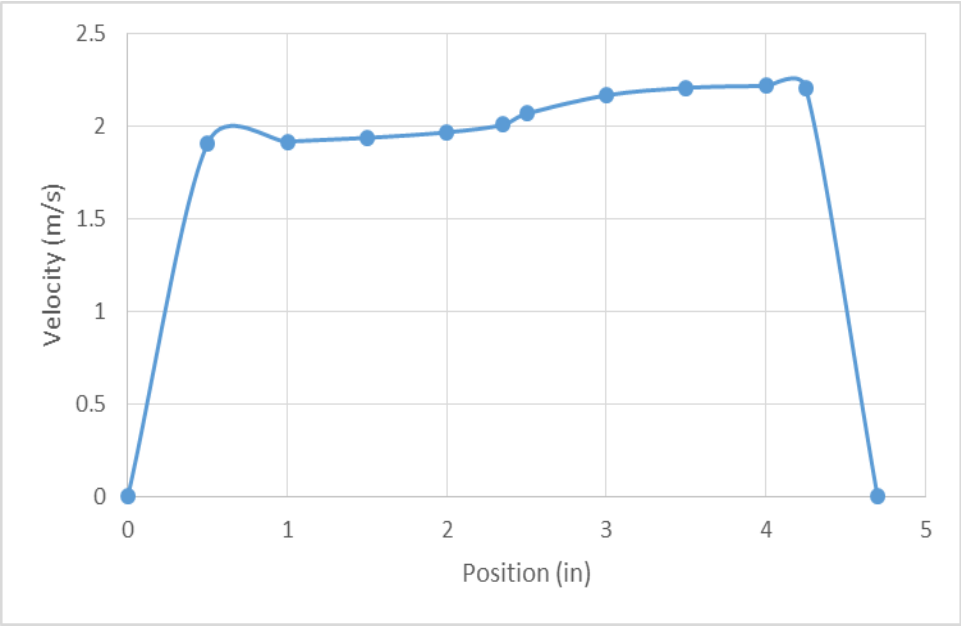

Figure 42. Sample measured velocity profile.

4.4 Determination of the Optimal Rack Movement Increment

In order to determine the optimal interval at which to move the racks, an experiment was carried out with a number of different increments. An experiment with a riser outlet temperature and velocity of 120^{o}C, and 5 m/s, respectively, was conducted. All four risers were in operation and increments of 0.5, 1, 2, 3, and 4" were used for the horizontal and vertical racks. The experiment was performed as per the procedure outlined in 4.5. The results of the experiment were post-processed using a Matlab script and Tecplot. Based on the results of the experiment described in the results section, a

0.5” was determined to be the optimal increment. Accordingly, all of the other experiments were ran at an interval of 0.5”.

4.5 Temperature Profile Measurement

The temperature distribution in the upper plenum was measured for the four different cases described previously. The procedure for each case was very similar with a few required modification for each experiment. Below is a chronological list of the necessary actions needed to measure the temperature distribution:

1. Start by writing a short summary of the intended experiment in the log book
2. Measure the ambient temperature at two different locations in the second floor using Fluke 52 II
3. Remove the glass from the front, top, and back sides of the upper plenum
4. Visually inspect the thermocouples, and racks in the upper plenum for any broken junctions or welds
5. Physically inspect the probes to ensure the intactness of the sensing end and proper positioning of the thermocouple
6. Start NI Signal Express and make sure that all the thermocouples are connected and functional
7. Start the blowers and set the voltage as per the velocity-voltage curve
8. Raise the vertical rack to allow velocity measurements to be taken

9. Measure the velocity profile across each riser using VelociCacl as described in section 4.3
10. Calculate the average velocity and write it down in the log book. If the average velocity is unsatisfactory, repeat 7 and 8 until a satisfactory result is obtained
11. Install the glass windows and insulate the upper plenum
12. Lower the vertical racks to their initial position
13. Set NI Signal Express on the recording mode so that it's running continuously and taking one temperature measurement per second. Add displays to allow interactive monitoring of the temperature inside the upper plenum during startup
14. Start the heaters as per the settings described in 4.2
15. Monitor the temperature using the displays from NI signal express
16. Record the ambient temperature every hour as described in step 2
17. Wait until the riser outlet temperatures measured using the probes positioned at the upper part of the risers converge to a temperature of 120^{o}C. If any of the risers outlet temperatures converge to a different value, change the PS settings on the heater and repeat 13,14 and 15
18. Wait until you're certain that there are no significant fluctuations in the measured temperatures and steady state is confirmed
19. Change the NI Signal Express Settings so that it can record the temperatures of the vertical racks, inlet and outlet of each chimney and outlet of the risers thermocouples using 900 samples and 90Hz frequency for one iteration when the run button is clicked

20. Position the vertical racks at 1” above the bottom plate and take a measurement using signal express. Keep moving the racks up at an interval of 0.5” while taking a measurement for each position. Make sure that you visually inspect the thermocouples at least three times while the measurement is being recorded. Keep moving the racks up until they are at an elevation of 17” inside the upper plenum
21. Withdraw the vertical racks to a position of 0.75” above the bottom plate of the upper plenum
22. Change the NI Signal Express Settings so that it can record the temperatures of the horizontal racks, inlet and outlet of each chimney and outlet of the risers thermocouples using 900 samples and 90Hz frequency for one iteration when the run button is clicked
23. Position the racks at 1” away from the right side of the upper plenum and take a measurement using signal express. Keep moving the racks towards the left side at a 0.5” interval while taking a measurement at each position. Make sure that you visually inspect the thermocouples at least three times while the measurement is being recorded. Keep moving the racks and taking measurements until they are 16.5” away from the right side
24. Withdraw the horizontal rack until they are 0.75” away from the right side
25. Turn off the heater while keeping the blowers on to cool the RCCS structure and the heaters
26. Remove the insulation from the upper plenum
27. Wait until the glass windows are cool and safe to touch

28. Remove the glass windows

29. Raise the vertical racks until they are 5” from the bottom plate

30. Measure the temperature profile and record it in the log book

31. Withdraw the vertical racks to their initial position

32. Turn off the blowers

5. RESULTS AND OBSERVATIONS

This section presented the results and observations from the experimental data recorded using the NI PIXe 1078 chassis. The raw data from the DAQ was refined using a Matlab script and visualized using Tecplot. A brief overview of the results obtained from the startup data was presented first, followed by the results from the initial experiments conducted for the selection of the spacing between each temperature measurement and the interpolation method. Then the results and observations from the four cases described earlier were shown and discussed. The section was concluded with the uncertainty of the experimental measurements. It was important to note that in this section the inlet temperature for all cases was 120 +/- 2^{o}C. However, temperature normalization was performed with respect to the maximum temperature recorded by the thermocouples inside the upper plenum which was not necessarily equal to 120^{o}C as the closest thermocouple rack was about an inch away from the outlet of the risers at its initial position.

5.1 Startup and Steady State

The startup was monitored and recorded for the purposes of observing any flow instabilities in the system and determining steady-state conditions. Steady-state was mainly determined based on the stability of the thermocouple readings at the risers and the upper plenum. Figure 43 below shows the startup temperature curve for the risers' outlet which is the upper plenum inlet for case 3. It can be concluded from the figure that it took that facility about five hours to reach steady state. It was important to note that at about 4 hours, the heater setting for riser 1 were adjusted to achieve an inlet temperature of 120^{o}C which explains the bump in the curve around that time.

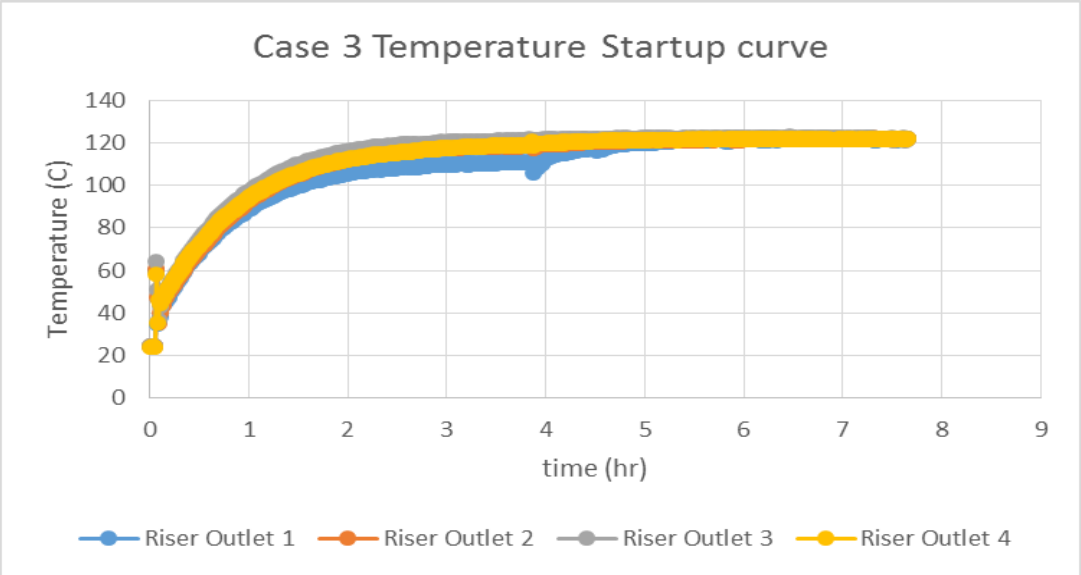

Figure 43. Case 3 riser inlet temperatures start-up curve. The heater controller settings for Riser 1 was reset to a new value in between 3 to 4 hours after start-up in order to reach the desired temperature.

The startup curve for case 4, depicted in Fig.44, was more interesting to watch. Even though risers 1 through 3 were not in operation, their outlet temperatures rose to a noticeable level. It was observed that the degree of temperature increase in risers 1 through 3 was dependent on their proximity from riser 4 which is in operation. Riser 3 which was the closest had the highest temperature increase with a final steady-state temperature of about 60^{o}C. On the other hand, riser 1 was least affected with an outlet temperature of 35^{o}C. Heat transfer through radiation was not expected due to the fact that there was insulation between the risers. Heat transfer due to conduction was also not expected to be significant due to the presence of insulation. This indicated that there might be air flowing through the outlet of risers 1-3.

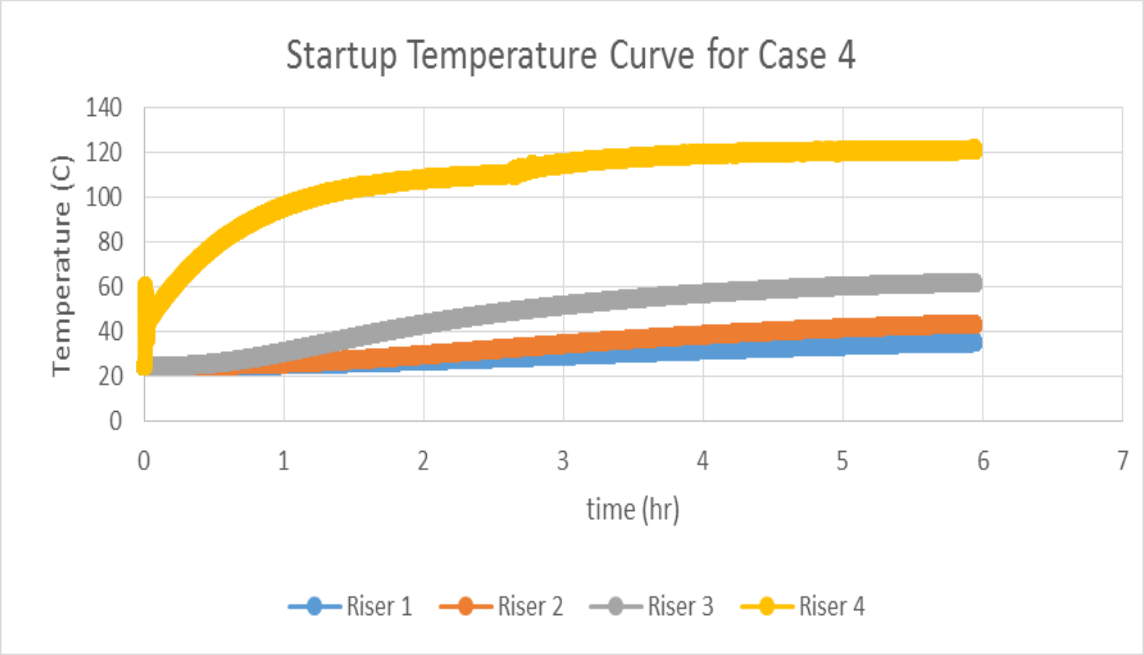

Figure 44. Case 4 riser inlet temperatures start-up curve. The heater controller settings for riser 4 was reset to a new value in between 2 to 3 hours after start-up in order to reach the desired temperature.

The chimney's start up temperature curve for case 3 grabbed most of the attention due to the occurrence of a perplexing phenomenon depicted in Fig.45. The temperature of the inlets and outlets were rising symmetrically until the two hour mark when the temperature of the right chimney dropped steeply. This implied that there was an uneven flow distribution with the flow preferring to exit through the left chimney. A similar phenomenon happened at ANL's test facility as shown in Fig.46. ANL experimental facility had a bypass in between the two chimneys. The phenomenon was mitigated by dampening the bypass valve which transported some of flow from the north to the south chimney until the flow balance was restoews. ANL's facility is a natural convection facility where the chimneys are open to the outside environment. They strongly believe that this was a flow reversal due to the wind changing speed or direction. However, this was not really applicable to TAMU's facility since the experiments were performed under a controlled environment. Interestingly, this phenomenon wasn't a coincidence as the same event took place again when the experiment was repeated as shown in Fig.47. The phenomenon will be discussed more later in the section.

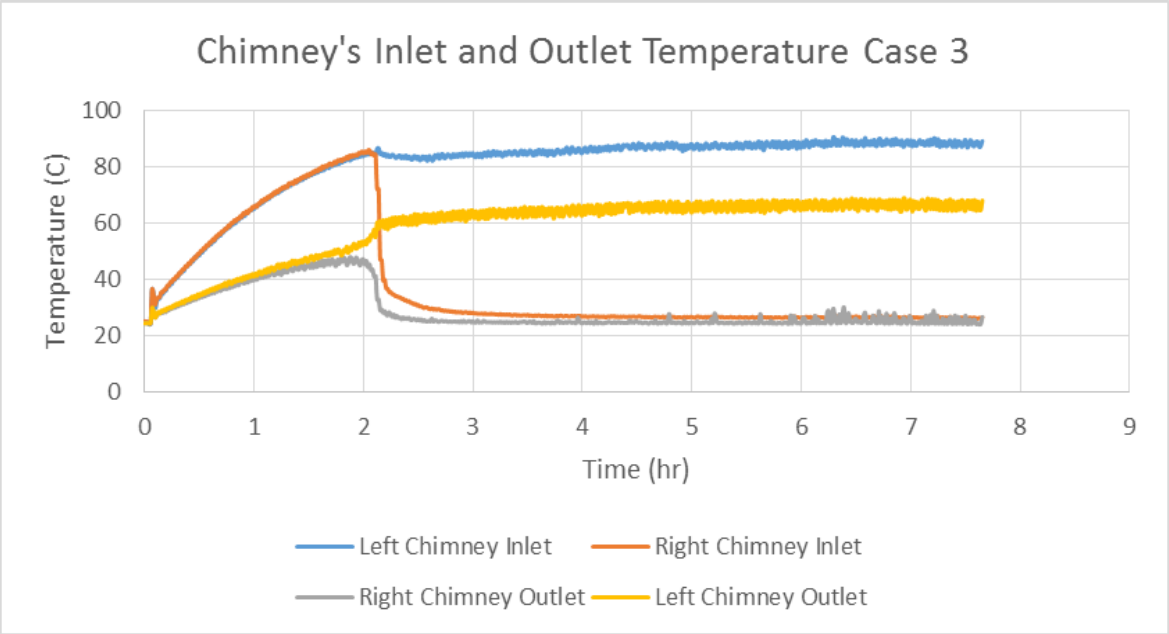

Figure 45.Perplexing phenomenon that occurred during the start-up of case 3. (Right) Uneven temperature distribution at the outlet of left and right chimneys; (left) Chimney in case 3.

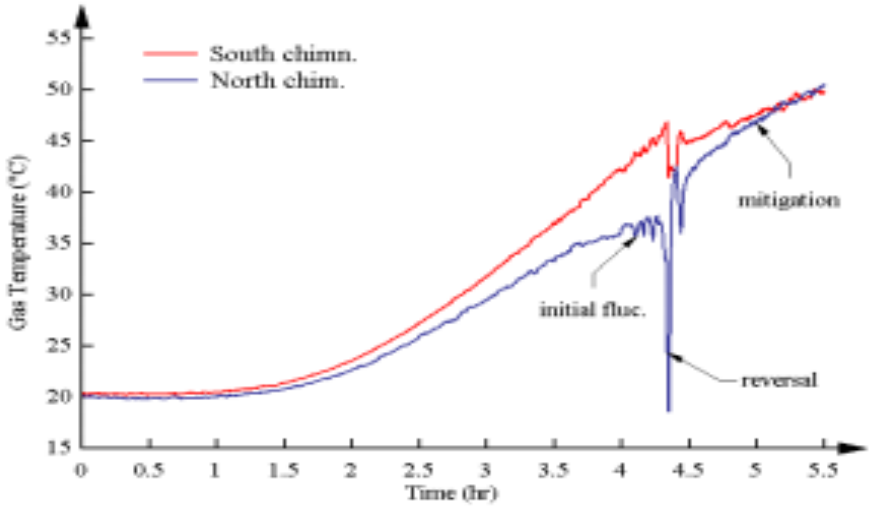

Figure 46. Similar phenomenon attributed to flow reversal in ANL RCCS facility. The phenomenon was mitigated by dampening the south chimney valve (Lisowski, et al, 2014).

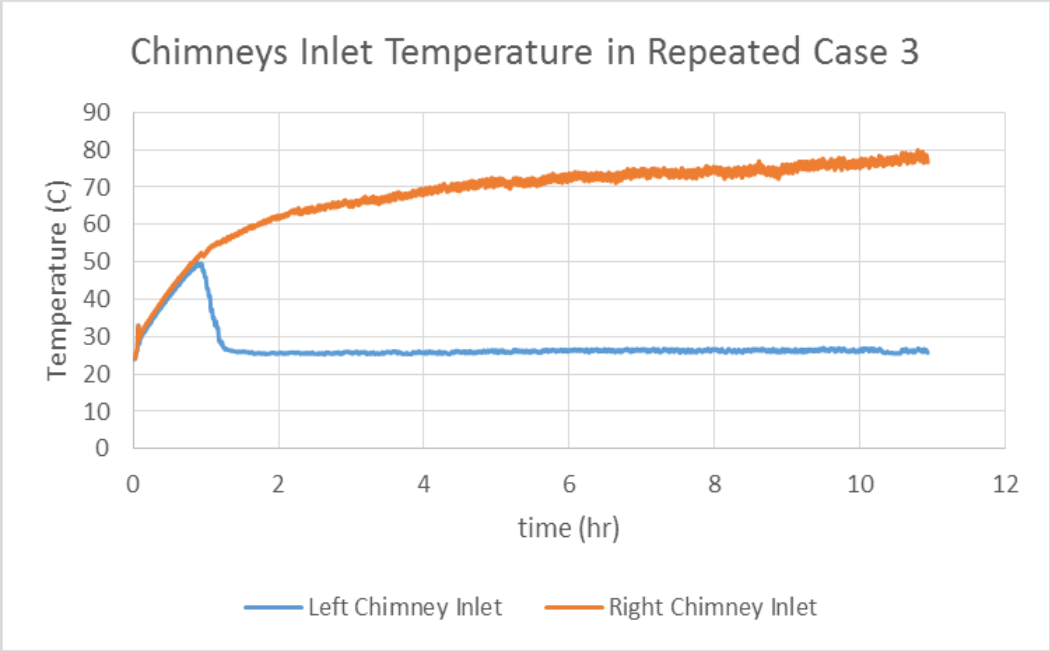

Figure 47. The same perplexing phenomenon occurring in a different experiment under the same conditions as case 3. The experiment wasn't completed due to some broken thermocouple junctions.

5.2 Rack Movement Interval and Interpolation Method

An experiment was performed to determine the rack movement interval. As discussed earlier, the thermocouple racks are moved at a given interval while taking measurements until 6 planes of temperature measurements, corresponding to the number of racks, are formed. The resulting six planes were depicted in Fig.48 and 49. The planes are named after the thermocouple racks. The three vertical planes were VTA, VTB and VTC, whereas the three horizontal planes were HTA, HTB and HTC as shown below. It's important to note that these planes did not cover the whole plane of the upper plenum. The planes extended as far as the distance between each parallel insertion rods.

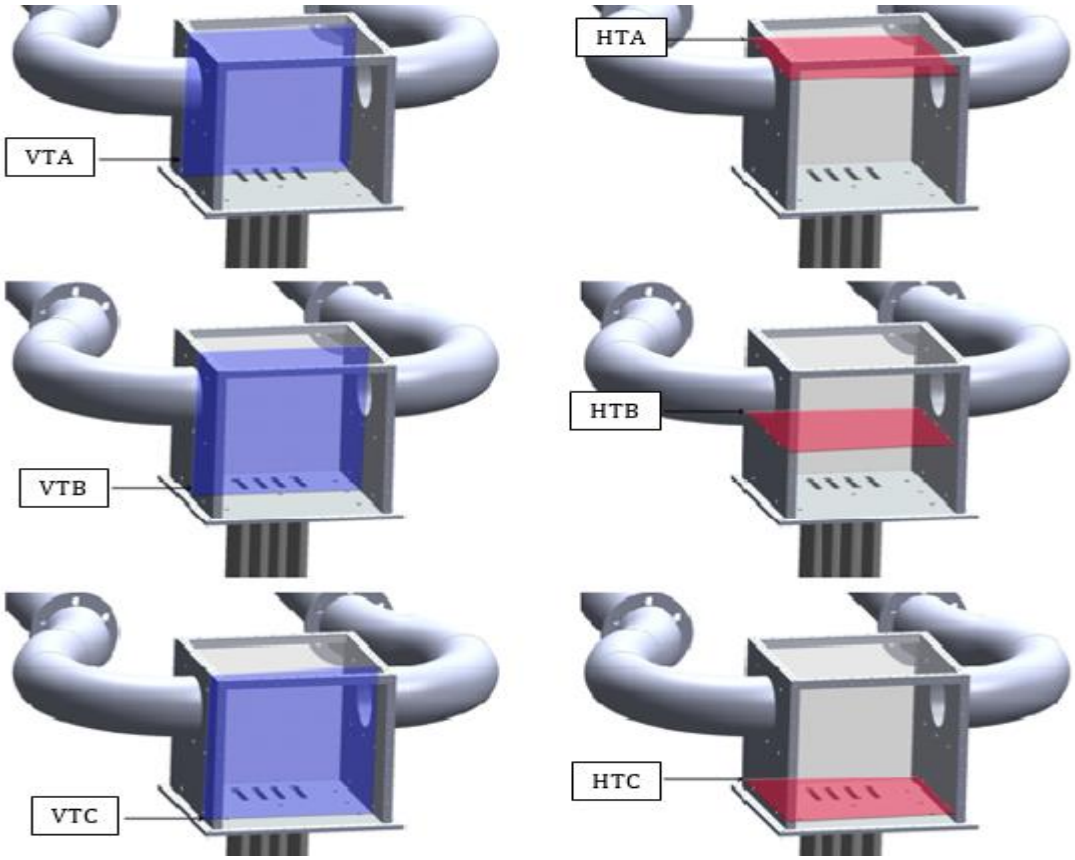

Figure 48. The planes formed by the movement of the vertical and horizontal racks. The vertical planes are on the left while the horizontal planes are on the right.

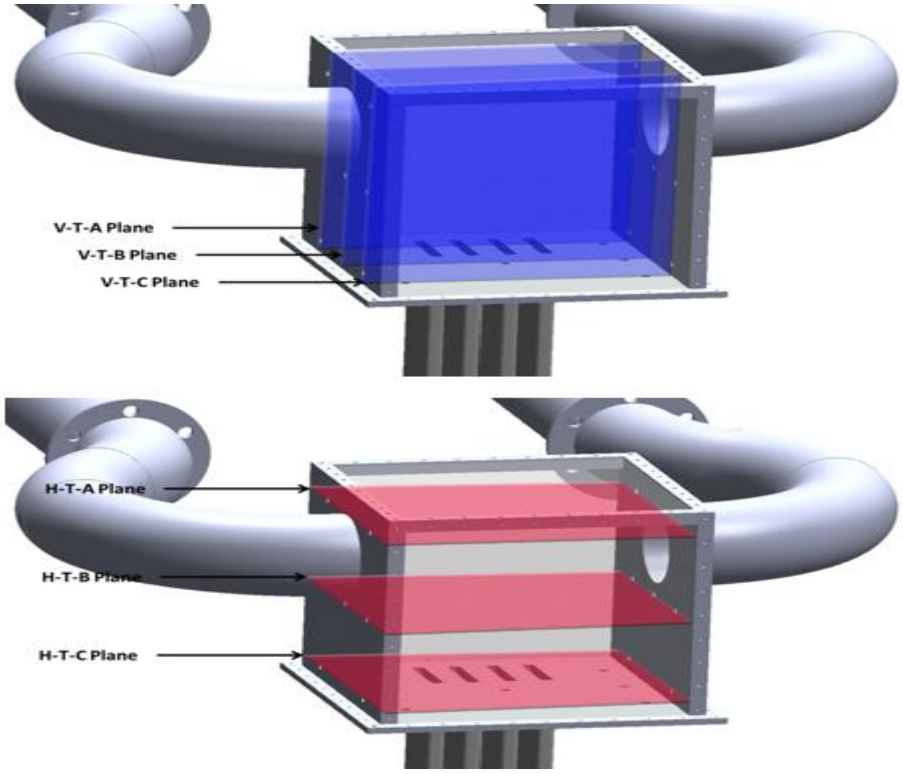

Figure 49. Vertical and horizontal planes superposed. Vertical planes at the top and horizontal planes underneath.

For this experiment, all four risers were running at an outlet velocity of 5 m/s and an outlet temperature of 120^{o}C. The racks were moved at an increment of 0.5, 1, 2, 3 and 4". Temperature measurements were recorded using the DAQ at these increments. The raw data was refined using a Matlab Script. The temperatures were interpolated using Tecplot to obtain continuous temperature planes. Inverse distance and Kriging interpolations were performed. In reality, it was not possible to get a continuous plane as shown in the above figure. A sample of the actual points where measurements were taken was shown below in Fig.50 for the 2" interval case. These measurements were interpolated to predict the values at the locations in between the measurements

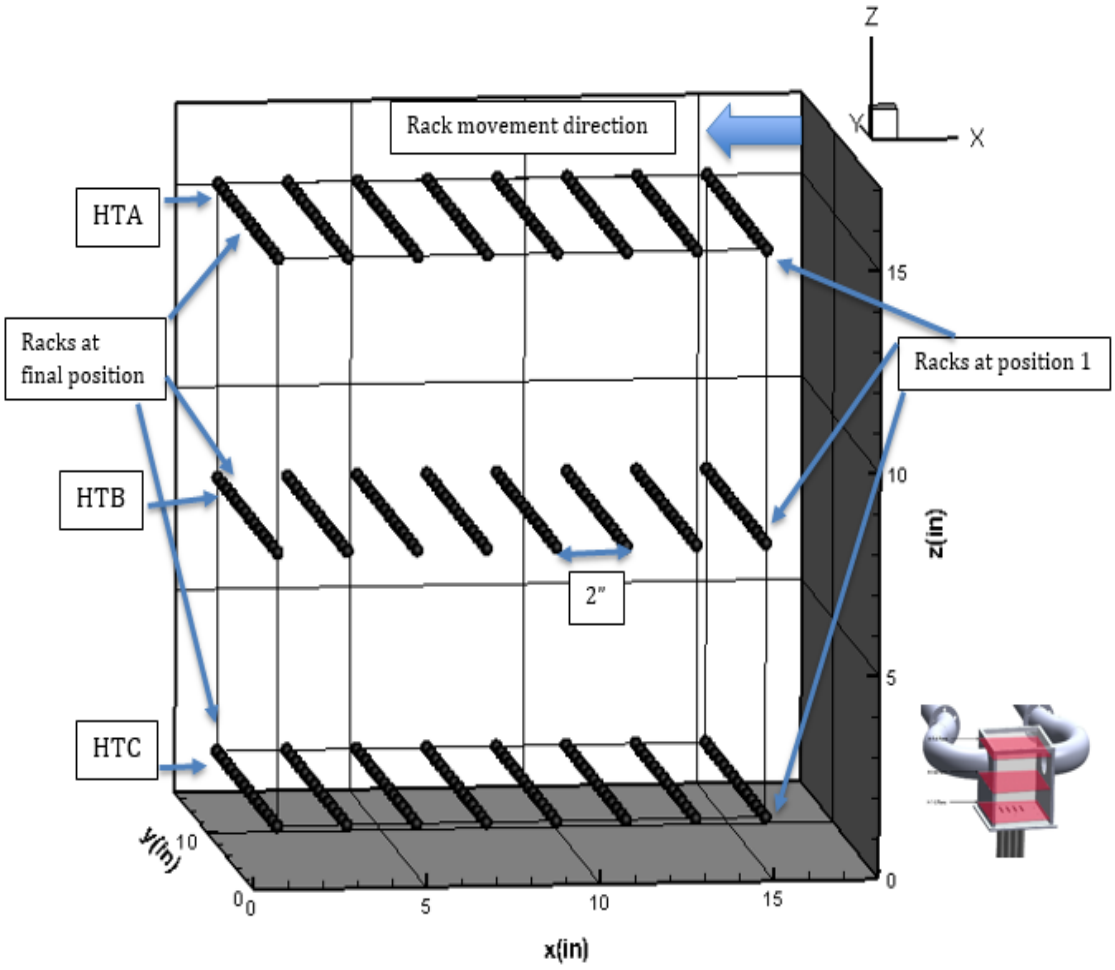

Figure 50. The locations of the temperature measurements for 2" interval.

The rack movement interval was determined based on the resolution of the temperature profiles for each interval. The temperature spatial profile for plane HTC with increment size of 0.5, 1, 2, 3 and 4" was plotted as shown in Fig.51 below. Note that the coordinate system represented the full upper plenum, while the smaller box represented where the temperature measurements were taken and interpolated. This plane (HTC) was specifically chosen for comparison due to its proximity from the outlet

of the risers. Apparently, the temperature of the risers' outlets cannot be distinguished for the 2, 3, 4" cases. The temperature at the risers' outlet was expected to be significantly higher than the rest of the plane. This implied that these increment sizes were large enough to skip some of the outlets of the risers. On the other hand, the risers could be clearly identified for the 0.5 and 1" cases. However, in the 1" case, it seemed that the risers were shifted by approximately half inch to the left side of the plenum. This was possibly due to the fact that the rack was very close to the end of one riser outlet and one measurement was taken at that location since the riser width was close to 1" as well. With the interpolation, this resulted in a shift of the locations of the temperatures possibly due to insufficient measurements. On the other hand, the riser outlets were symmetrically centered for the 0.5" case possibly indicating more than one temperature measurement across the risers. It was clear that the 0.5" had a better resolution than the rest of the cases due to the larger number of measurements. As expected, the larger number of measurements yielded an improved resolution compared to the 1" case.

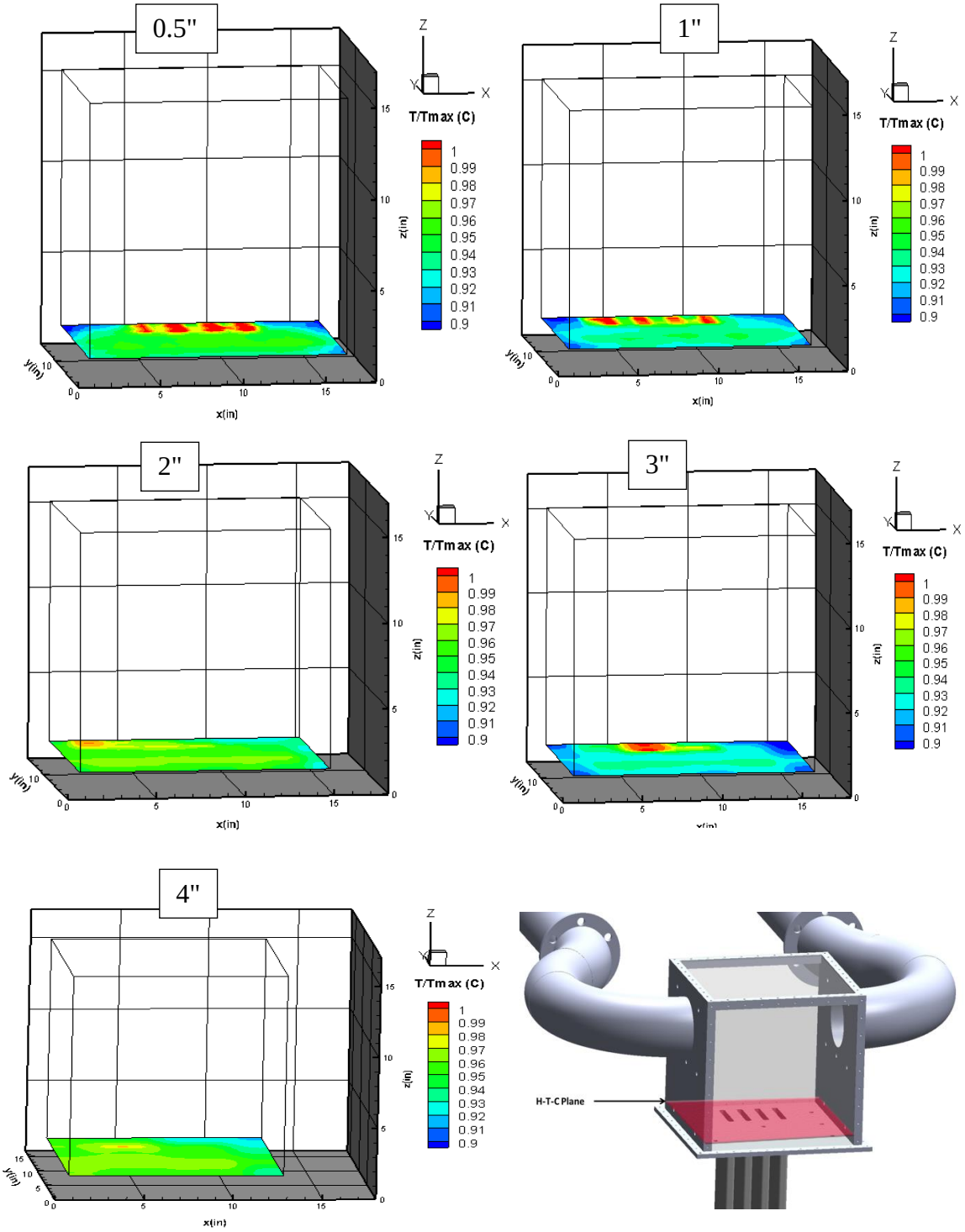

Figure 51. Normalized Temperature spatial profile at plane HTC with interval size of 0.5, 1, 2, 3 and 4" using Inverse Distance Interpolation.

In order to choose between 0.5 and 1” interval, some of the interpolated values for the 1” case were compared to the measured value obtained from the 0.5”. Since the 1” size was double the size of the 0.5”, the latter measured the temperature for points that happened to be in between the 1” case measurements. For instance, the 1” case took measurements at x= 1, 2, 3, 4” until the 16”, whereas the 0.5” took measurements at x=1, 1.5, 2, 2.5” until 16.5”. This meant that the interpolated value at x=1.5” for the 1” case can be compared to the measured value at x=1.5” from the 0.5” case. Similarly, other points can be compared as well. Figures 52, 53 and 54 below compared the temperatures interpolated using the Inverse Distance and Kriging methods from the 1” case with the actual values obtained from the 0.5” case for selected thermocouples from three different planes. While the overall behavior of the interpolated curves was always similar to the actual curve, significant discrepancy was found in the comparison for the HTC1 thermocouple shown in Fig.54. While the average temperature difference between the interpolated (Inverse Distance) and the actual values for thermocouple HTC1 was about 0.75^{o}C, localized differences could go up to 2^{o}C. For the HTB14 and HTA5 thermocouples the average temperature difference was about 0.7 and 0.45^{o}C with maximum differences of 1.1 and 1.6^{o}C. Overall, the interpolated values for the horizontal thermocouples closely matched the measured values. The interpolation seemed to be slightly over predicting the temperatures.

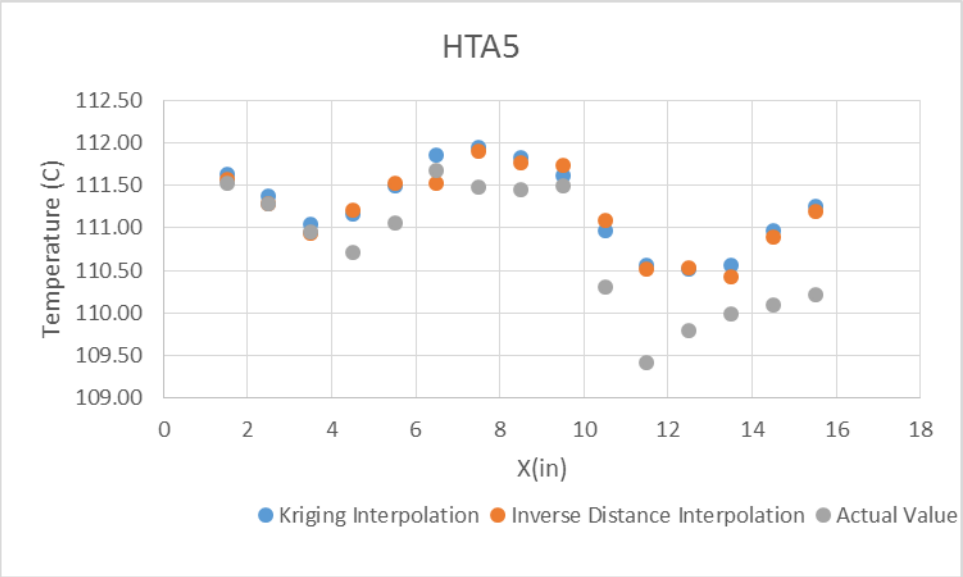

Figure 52. Comparison of the interpolated temperature for from the 1" case with the measured value from the 0.5" case for thermocouple HTA5.

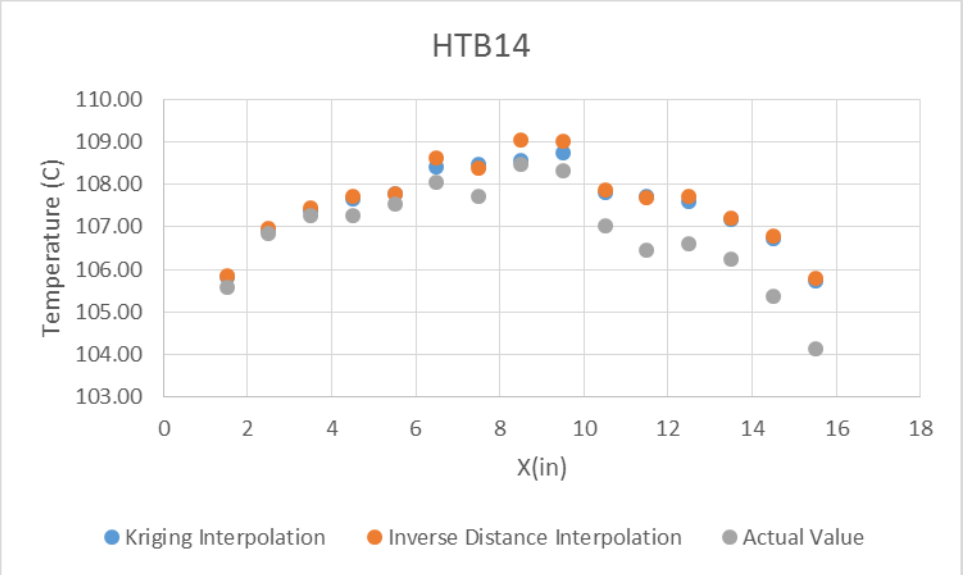

Figure 53.Comparison of the interpolated temperature for from the 1" case with the measured value from the 0.5" case for thermocouple HTB14.

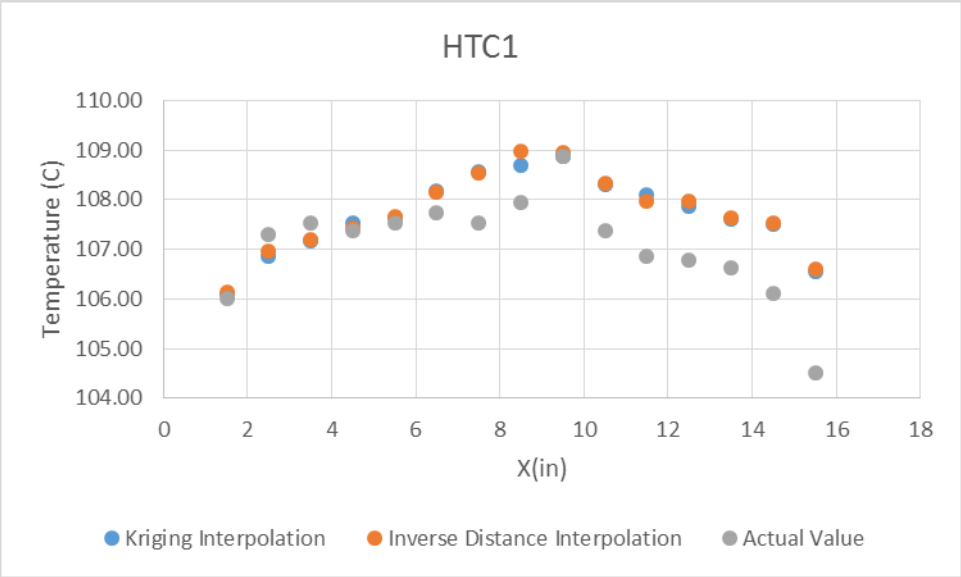

Figure 54. Comparison of the interpolated temperature for from the 1" case with the measured value from the 0.5" case for thermocouple HTC1.

Interpolations for the vertical thermocouples, Kriging and Inverse Distance, succeeded in predicting the temperature values with a very good degree of accuracy as shown in the figures below. Three thermocouples were selected randomly from each thermocouple rack. The average and maximum temperature difference with respect to the inverse distance interpolation for VTA2, VTB6, and VTC1 were 0.27, 0.28, 0.22 and 0.46, 0.6, 0.47^{o}C, respectively. Even though the difference between the measured and interpolated temperatures was relatively insignificant for both horizontal and vertical thermocouples, the shift in the risers' locations on plane HTC discussed earlier geared the RCCS team towards picking the 0.5" interval to achieve better resolution. Moreover, with the smaller interval the localized variations were expected to be minimal. With regards to the interpolation method, both Kriging and Inverse distance provided a good

estimate for the temperature. Figures 55, 56, and 57 compared the two interpolation methods with the actual value obtained from the 0.5” case.

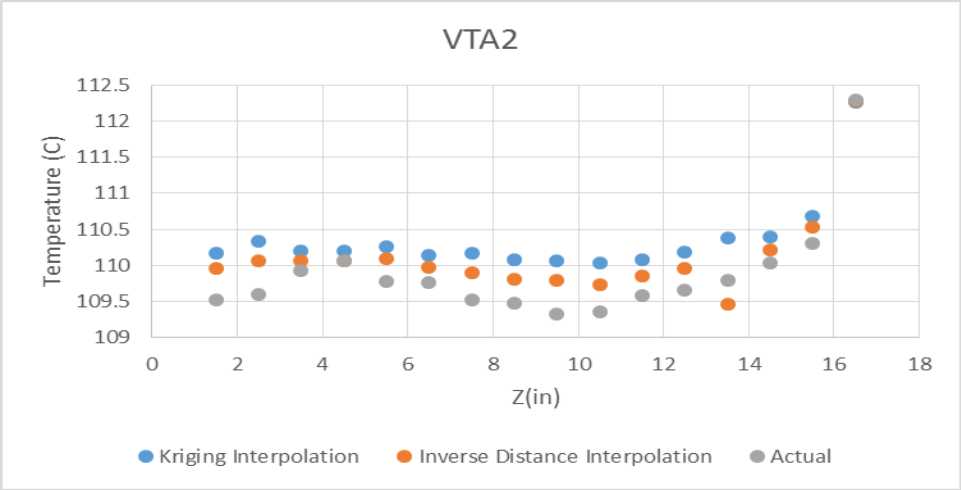

Figure 55. Comparison of the interpolated temperature for from the 1" case with the measured value from the 0.5" case for thermocouple VTA2.

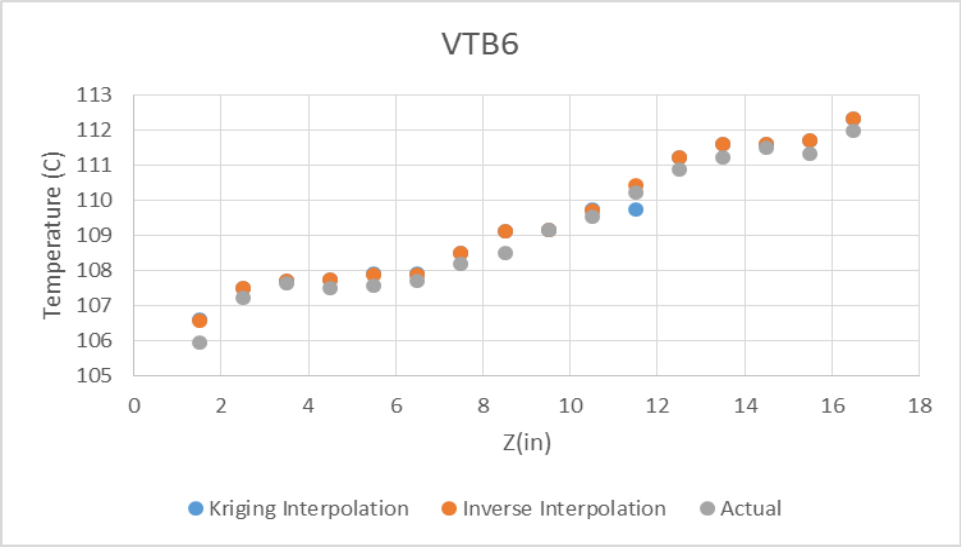

Figure 56. Comparison of the interpolated temperature for from the 1" case with the measured value from the 0.5" case for thermocouple VTB6.

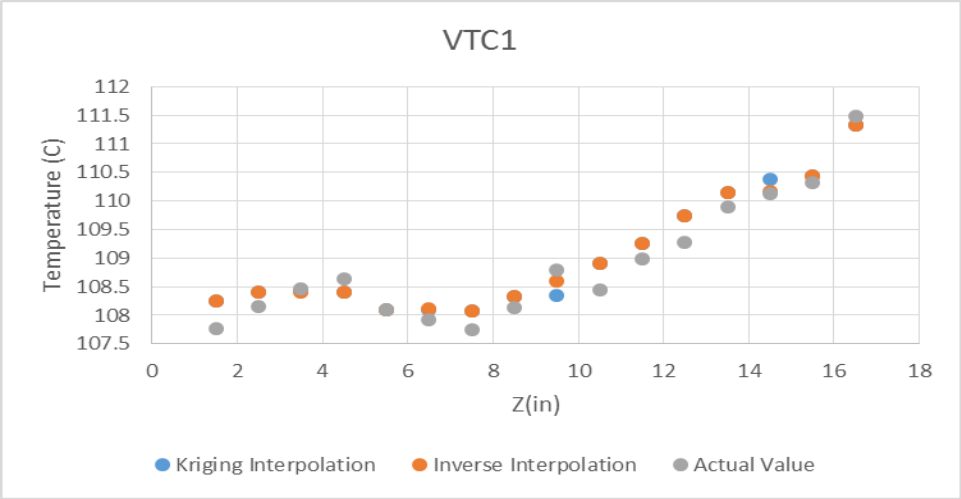

Figure 57. Comparison of the interpolated temperature for from the 1" case with the measured value from the 0.5" case for thermocouple VTC1.

Table 5 showed the error associated with each type of interpolation with respect to the measured value for the selected thermocouples. Although the error was infinitesimally small for both types, Inverse Distance interpolation had a smaller error consistently. Accordingly, it was the method used for interpolation for the rest of the experiments.

Table 5. Comparison of the error associated with Kriging and Inverse Distance Interpolations. The error was calculated with respect to the measured value.

Thermocouple	Kriging Maximum Error	Kriging Average Error	Inverse Distance Maximum Error	Inverse Distance Average Error
HTA5	1.05%	0.44%	1.01%	0.42%
HTB14	1.55%	0.60%	1.59%	0.69%
HTC1	2%	0.70%	2%	0.70%
VTA2	0.67%	0.43%	0.42%	0.25%
VTB6	0.61%	0.28%	0.58%	0.26%
VTC1	0.67%	0.43%	0.42%	0.25%

5.3 Case 1

In case 1, all four risers were in operation with an inlet temperature of 120^{o}C and an average velocity of 5m/s. The average ambient temperature was 25.8^{o}C when the data was acquired. Due to the symmetry of the boundary conditions, the temperature profile was expected to be symmetric due to the expected symmetry in the flow distribution. Figure 58 showed the lower horizontal plane normalized temperature contour for case 1. As anticipated, the temperature profile was symmetric across the plane which was suggestive of even flow distribution. The jets at this elevation (z=1.25") could be clearly distinguished. This meant that at this elevation the jets did not merge yet. The attention grabbing feature of the below contour was the prominently lower temperature at the corners of the upper plenum. This suggested the existence of recirculation zones at the corners' of the bottom plate. Interestingly, similar cold regions at the corners were predicted by the preliminary results of the computational fluid dynamics model created using STAR CCM+ (Sulaiman, et al., 2014).

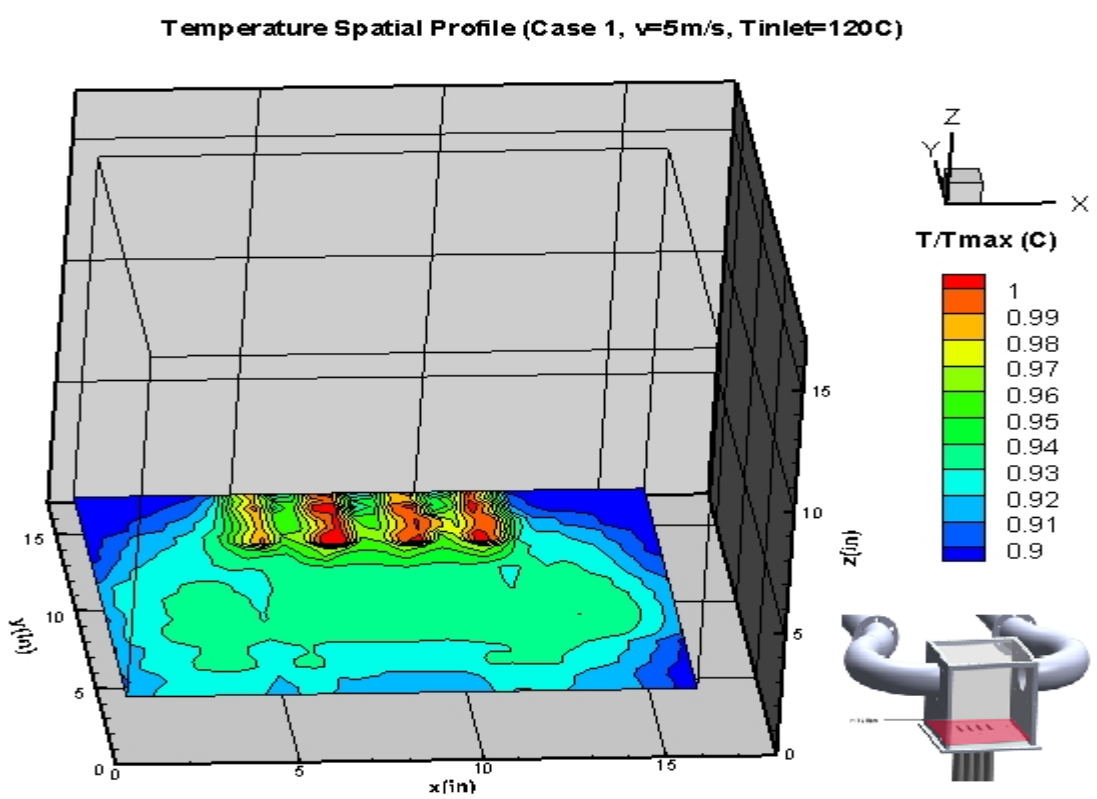

Figure 58. Normalized temperature spatial contour at plane HTC (The bottom of the plenum) for case 1. The maximum temperature is 118^{o}C.

The temperature contour for the HTB plane depicted in Fig.59 confirmed the temperature profile's symmetry. At this plane, the average temperature was relatively higher than the HTC plane. It was apparent that the jets had merged as identification of the separate jets wasn't possible at this elevation (z=8"). The lower temperature contour lines located at the left and right sides of the plane were very close to the inlet of the chimneys.

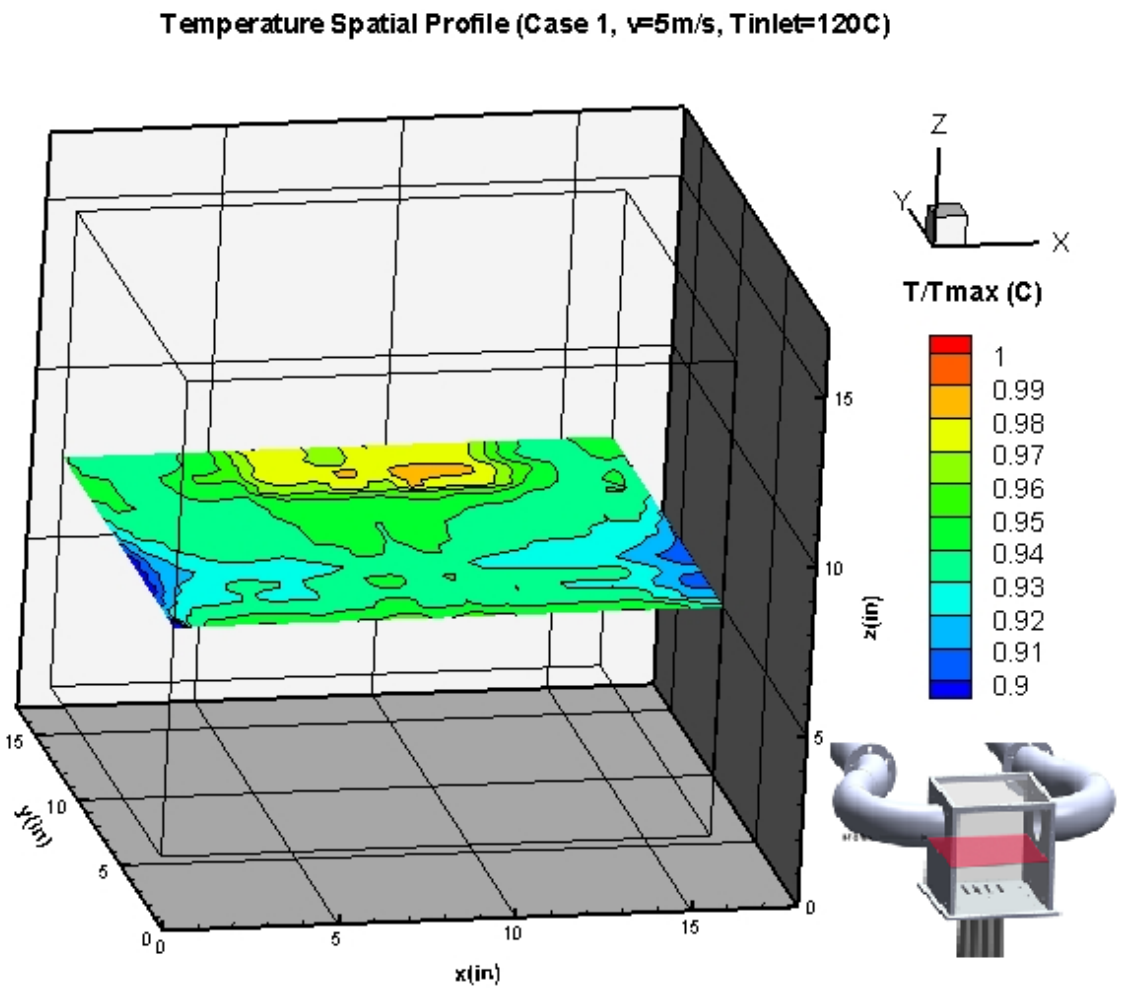

Figure 59. Normalized temperature spatial contour at plane HTB for case 1. The maximum temperature is 118^{o}C.

The top plane (HTA) had the highest temperature amongst all three planes shown in Fig.60. This could be attributed to the effects of buoyancy as air with higher temperature has lower density and always tries to travel upwards. The impingement of the jets, although appeared to be asymmetric, can be clearly seen at plane HTA. The reason behind the asymmetry can be due to the fact that the difference between the

contour levels was very small. Thus, the asymmetry could be due to the thermocouple's accuracy and its associated uncertainty.

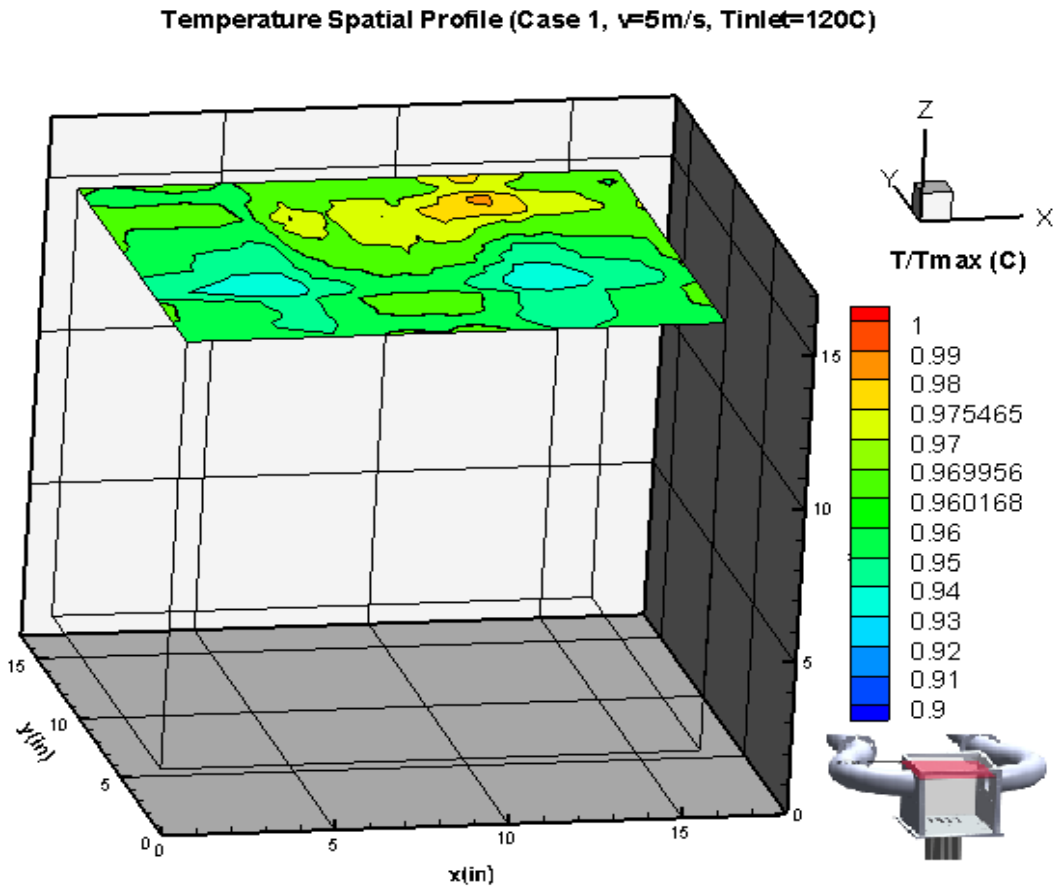

Figure 60. Normalized temperature spatial contour at plane HTA for case 1. The maximum temperature is 118ºC.

The vertical plane VTA also showed that the temperature profile was fairly symmetric as displayed in Fig.61. This plane was very special as it's located directly above the location of the jets. What was noteworthy in the below contour was the fact that the jets from risers 1 and 2 seemed to mix initially on their own forming a single jet.

Similarly, the jets from risers 3 and 4 mixed separately away from the rest of the jets forming another single jet. In other words, each pair of jets seemed to act as a separate twin jet. It was postulated that the reason behind the lack of interaction between the two middle jets was due to a condition imposed by the two symmetric chimneys. The phenomenon was not very well understood and would require velocity measurements at different planes for better understanding. The contour lines in between risers 2 and 3 showed the separation between the jets formed by the two pairs. It was also believed that the contour lines in between the jets were representing recirculation zones as predicted by multiple parallel jet theory. According to the contour line in between risers 3 and 4 on the right, the two jets started to merge at an elevation of about 3". The jets from the other two risers begun to merge at a lower elevation of 2.85". The two formed jets seemed to impinge before getting the chance to merge. Determination of the merging point is dependent on velocity field. These were estimates from the temperature contour and are subject to significant error. Another important observation was the separate circle-like contour found at the middle top of the temperature contour. This could probably be a recirculation zone created due to the interaction of the newly formed jets or it could just be related to the uncertainty of the measurement since the difference between the contour levels was relatively low.

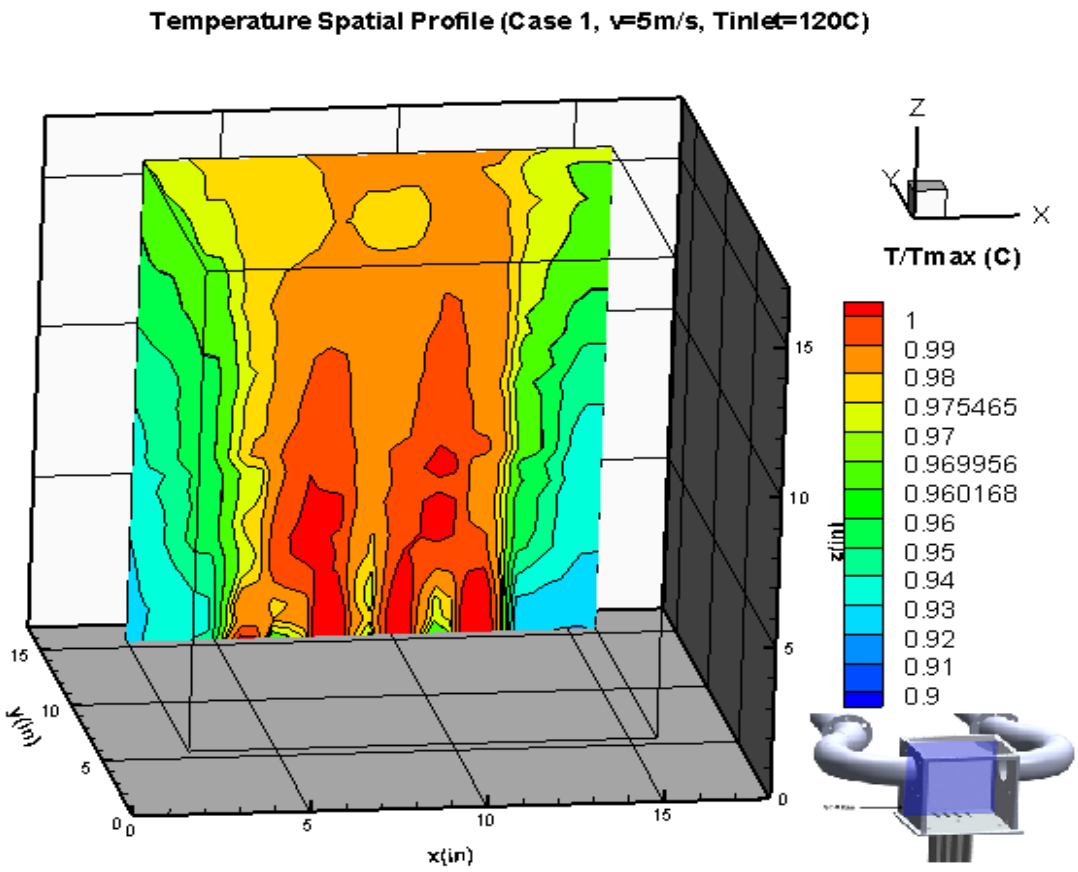

Figure 61.Normalized temperature spatial contour at plane VTA for case 1. The maximum temperature is 118ºC.

The temperature fluctuations for case 1 were unexpectedly small. It was projected that this case would have high temperature fluctuations due to the higher velocity. However, as shown in the Fig.62 and 63 the temperature fluctuation as a percentage of the maximum temperature had maximum values of 0.38 and 0.8 % for the horizontal and vertical measurements, respectively.

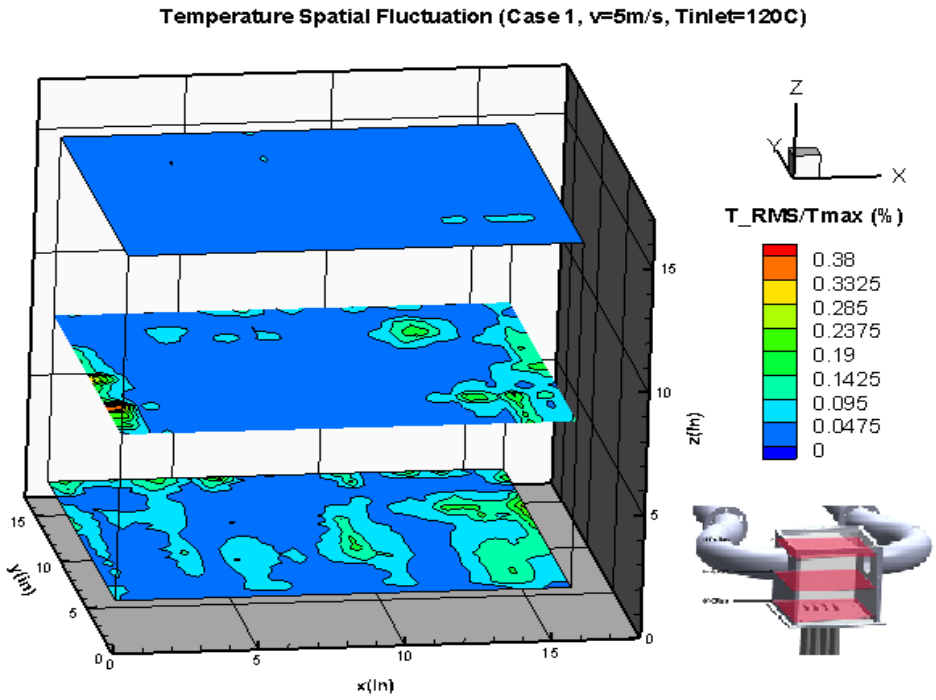

Figure 62. Temperature fluctuation percentage for the three horizontal planes. It is calculated by dividing the RMS (Root Mean Square) by the maximum temperature which is 118ºC.

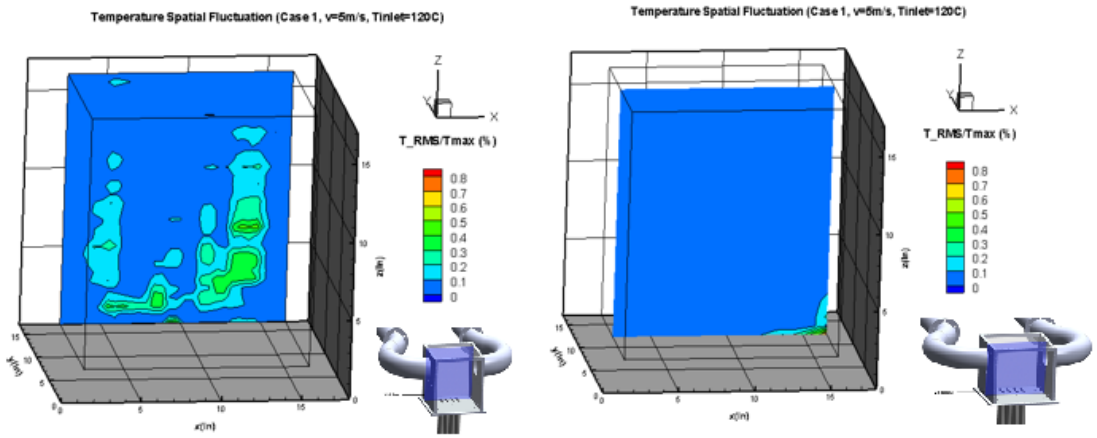

Figure 63. Temperature fluctuation percentage for the vertical planes VTA and VTB. It is calculated by dividing the RMS (Root Mean Square) by the maximum temperature which is 118ºC.

5.4 Case 2

In case 2, riser 4 was the only riser in operation with an average velocity of 5 m/s and an outlet temperature of 120^{o}C. The average room temperature was 25.6^{o}C when the measurements were taken. In this case it was observed from the temperature measurements that the flow was preferring to exit through one chimney. The inlet and outlet temperature for the left chimney was around 66 and 53^{o}C, respectively. On the other hand, the right chimney had room temperatures of 26.9 and 25.3^{o}C, for the inlet and outlet, respectively. It was important to mention that riser 4 was located on the right side of the upper plenum closer to the right chimney. It was also important to note that the experiment was conducted under controlled environment with both chimneys being exposed to the same conditions. The normalized temperature contours for the horizontal planes were asymmetric which was expected due to the flow coming from a point that was asymmetric with respect to the upper plenum geometry. The temperature gradient for this case was very large compared to case 1. In case 1 the temperature ranged from 90 to 100% of the maximum temperature, whereas the temperature ranged from 40 to 100% of the maximum temperature in this case which suggested the presence of thermal stratification and poor mixing. Similar to case 1, the upper plane had a higher average temperature relative to the other two planes due to buoyancy effects suggesting the presence of thermal stratification. The temperature did not vary considerably within the HTA plane (the upper plane) with one contour line separating two regions. Clearly, the hotter region was due to the impingement of the jet which according to Fig.64 had

dropped in temperature by almost 20%. The temperature contour for the HTB (the middle plane) plane exhibited remarkable variations in temperature. While the region above the jet can be clearly distinguished and justified in this plane, a significantly colder separated region which looked similar to an ellipse existed close to the right chimney. It was not really clear whether this region was due to a recirculation zone or some other kind of phenomenon related to the chimney. Another hotter than average region located on the left of the plane and separated from the mainstream temperature of this plane was present close to the left chimney. This supported the observation of the flow being diverted through the left chimney only. The lower plane (HTC) had a generally lower temperature average than the upper two planes. A small colder contour line near the outlet of risers 1 and 2 (not in operation during this experiment) was observed. It was not likely that the presence of this region was a result of the uncertainty of the thermocouple as the difference in the levels of the contour lines was substantial in this case.

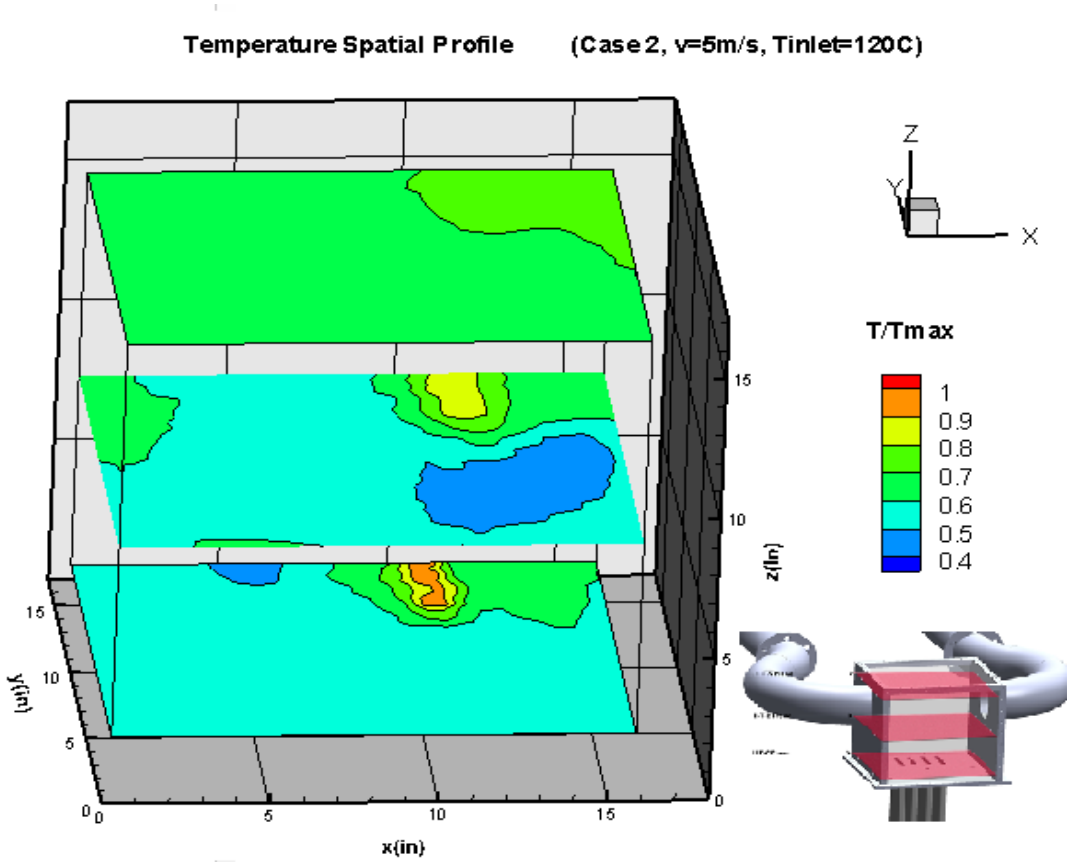

Figure 64. Normalized temperature spatial contour for the horizontal planes for case 1. The maximum temperature is 113°C.

The vertical temperature contour showed a larger temperature gradient ranging from 30 to 100% of the maximum temperature, which translated into 38 and 117°C. Plane VTA's temperature spatial profile gave a clear image of the jet development. It can be observed from Fig.65 that the jet started at a high temperature. The temperature decreased as the jet grew with elevation. The jet's temperature also widened in the lateral (x) direction as it traveled upwards. The contour then indicated that the jet impinged on the upper wall to right side corner and changed direction to end up traveling

to the left side. The cold region above the outlet of riser 1 was also present and distinguished in this profile.

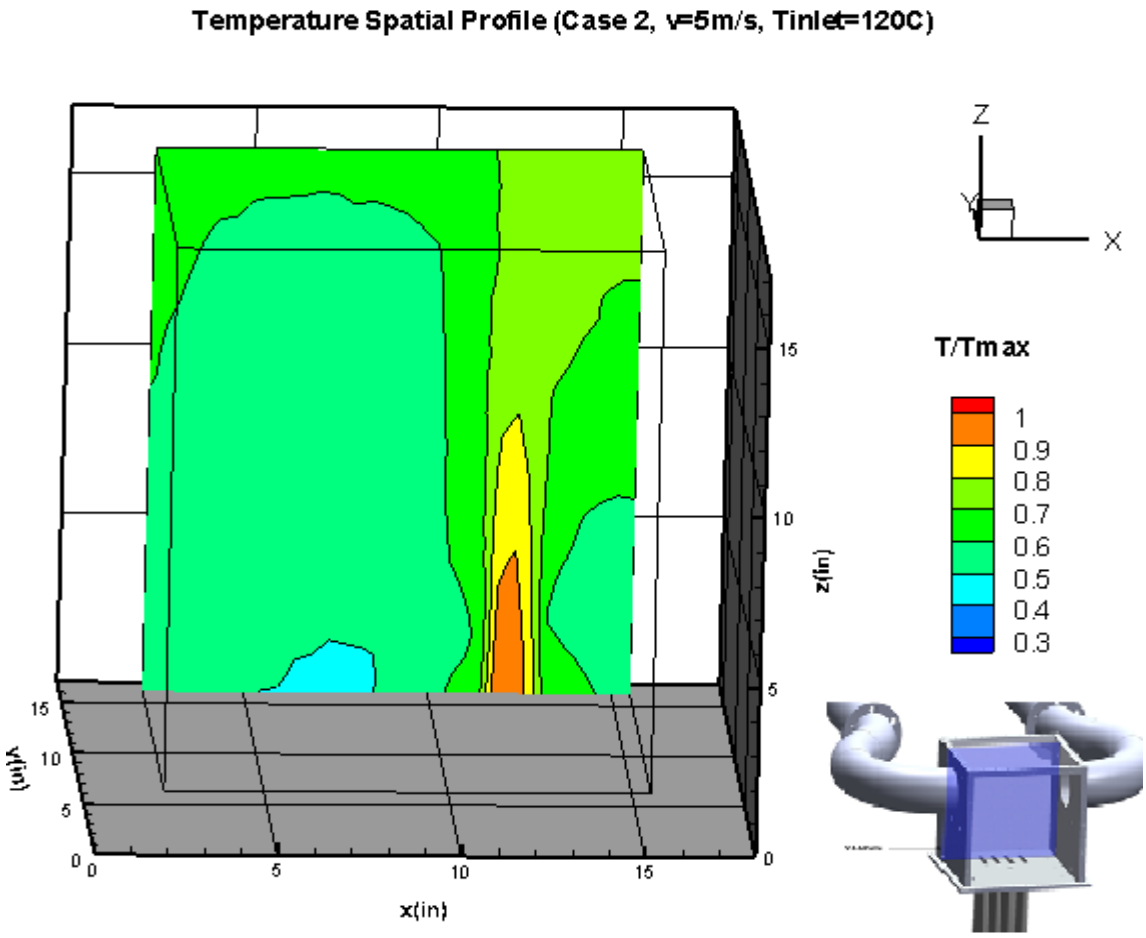

Figure 65. Normalized temperature spatial contour for the vertical plane VTA. The maximum temperature is 117ºC.

The most notable feature of the temperature profile in VTB plane was the cold region extending from the right side (near the right chimney) to the middle of the upper plenum as displayed in Fig.66. This was the same region as the elliptical region found in

plane HTB earlier. It was not really clear what's the reason behind the presence of this region, but it's very likely that it's related to the cold right chimney.

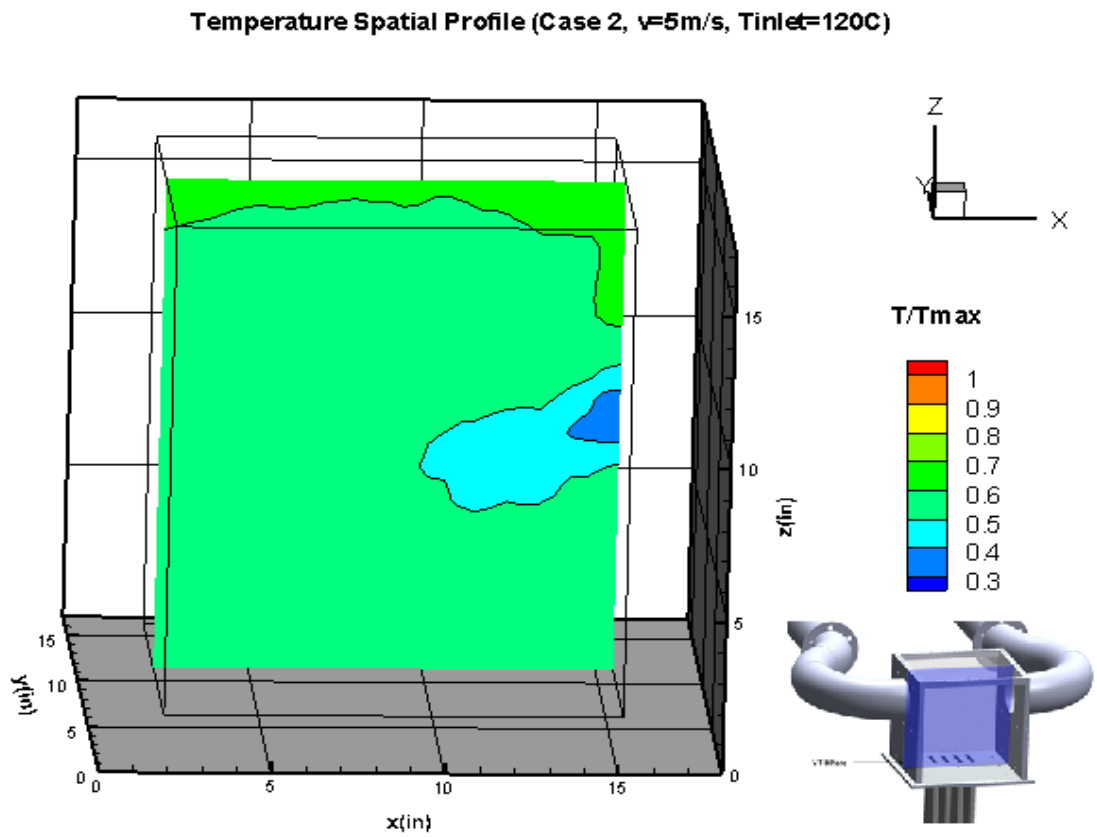

Figure 66. Normalized temperature spatial contour for the vertical plane VTB. The maximum temperature is 117°C.

Figure 67 showed a continuation of the puzzling phenomenon with the cold region extending beyond the middle of the upper plenum now. It was very difficult to make any conclusions pertaining this phenomenon with temperature measurements alone.

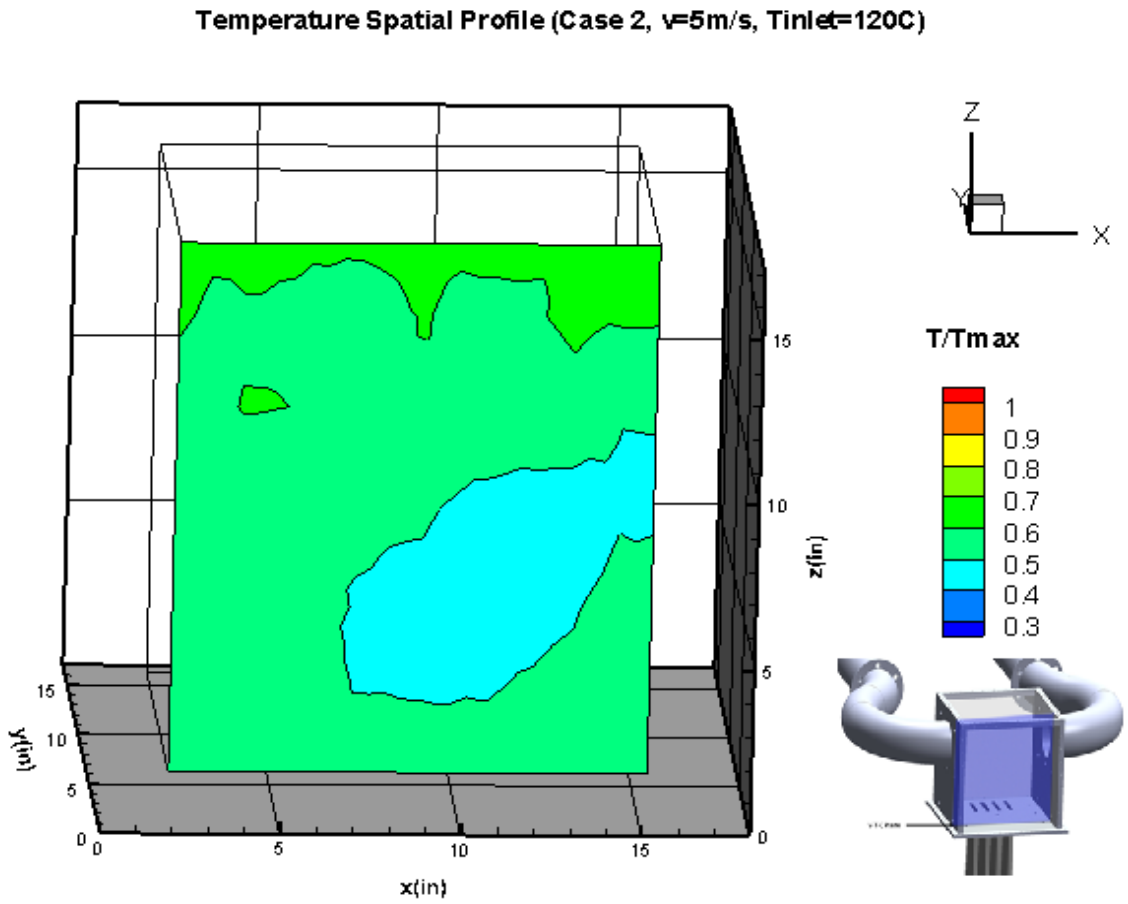

Figure 67. Normalized temperature spatial contour for the vertical plane VTC. The maximum temperature is 117ºC.

Isosurfaces were created for this case to get an indication of the flow behavior from the temperature measurements. The isosurface is basically a surface created from points the lie within a given temperature range. While not very accurate for flow characterization, the isosurfaces could be insightful with regards to the flow progression. It was assumed that the flow started with the highest temperature in descending order as shown in Fig.68. Steps 1 through 4 showed the jet progression, while step 5 was indicative of the preferential flow towards the left side of the plenum. Step 6 showed an

isosurface extending from the jet region towards the left chimney. Steps 7 and 8 showed isosurfaces declining from the right chimney to the middle of the plenum, and ascending through risers 1 and 2. The last two steps were representative of the puzzling phenomenon. It was suspected that this could be due to reverse flow from the right chimney inducing cross flow in the upper plenum. The theory was that the jets entered the plenum with a large momentum and high velocity relative to the stagnant flow. The high velocity created low pressure which attracted some of the stagnant air to join the flow (flow entrainment) which could describe the widening of the jet in steps 3, 4, 5 and 6. The entrainments of the surrounding air left room in the upper plenum for reverse flow from the right chimney. The declining isosurface also supported the reverse flow theory. It was noticeable that the isosurface was declining towards the bottom of the plenum. This was due to the fact the air coming from the right chimney was cold which meant it was denser and thus tended to flow down. This theory might explain the large temperature gradient in this case. However, these are temperature measurement, therefore, solid conclusions cannot be made unless the velocity profile is measured.

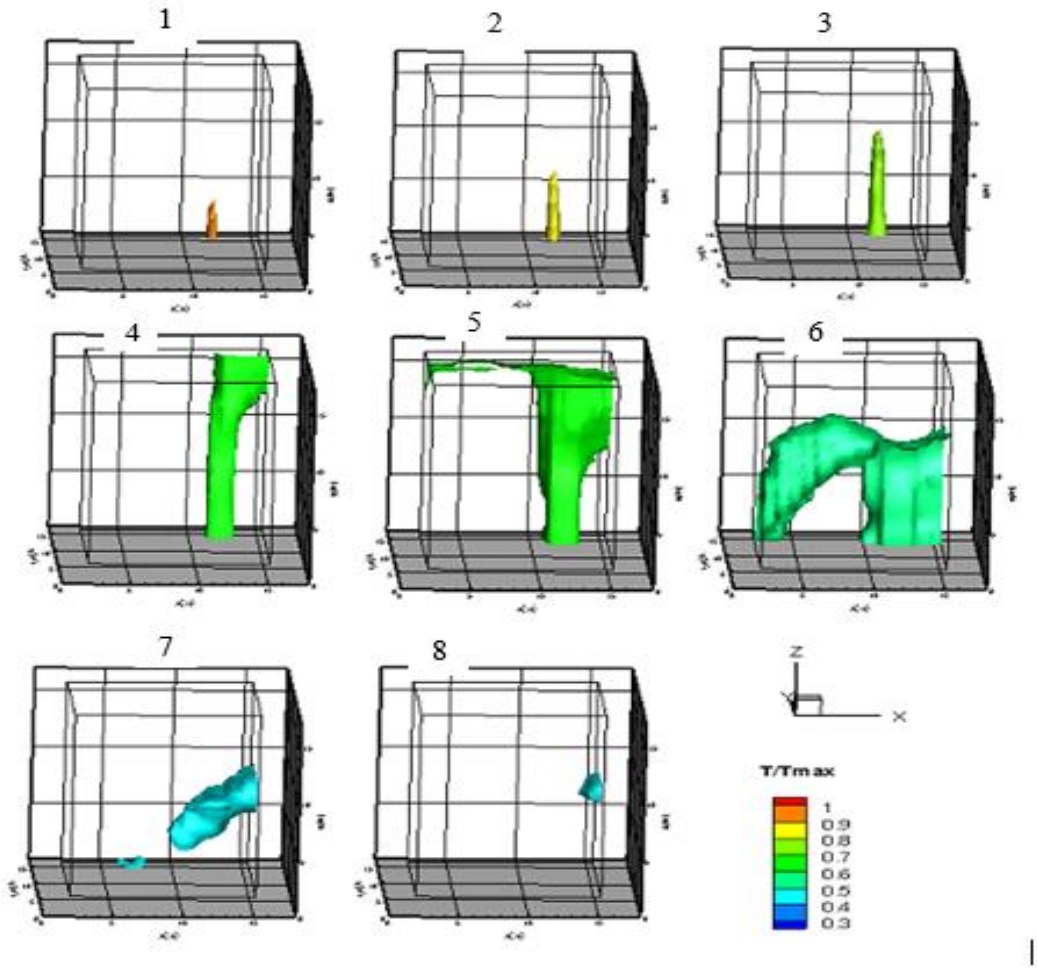

Figure 68. Isosurfaces for case 2 starting from the highest to the lowest temperature.

The temperature fluctuations for the horizontal planes in case 2 were markedly higher than case 1 ranging from 0 to 3.5% of the maximum temperature as presented in Fig.69. Interestingly, most of fluctuations occurred near the right chimney where the earlier discussed phenomenon was taking place. Significant fluctuations were also present near the outlet of risers 1 and 2. High temperature fluctuations supported the reverse flow hypothesis as the possible induced cross flow was causing mixing between the hot and cold streams which resulted in high fluctuations. Figure 70 for the vertical

planes also showed increased fluctuations relative to case 1 with a maximum of 4.5%. The high fluctuations regions were the same as the ones found in the horizontal profiles. In addition, fluctuations were observed along the vertical path of the jet indicating, possibly due to the turbulent shear layer in between the jet and the ambient air.

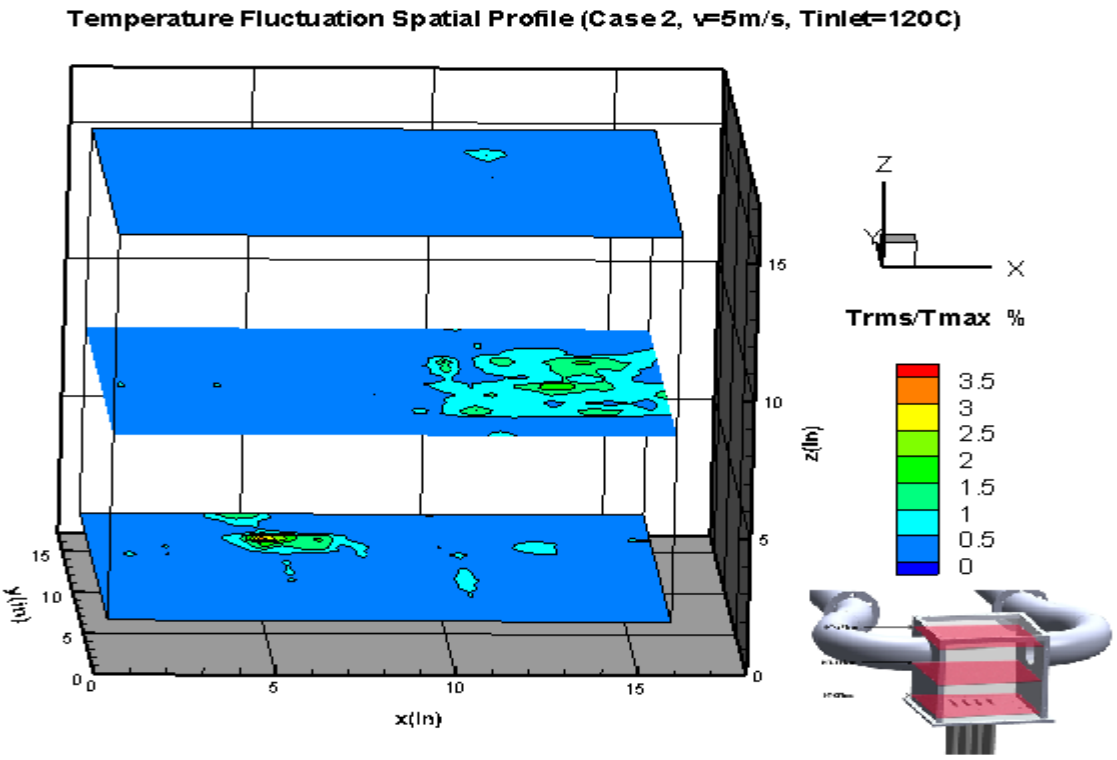

Figure 69.Temperature fluctuation percentage for the three horizontal planes. It is calculated by dividing the RMS (Root Mean Square) by the maximum temperature which is 113°C.

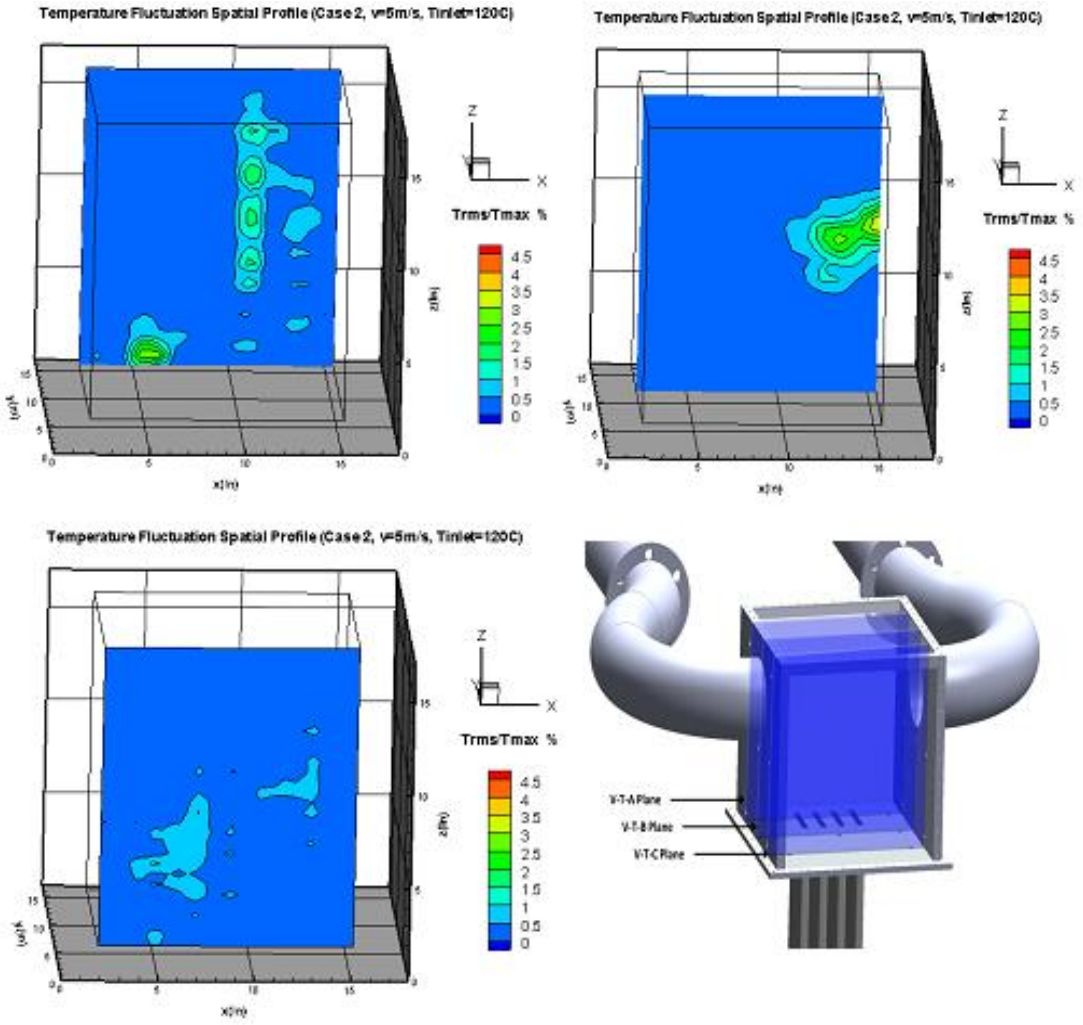

Figure 70. Temperature fluctuation percentage for the three vertical planes. It is calculated by dividing the RMS (Root Mean Square) by the maximum temperature which is 118°C.

Since the above temperature and fluctuation profiles were interpolated, another method was used to verify the obtained results. Cross correlations was used to correlate different thermocouple signals at different locations in the upper plenum. In particular, thermocouple VTB1 (first vertical thermocouple located in rack B on the right) with VTB2, VTB8 and VTB13. These thermocouples were located to the left of VTB1 with

VTB2 being the closest and VTB13 being the furthest. The thermocouple signals were correlated at three different elevations of 1, 8.5 and 17”. The cross-correlation was applied to this specific rack because it had the most fluctuations and it passed by the chimneys as it was moved up. The cross correlation plotted in Fig.71 showed that the signals of the thermocouples were very similar at 1” height.

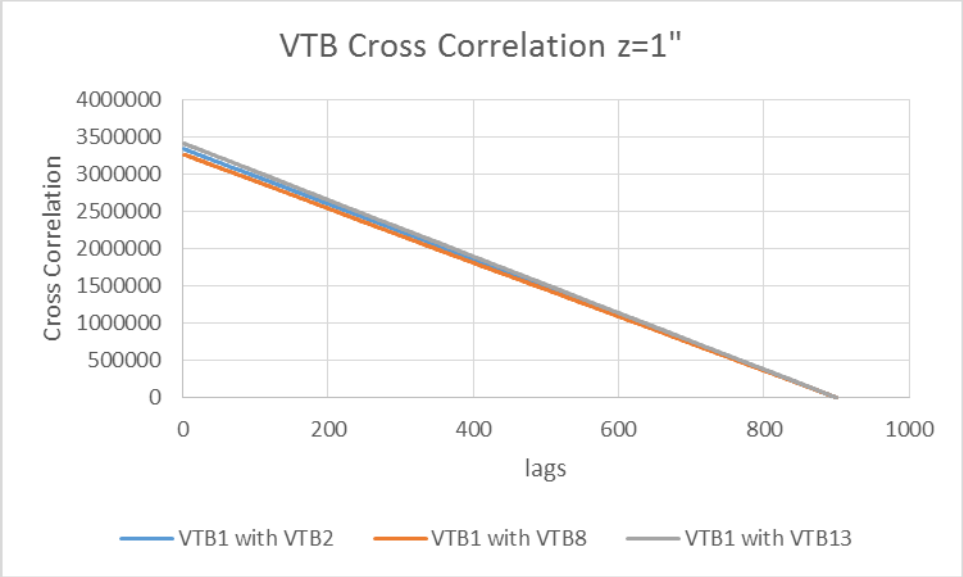

Figure 71. Cross correlation for plane VTB at an elevation of 1" from the bottom of the plenum.

At a height of 8.5”, the similarity of the signals appeared to be dying as shown in Fig.72. While VTB8 and VTB13 seemed to have a similar correlation with VTB1, the cross correlation with VTB2 was clearly different. This verified that there was actually some kind of phenomenon as suggested by the interpolated data. The reason why the VTB2 correlation differed was due to its proximity from the right chimney. Therefore, it

was reasonable to assume that the postulated reverse flow would have a larger influence on VTB2 which explained the disagreement between the cross correlations.

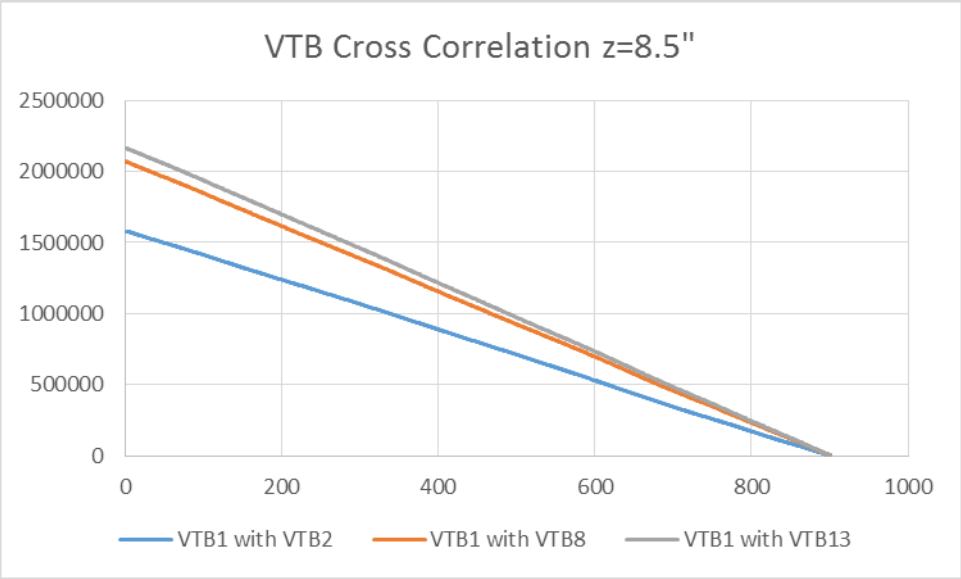

Figure 72. Cross correlation for plane VTB at an elevation of 8.5" from the bottom of the plenum.

At an elevation of 17”, the cross correlation between VTB1 and VTB13 seemed to be different from VTB2 and VTB8 correlations. This was logical since VTB 13 was located at the left of the rack along the hypothesized flow path of the jet. Therefore, the discrepancy in the correlation was sensible. Figure 73 showed the discrepancy in the correlation.

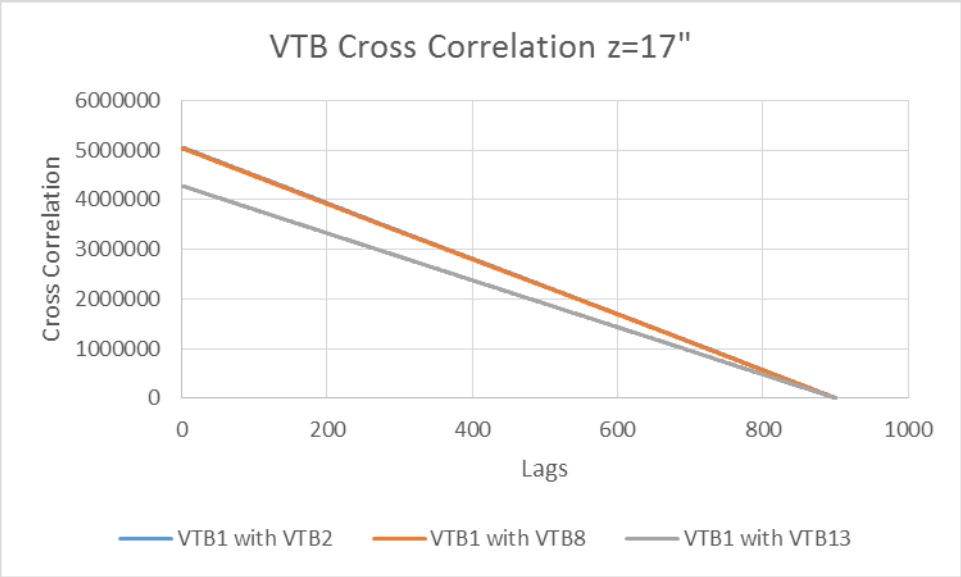

Figure 73. Cross correlation for plane VTB at an elevation of 17" from the bottom of the plenum.

5.5 Case 3

Case 3 had the same conditions as case 1 with the exception of the velocity. All four risers were in operation with an average outlet velocity of 2.25 m/s, and an outlet temperature of 120^{o}C. The average ambient temperature was measured to be 24.8^{o}C. As mentioned earlier in the section, a perplexing phenomenon was encountered during the startup of this experiment, more specifically around two hours from the startup. It was anticipated that this case would be similar to case 1 as a result of the symmetric boundary conditions. However, this case exhibited a very complex behavior which deserved to be investigated further.

The temperature contour for the horizontal planes in Fig.74 was strikingly asymmetric. What was also not expected was the high temperature gradient ranging from

43 to 100% of the maximum temperature suggestive of the presence of thermal stratification. This was not expected due to the symmetry of the boundary conditions. What was more striking was the cold contour appearing in the middle plane which was similar to the hypothesized reverse flow from case 2. However, the results from this experiment were supposed to be similar to those found in case 1 due to the boundary conditions similarity.

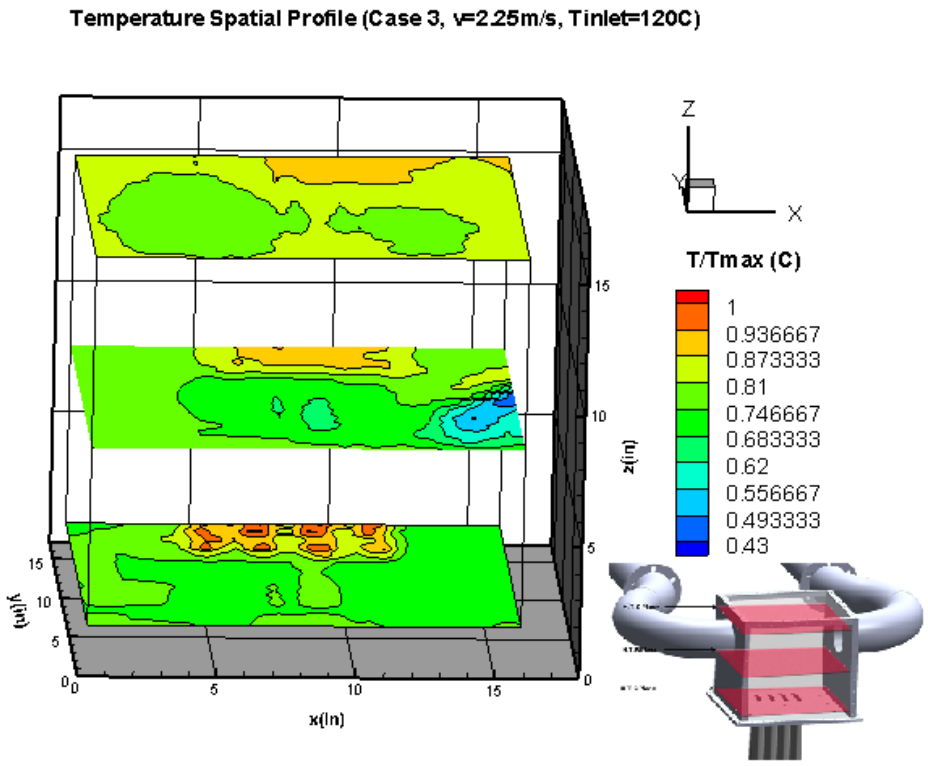

Figure 74. Normalized temperature spatial contout for the horizontal planes. The maximum temperature is 115ºC.

Similarly, the vertical planes did not have a symmetric temperature profile as shown in Fig.75. The similarity to the hypothesized reverse flow from case 2 was very

clear from the vertical profiles. In fact the reverse flow in this case was more prominent as the cold region extended from near the right chimney to a point significantly beyond the middle of the upper plenum. The main difference between this phenomenon and the one encountered in case 2 was that in the former the flow distribution seemed to be even until after two hours when the temperature of the right chimney suddenly dropped to room temperature. While in the latter, the flow was uneven from the beginning and the right chimney temperature was at room temperature from the beginning. This suggested that the flow in case 3 was perturbed due to some unknown reason which triggered the reverse flow and the uneven flow and temperature distribution. Changes in the outside conditions surrounding the chimneys were not likely since the experiment was conducted inside a closed laboratory under a controlled environment. Thermal stratification was obvious in the vertical contours. A contour line separated the top hot portion from the rest of the planes as shown in the VTB and VTC planes.

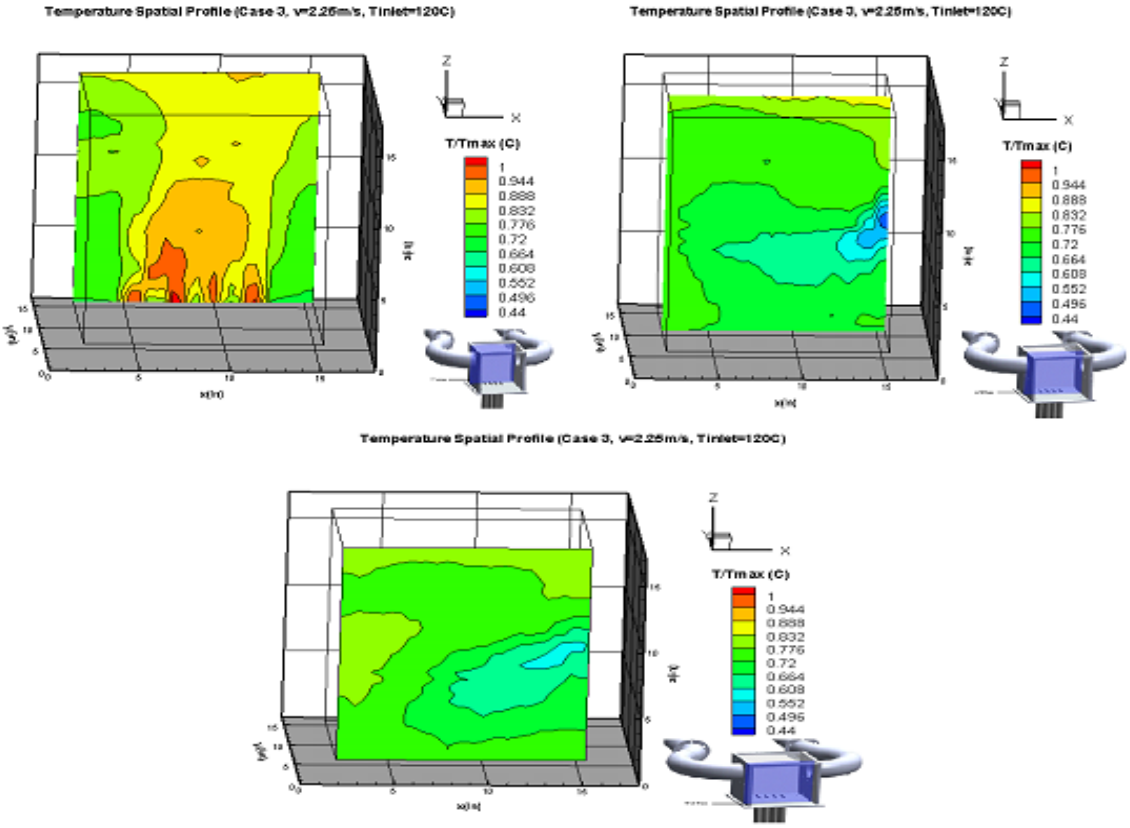

Figure 75. Normalized temperature spatial contour for the vertical planes. The maximum temperature is 118°C.

This case also had a very large temperature fluctuations near the postulated reverse flow region. The fluctuations ranged from 0 to 14% and 0 to 17% for the horizontal and vertical measurements, respectively. Similar to case 2, the high fluctuations were due to the assumed reverse flow causing high mixing between the cold and hot streams. The fluctuations can be seen in Fig.76 and 77 below.

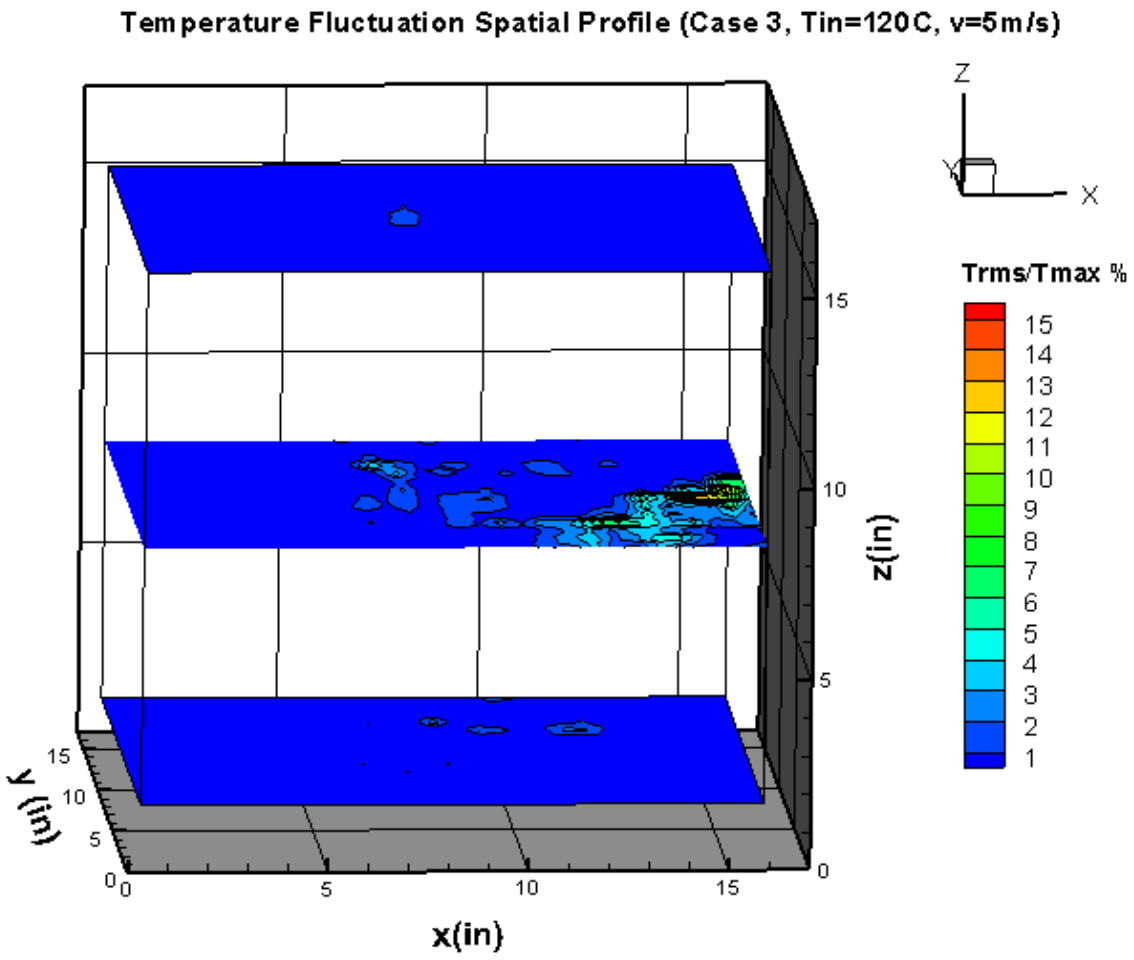

Figure 76. Temperature fluctuation percentage for the three horizontal planes. It is calculated by dividing the RMS (Root Mean Square) by the maximum temperature which is 115ºC.

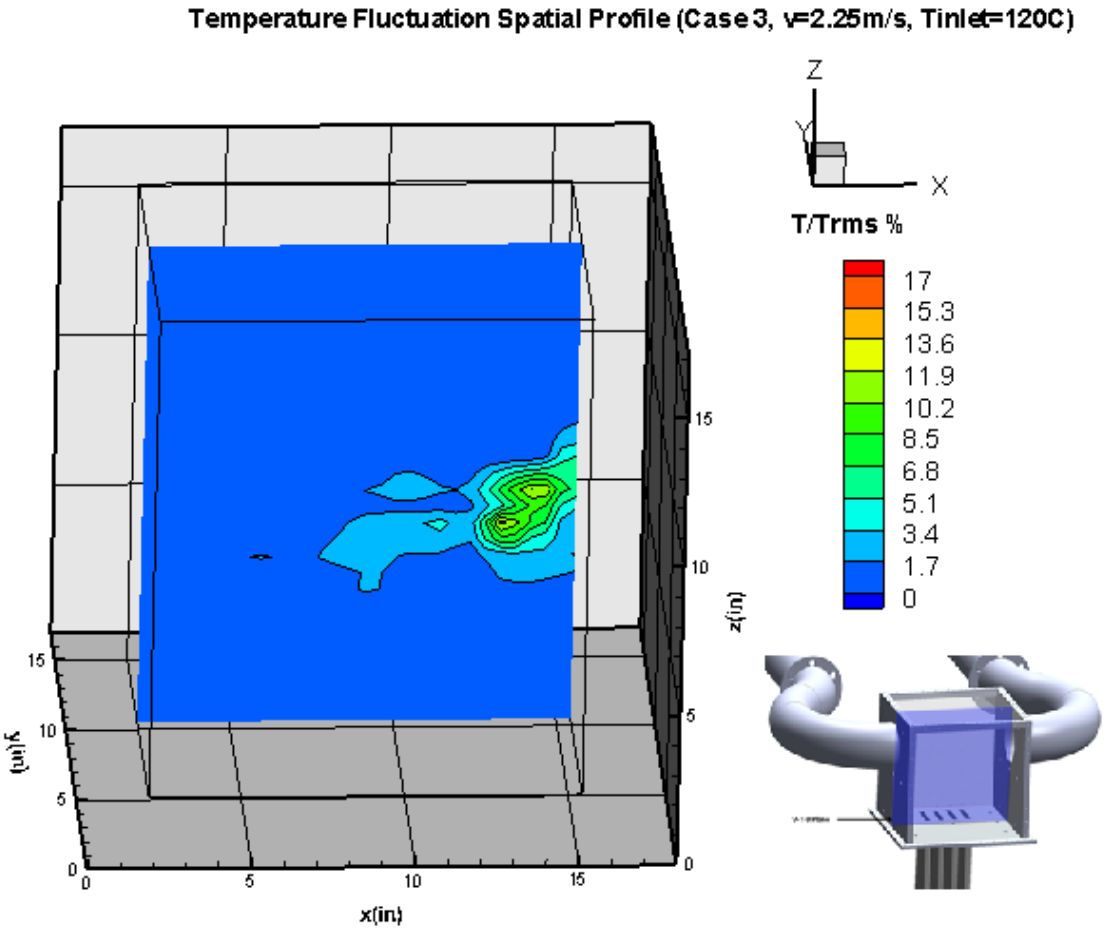

Figure 77. Temperature fluctuation percentage for the three horizontal planes. It is calculated by dividing the RMS (Root Mean Square) by the maximum temperature which is 118°C.

The uneven flow distribution was suggestive of uneven boundary conditions at the outlet of the risers. The temperatures were continuously monitored throughout the experiment with thermocouple probes. The velocity profile for each riser was measured before the experiment, but not during the experiment. The velocity profiles were shown in Fig.78. Since the experiment started normally for the first two hours, it was suspected that a velocity variation was present due to instrumentation fault. Hence, the velocity

profile was measured again after the experiment to check for any inconsistency. While there was a discrepancy between the before and after profiles for all the risers, it seemed that the chief culprit was riser 2 which was consistently lower after the experiment. The hypothesis was that all risers started with an even velocity, however, after two hours a decline in riser 2 velocity perturbed the system and induced the postulated reverse flow phenomenon. Theoretically, the jet from riser 2 was bent towards the jet from riser 1 due to the created low pressure. The merging of twin jets with uneven velocities occurred at a higher elevation compared to those with equal ones. In symmetric conditions as in case 1, each twin jets merged at the same point and a state of equilibrium existed which resulted in even flow distribution. However in this case, the twin jet on the left merged at a higher elevation which perturbed the system. The combined jet from risers 3 and 4 had a greater momentum and higher velocity. The higher velocity introduced low pressure which possibly attracted the other formed jet with lower momentum and resulted in the flow exiting through the left chimney only. The combined flow of the jets entrained stagnant air particles by making them join the mainstream flow creating room for air from the right chimney to flow into the plenum.

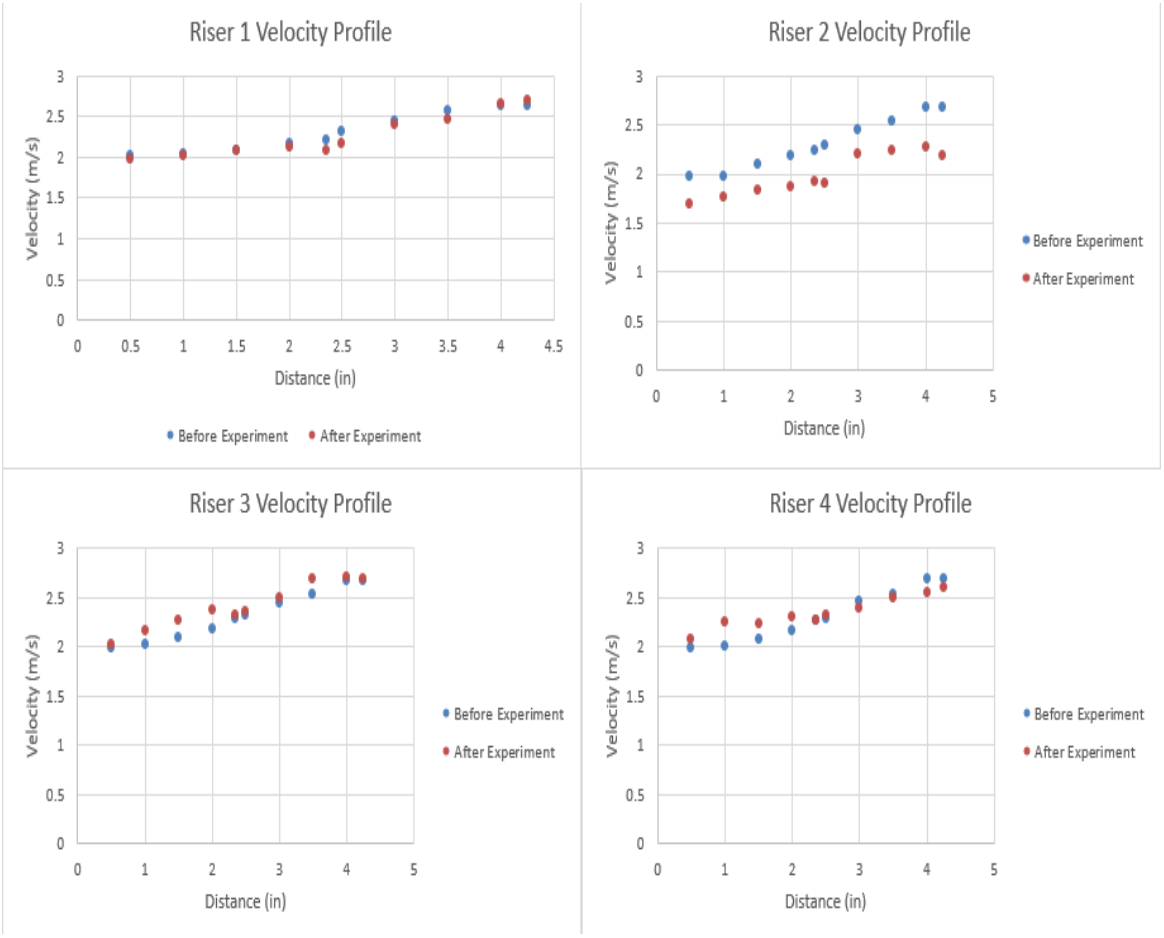

Figure 78. Riser velocity profile measured before and after the experiment.

It was believed that the culprit behind the uneven before and after experiment velocity profiles was the variable autotransformer. Figures 37-40 showed that between 10 and 15V the velocity-voltage curve had a sharper curve with a larger slope compared to voltages above 15 which were linear with a lower slope. The 2.25 m/s velocity happened to fall within the former. At this region of the curve, any voltage fluctuations could cause a relatively significant velocity change. It was noticed that the voltages fluctuated by +/- 0.2V throughout the experiment. While not significant for large

velocities such as the 5 m/s case, lower velocities can be affected by such variation. The fluctuation in the voltage could be attributed to the noise picked up by the system.

Cross correlation was also used in this case to support the interpolated data. Despite the boundary conditions differences between case 3 and 2, the cross-correlation yielded a very similar behavior in both cases. At the first position near the bottom of the plenum, all three thermocouples had a similar correlation with VTB1 as displayed in Fig.79. Looking at the horizontal temperature contour, it can be observed that the lower plane looked fairly isothermal if the jets were neglected. This justified the strong correlation between the signals.

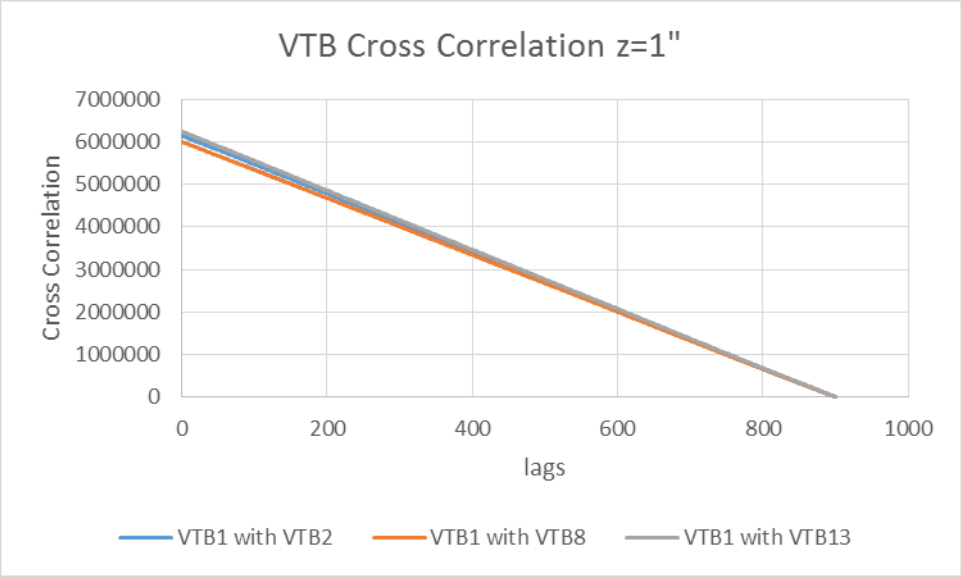

Figure 79. Cross correlation for plane VTB at an elevation of 1" for case 3.

Similar to case 2, the cross correlation for VTB8 and VTB13 were very different from VTB2 the closest thermocouple to the cold chimney. This proved that the

phenomenon was not due to an error in the interpolation. The cross-correlation at an elevation of 8.5” was shown in Fig.80. Moreover, at z=17” VTB13, the closest thermocouple to the left chimney, had a correlation that was obviously different from the other two. This was also similar to the cross-correlation obtained for case 2 when the flow was found to be exiting through the left exhaust only. The cross-correlation for z=17” was presented in Fig.81.

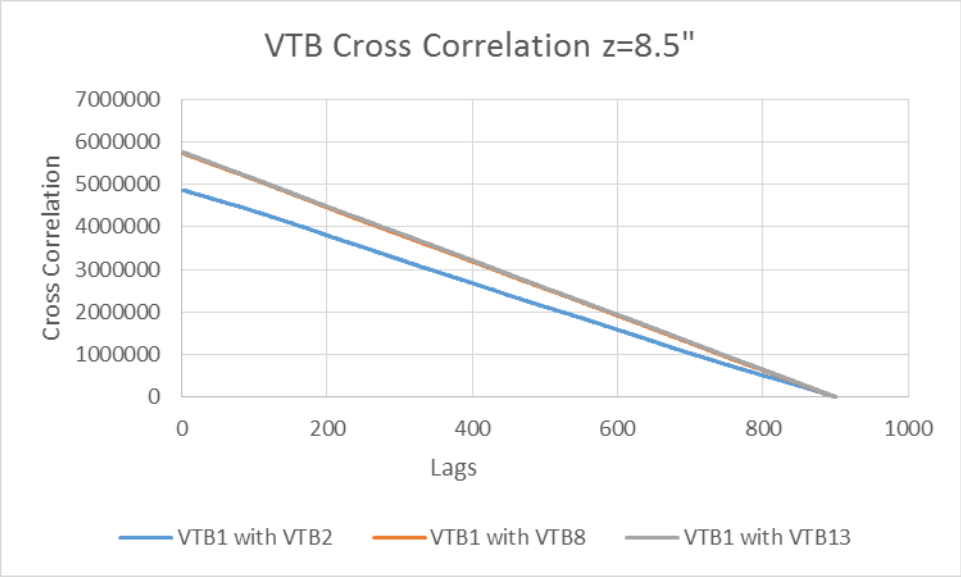

Figure 80.Cross correlation for plane VTB at an elevation of 8.5" for case 3.

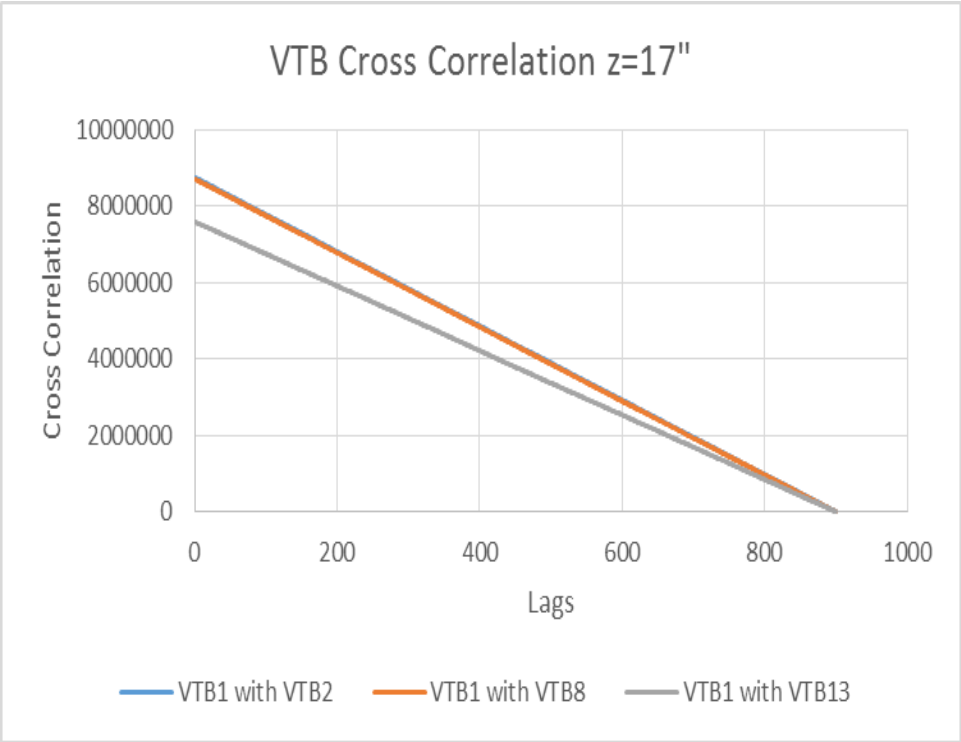

Figure 81. Cross correlation for plane VTB at an elevation of 17" for case 3.

5.6 Case 4

Only riser 4 was in operation in this case with an outlet temperature and velocity of 120^{o}C and 2.25m/s. This case was basically a repetition of case 2 with a lower velocity. The temperature gradient was larger in this case ranging from 25 to 100% of the maximum temperature which was 114^{o}C in this case from the vertical measurements. This case was very similar to case 1 with assumed reverse flow from the right chimney. However, from the middle horizontal and vertical planes (HTB and VTB) it was observed that the cold region in this case extended from the right chimney to the other side of the upper plenum. From planes VTA and HTA it was clear that the jet was

geared to the left side after impingement. The jet also seemed to widen at a quicker rate in this case. While this jet had a lower velocity relative to case 2, it appeared to be attracting more flow towards it compared to the latter. The theory was that even though the low pressure created by the jet was not as low as in case 2, the fact that the jet had lower momentum meant that it would spend more time in the box. This allowed the jet to have a better mixing and inevitably displacing more stagnant air particles. The displacement of a large amount of the stagnant air induced a stronger flow reversal as can be seen from the temperature measurements. The vertical contours illustrated the presence of thermal stratification in this case. It was clear from the contours that hot air was at the top of the upper plenum sitting on top of the cold air in the bottom of the plenum. The thermal stratification indicated poor mixing between the jet and the air in the upper plenum which resulted in a huge temperature gradient. Thermal stratification is very undesirable and may inhibit natural circulation in the actual system. The horizontal and vertical planes were shown in Fig.82 and 83, respectively.

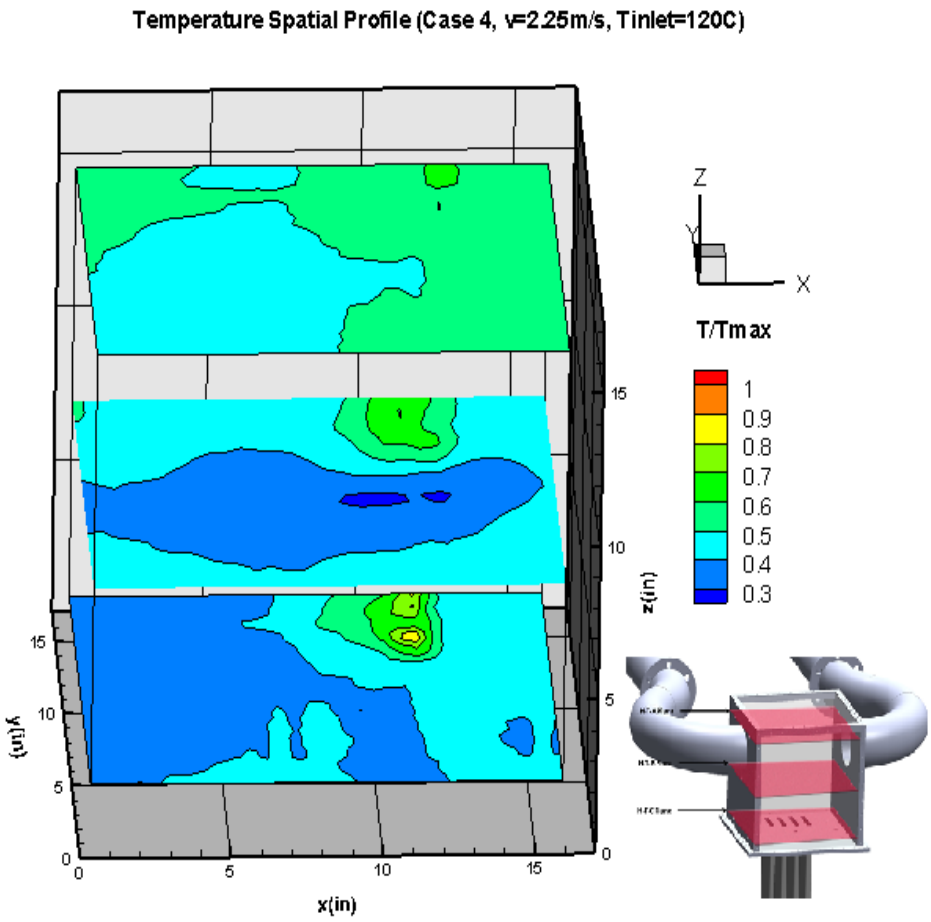

Figure 82. Normalized temperature spatial contout for the horizontal planes. The maximum temperature is 105ºC.

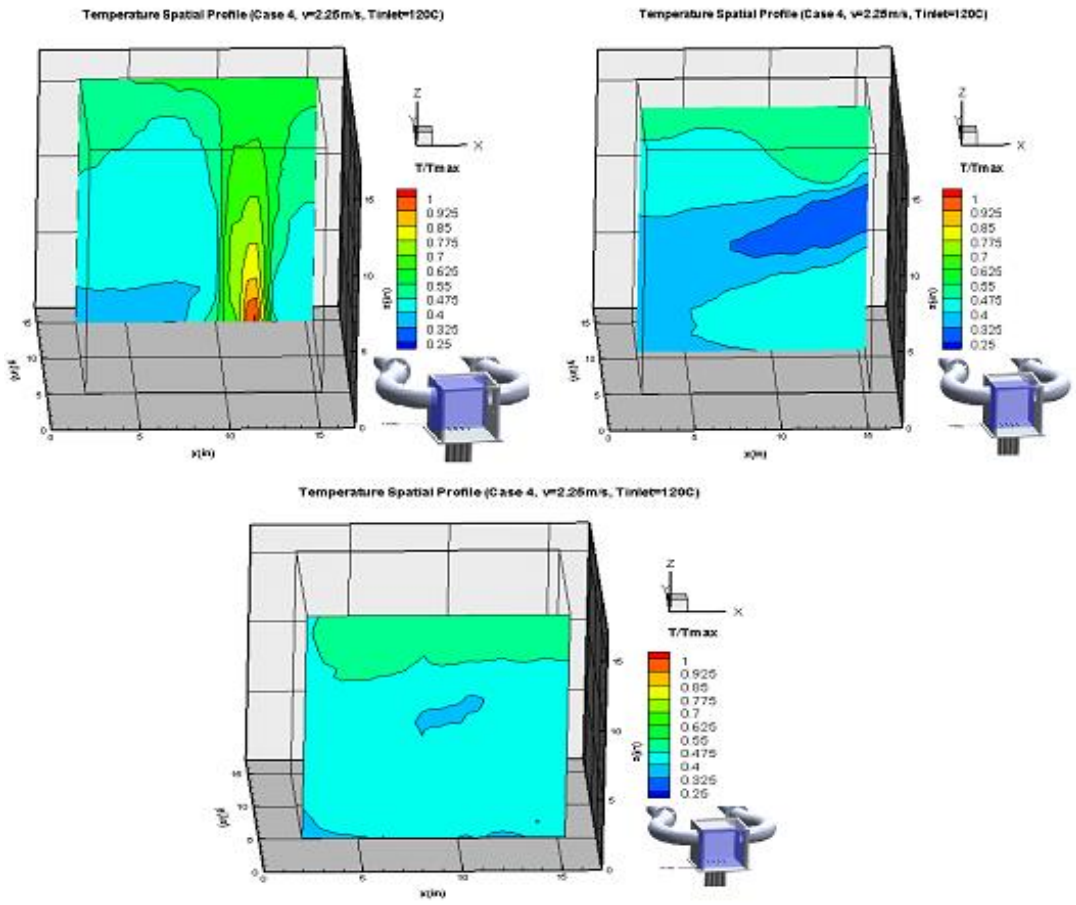

Figure 83. Normalized temperature spatial contout for the vertical planes. The maximum temperature is 114ºC.

Most of the temperature fluctuations appeared near the reverse flow region where cross flow was postulated. The maximum temperature fluctuation was around 7% of the maximum temperature. The locations of the high fluctuations were close to those found in case 2. The horizontal and vertical planes fluctuations were shown in Fig.84 and 85, respectively.

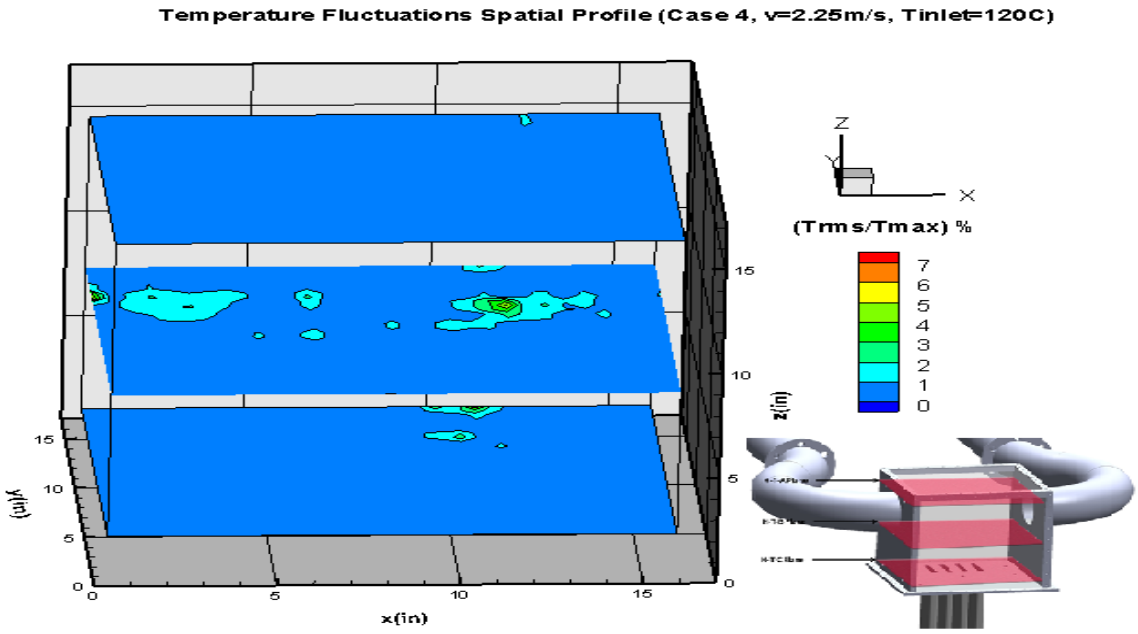

Figure 84. Temperature fluctuation percentage for the three horizontal planes. It is calculated by dividing the RMS (Root Mean Square) by the maximum temperature which is 114ºC.

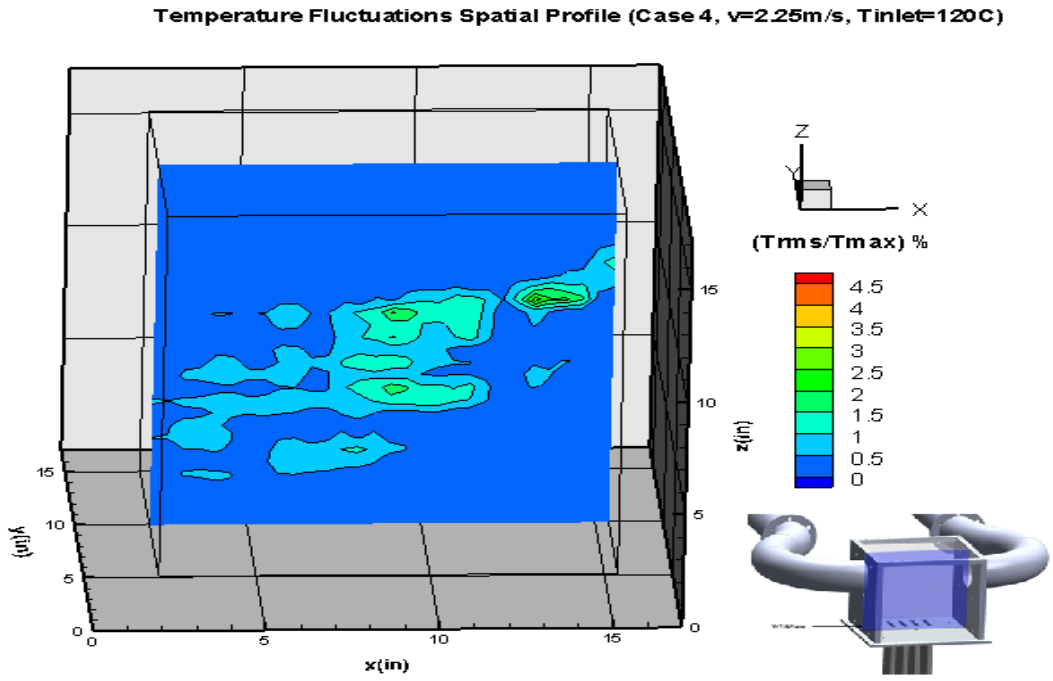

Figure 85. Temperature fluctuation percentage for the VTB plane. It is calculated by dividing the RMS (Root Mean Square) by the maximum temperature which is 114ºC.

5.7 Uncertainty Analysis

The uncertainty analysis for the temperature measurements was performed based on a model developed by Sandia National Lab. Both systematic and random errors were incorporated in the analysis. It was found that the systematic error had a greater influence on the uncertainty of the measurements. The random error was relatively low due to the large sample (900 measurements per thermocouple in each location) collected for each measurement. The analysis assumed that the connectors were made of material similar to but not the same as thermocouple wire. Based on this assumption, the error for associated with connector was estimated to be 1.1^{o}C. The DAQ error was calculated using formulas provided in the NI manuals. Refer to Ni PIXe 4345 for sample calculation of the DAQ induced error. The error used for the conversion formula was 0.03^{o}C. Equation 4 was used to calculate the error due to the length of the thermocouple wires. The random error was obtained using equation 3. The systematic error was applied to the average of each thermocouple measurement. The error was calculated for all of the measurements and the maximum was 1.6^{o}C, whereas the minimum was 1.2^{o}C. Below are figures of the temperature of rack VTA at three different elevations (z=1, 8.5 and 17") for the discussed four cases. The error bars were included in the plots. The temperature as a function of distance for case 1 was shown in Fig.86 below.

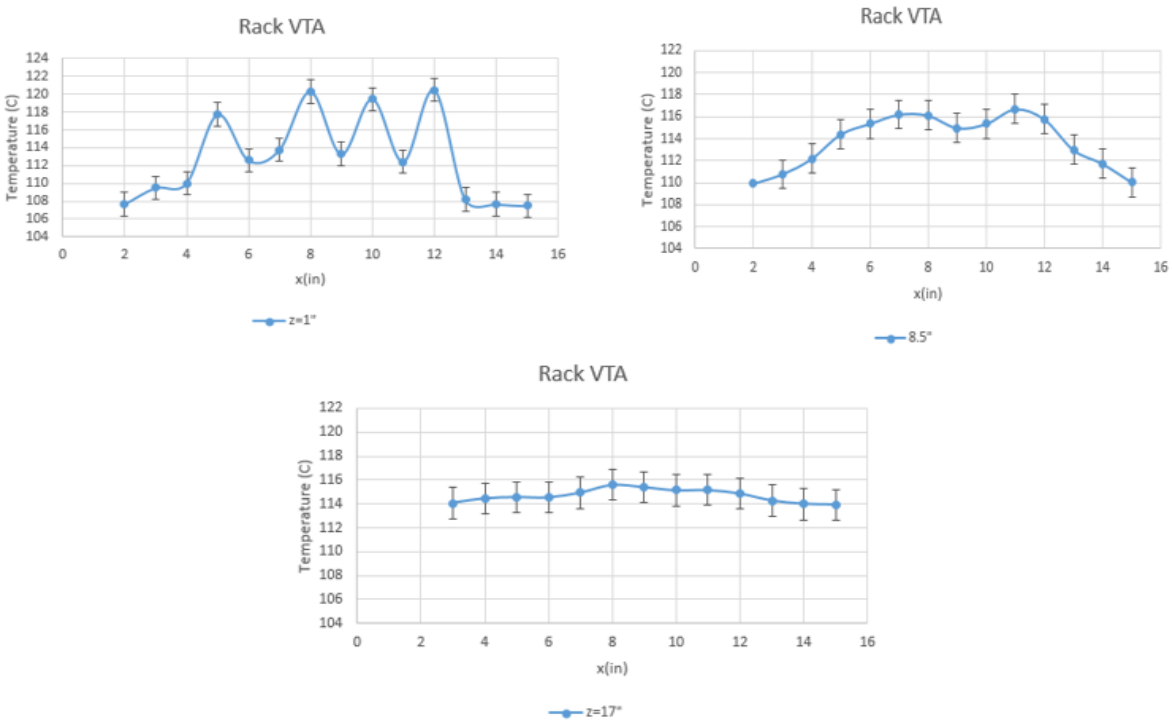

Figure 86. Rack VTA temperature as function of the x direction. This profile was for case 1.

Figure 87 showed the temperature as a function of distance for case 3 at three different elevations. The four jets could be clearly distinguished at position z=1". The obviousness of the jets disappear as the rack was moved up. It was clear from the plots that the error was fairly insignificant.

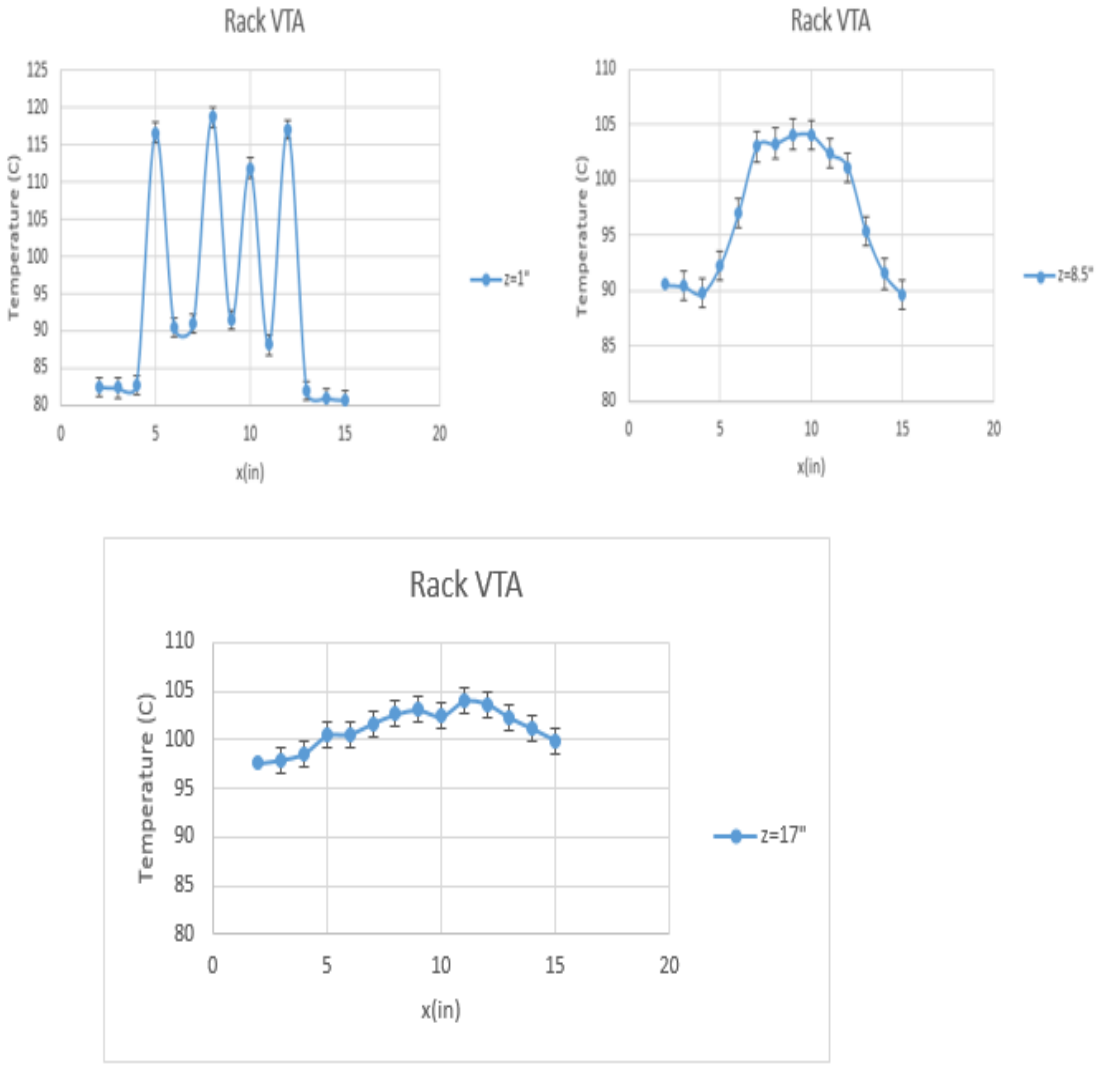

Figure 87. Rack VTA temperature as function of the x direction. This profile was for case 3.

Similarly, Fig.88 and 89 showed the temperature as a function of the x distance for cases 4 and 2. Due to the similarity of the two cases, the plots were very similar in shape, but different in magnitude.

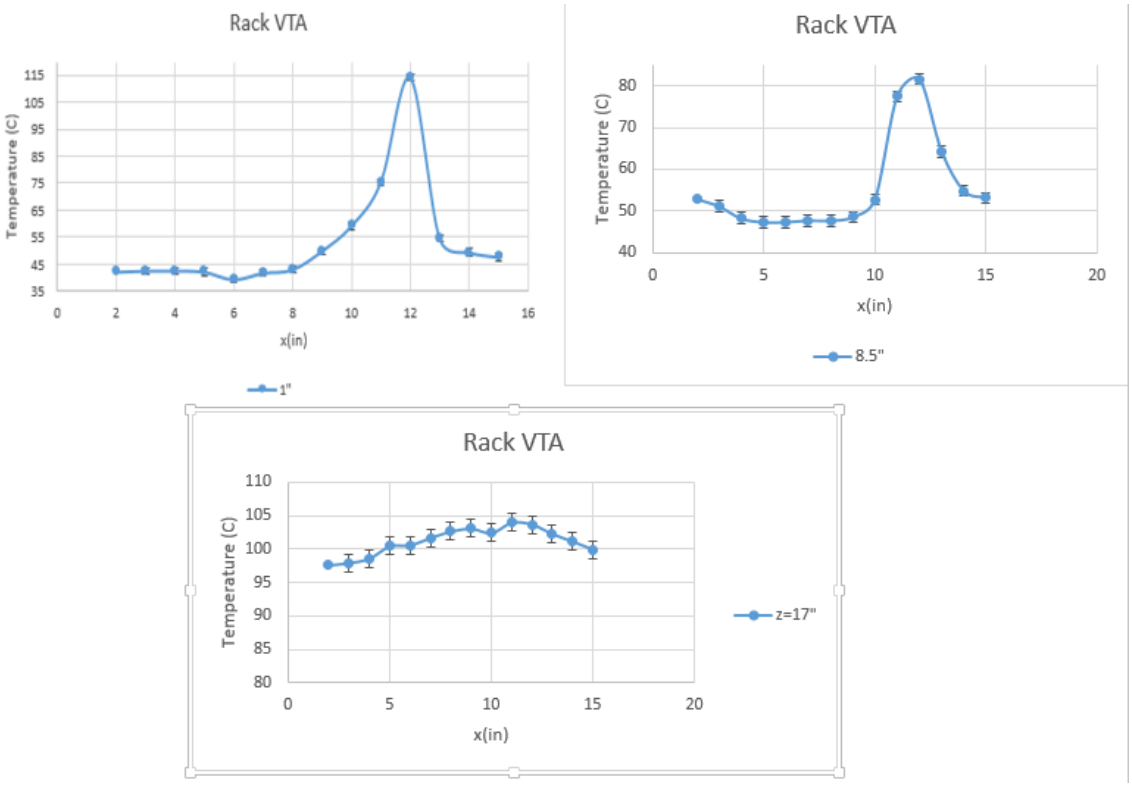

Figure 88. Rack VTA temperature as function of the x direction. This profile was for case 4.

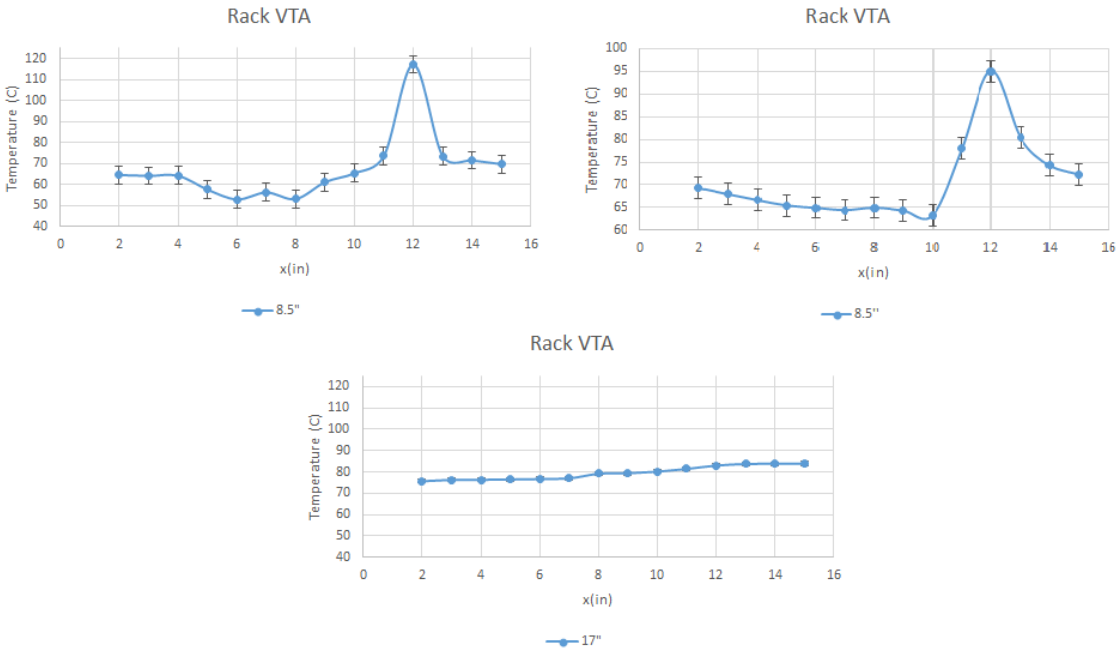

Figure 89. Rack VTA temperature as function of the x direction. This profile was for case 2.

6. CONCLUSIONS

Six temperature spatial contours of the upper plenum of the air-cooled RCCS experimental facility were measured using thermocouples with a maximum error of +/- 1.6^{o}C. The temperature measurements were interpolated using an inverse distance weighting technique to obtain a continuous temperature profile across the planes. An interval of 0.5" was determined to be optimal for the movement of the thermocouple racks based on resolution and interpolation considerations. It was observed that the temperature profile was symmetric in the plenum when the boundary conditions were equivalent for all four risers suggesting an even flow distribution in the upper plenum. The temperature contour lines suggested that the jets from risers 1 and 2 combined to form a single jet and so did the jets from riser 3 and 4. For the case of one riser being in operation (cases 2 and 4), the distribution of temperature was asymmetric in the box. Moreover, it was concluded that the flow tended to exit through the opposing chimney which in this case was the left one. It's predicted that if riser 1 was in operation only, the flow would be directed to the right chimney. The single riser case also suggested the presence of reverse flow based on the upper plenum temperature profile. It's believed that the reverse flow was caused by the low pressure formed by the high velocity jet which displaced stagnant air particles along its path to the left chimney inducing reverse flow from the right chimney. The single riser case also exhibited a wide temperature range supporting the reverse flow hypothesis. Case 3 indicated that the boundary conditions for the RCCS experimental facility were not reliable at low velocities,

especially when the velocity falls within the 10-15V range on the velocity-voltage curve. This case which was supposed to be similar to case 1 with anticipated symmetric temperature and flow distribution exhibited a perplexing behavior similar to the conditions encountered in the single jet cases. Reverse flow from the right chimney was observed based on the temperature measurements during startup and from the steady-state profiles. It was strongly believed that the postulated presence of reverse flow in this case was due to the variation of riser 2 velocities after the start of the experiment. The variable autotransformer was the main suspect behind the variation in velocity. In conclusion, the experiments predicted that the flow behavior in the RCCS upper plenum was strongly linked to the boundary conditions especially at lower velocities. Small perturbations to the system can cause the flow to be directed to one chimney and consequently induce reverse flow. Similar boundary conditions are required on the outlets of the risers for better heat transfer performance of the RCCS.

If the postulated reverse flow is confirmed with velocity measurements the air-cooled RCCS stability will be questionable. Reverse flow from a chimney in the real design will mean that the load on the other chimneys will increase. This will raise the pressure of the upper plenum and may eventually inhibit the natural circulation in the system by blocking the risers' outlets. Eventually, the RPV and reactor cavity temperature will increase the RCCS will not be capable of removing the generated heat.

7. FUTURE WORK

The variable autotransformers for riser 2 should be investigated so that voltage fluctuations do not occur at all. The TAMU air-cooled RCCS test facility is unique due to its ability to manipulate the boundary conditions and simulate different scenarios. Without reliable boundary conditions for low velocities, the facility will not be able to accurately simulate natural convection conditions in the upper plenum.

The installation of pressure transducers seemed necessary after looking at the temperature results. Pressure transducers would confirm the presence of reverse flow in the system. Moreover, variation in pressure due to the fast jets should be monitored in future experiments.

All of the observations and hypotheses regarding the flow behavior in this thesis were based on temperature measurements. Although temperature is a good indication of the flow behavior, velocity measurements are necessary to confirm the hypotheses made based on temperature. Non-intrusive methods such as particle image velocimetry must be implemented in the future to measure the velocity profile in the upper plenum and to study the occurring multifaceted phenomena in the upper plenum.

The data acquired in this thesis can also be used for one to one comparison with the STAR CCM+ computational fluid dynamic (CFD) models which currently under development.

REFERENCES

Bohling, G. (2005). Kriging [PDF document]. Kansas University, Lawerence, Kansas. Retrieved from http://people.ku.edu/~gbohling/cpe940/Kriging.pdf. Date accessed: Oct-5-2014.

Corradini, M, Anderson, M, Hassan, Y, Tokuhiro, A. (2012). Experimental Studies of NGNP Reactor Cavity Cooling System With Water (Project No. 09-781). Department of Energy, Washington, D.C.

DATAQ Instruments. (2012). Maximum Thermocouple Wire Length. DATAQ Instruments, Akron, Ohio. Retrieved from http://www.dataq.com/blog/data-acquisition/thermocouple-data-acquisition/maximum-thermocouple-wire-length/. Date accessed: Oct-7-2014.

Flitter, H, Weckenbrock, P, Weibel, R, Wiesmann, S. (2013). Continuous Spatial Variables [PDF document]. Geographic Technology Training Alliance, Zurich, Switzerland. Retrieved from http://www.gitta.info/ContiSpatVar/en/text/ContiSpatVar.pdf. Date accessed: Oct-5-2014.

Fluke Corporation. (1999). Fluke 51 & 52 Series II User Manual [PDF document]. Fluke Corporation, Everett, Washington. Retrieved from http://assets.fluke.com/manuals/5152____umeng0100.pdf. Date accessed: Oct-5-2014.

Idaho National Laboratory. (n.d.). High Temperature Engineered Test Reactor Physics Benchmark [PDF document]. Idaho National Laboratory, Idaho Falls, Idaho. Retrieved from http://www.inl.gov/technicalpublications/Documents/4247200.pdf. Date accessed: Oct-5-2014.

International Atomic Energy Agency. (2011). Status Report 70- Pebble-Bed Modular Reactor [PDF document]. International Atomic Energy Agency, Vienna, Austria. Retrieved from https://aris.iaea.org/sites/..%5CPDF%5CPBMR.pdf. Date accessed: Oct-5-2014.

Lisowski, D, Farmer, M. (2014). Experimental Observations of Natural Circulation Flow in the NSTF at Steady-State Conditions (Paper HTR2014-6-143). Argonne National Laboratory, Lemont, Illinois.

Lomperski, S, Pointer, W, Tzanos, C, Wei, T, Krauss, A, 2011. Generation IV Nuclear Energy System Initiative: Air Cooled Option RCCS Studies and NSTF Preparation (ANL-GenIV-179) [PDF document]. Argonne National Lab, Lemont, Illinois. Retrieved from http://www.ipd.anl.gov/anlpubs/2012/11/71292.pdf. Date accessed: Oct-5-2014.

Makhnin, O. (2014). Introduction to Kriging: Lecture 10, Math 586 [PDF document]. New Mexico Tech, Socorro, New Mexico. Retrieved from http://infohost.nmt.edu/~olegm/586/HYD10.pdf. Date accessed: Oct-8-2014.

Nakos, J. (2004). Uncertainty Analysis of Thermocouple Measurements Used in Normal and Abnormal Thermal Environment Experiments at Sandia's Radiant Heat

Facility and Lurance Canyon Burn Site (SAND2004-1023) [PDF document]. Sandia National Laboratories, Albuquerque, New Mexico. Retrieved from http://prod.sandia.gov/techlib/access-control.cgi/2004/041023.pdf. Date accessed: Oct-8-2014.

National Instruments. (2012). NI PXIe-4353 Specifications (375508B-01) [PDF Document]. National Instruments, Austin, Texas. Retrieved from http://www.ni.com/pdf/manuals/375508b.pdf. Date accessed: Oct-8-2014.

Oh, C, Davis, C, Park, G. (2007). RCCS Experiments and Validation for High Temperature Gas-Cooled Reactor. Proceedings from NURETH 07': The 12th International Topical Meeting on Nuclear Reactor Thermal Hydraulics. Pittsburgh, Pennsylvania.

Omega. (2014). Quick Disconnect Thermocouples with Miniature Connectors. Omega, Stamford, Connecticut. Retrieved from http://www.omega.com/pptst/jmqss.html. Date accessed: Oct-7-2014.

Pyromation Incorporation. (2014). Thermocouple Theroy [PDF document]. Pyromation Incorporation, Fort Wayne, Indiana. Retrived from http://www.pyromation.com/Downloads/Doc/Training_TC_Theory.pdf. Date accessed: Oct-7-2014.

Sulaiman, S, Dominguez, E, Alhashimi, T, Budd, J, Matos, M, Hassan, Y. (2014). TAMU Air-Cooled RCCS Status Update (Unpublished report). Texas A&M University, Nuclear Engineering Department, College Station, Texas.

TSI Incorporated. (2014). VelociCalc Air Velocity Meter 9535. TSI Incorporated, Shoreview, Minnesota. Retrieved from http://www.tsi.com/velocicalc-air-velocity-meter-9535/. Date accessed: Oct-6-2014.

Vaghetto, R. (2011). Experimental Study of Thermal-Hydraulic Phenomena in the Reactor Cavity Cooling System and Analysis of the Effect of Graphite Dispersion (Master's thesis).Texas A&M University, College Station, Texas.

Wei, H. (2009). Reactor Cavity Cooling System Heat Removal Analysis for a High Temperature Gas Cooled Reactor (Master's thesis). University of Florida, Gainesville, Florida.